THE UNIVERSITY OF HULL

Development of a Heterogeneous Microwave Network, Fade Simulation Tool Applicable to Networks that Span Europe

being a Thesis submitted for the Degree of

Doctor of Philosophy in Electronic Engineering

in the University of Hull

by

HAFIZ BASARUDIN

(MEng.)

(HND, British Malaysian Institute)

January, 2012

ACKNOWLEDGEMENTS

First and foremost, my utmost gratitude to Dr. K. S. Paulson, my supervisor, whose sincerity, guidance and encouragement I will never forget and has helped me to finish this work. I would also like to extend my gratitude to others including Mr. N. G. Riley, Dr. Franklin Mung'au, the department and Graduate School. I would also like to acknowledge the support of the British Atmospheric Data Centre and the National Oceanic and Atmospheric Administration, Physical Science Division for providing the critical datasets for this research. Last but not least, my sincere gratitude to my family and friends who helped me a lot in finishing this project through continuous encouragement and support during my study.

ABSTRACT

Radio communication systems operating at microwave frequencies are strongly attenuated by hydrometeors such as rain and wet snow (sleet). Hydrometeor attenuation dominates the dynamic fading of most types of radio links operating above 10 GHz, especially high capacity, fixed, terrestrial and Earth-Space links. The International Telecommunication Unions – Radio Section (ITU-R) provides a set of internationally recognized models to predict annual fade distributions for a wide variety of individual radio link. However, these models are not sufficient for the design and optimisation of networks, even as simple as two links. There are considerable potential gains to be achieved from the optimized design of real-time or predictive Dynamic Resource Management systems. The development of these systems requires a joint channel simulation tool applicable to arbitrary, heterogeneous networks. This thesis describes the development of a network fade simulation tool, known as GINSIM, which can simulate joint dynamic fade time-series on heterogeneous networks of arbitrary geometry, spanning Europe.

GINSIM uses as input meteorological and topological data from a variety of sources and numerically calculates the joint effects on fading on all links in a specified network. ITU-R models are used to transform rain rate into specific attenuation and to estimate the specific attenuation amplification due to non-liquid hydrometeors. The resulting simulation tool has been verified against ITU-R models of average annual fade distributions, fade slope and fade duration distributions, in the southern UK. Validation has also been performed against measured terrestrial and Earth-space link data, acquired in the Southern UK and Scotland.

CONTENTS

LIST OF FIGURES AND TABLES

NOTATION

a and b	Parameters of the Z-R relationship equation
A	Attenuation level in dB
$A_{0.01}$	Attenuation exceed for 0.01% of the time in dB
b and a	major and minor axis length of the water drop
C	(1) Coefficient formed by merging of all constant parameters in the radar equation. (2) Autocovariance
d	Path length
D	Drop diameter
D_0	Drop mean diameter
Dx and Dt	Spatial and temporal decorrelation distances
E	Expected value
f	Frequency in Hz
f_B	3 dB cut off frequency of the low pass filter (Hz)
G	Antenna gain
h	Pulse length
k and α	Frequency and polarization dependent coefficients
Kl	Specific attenuation coefficient ((dB/km)/(g/m^3))
m	Order of gamma distribution
M	Liquid water density in the cloud or fog (g/m^3).
$N(D)$	Drop size distribution
N_0	Drop concentration at D = 0
$N"(f)$	Imaginary part of the frequency dependent complex refractivity
P_r	Received power
P_t	Transmitted power
$\overline{P_r}$	Averaged received power for precipitation illuminated by the radar
r	(1) Path reduction factor, (2) Distance between the radar and target
R	Rain rate in mm/hr

$R_{0.01\%}$	Rain rate exceeded for 0.01% of the time in mm/hr
$R_{0.001\%}$	Rain rate exceeded for 0.001% of the time in mm/hr
T	Temperature
z	Altitude
Z	Radar reflectivity in dBZ
Z_V and Z_H	Radar reflectivity of a vertically and horizontally polarised pulse
¥	Lapse rate in units of temperature divided by units of altitude
γ_R	Specific attenuation of rain in dB/km
γ_C	Specific attenuation within the cloud in dB/km
Λ	Slope of the drop size distribution
Δh	Altitude relative to the rain height in metres
ΔV	Volume illuminated at any instant
Δx and Δt	Spatial and temporal sampling
$\Gamma(\Delta h)$	Sleet fade multiplication factor for specific attenuation of rain
a= =	Wavelength==
$\varepsilon(f)$	Dielectric permittivity of water
±	Backscattering cross section of the target
± ¸	Standard deviation of the conditional fade slope
¤ and ¯	Vertical and horizontal beam widths of an antenna
¸	Fade slope in dB/s

GLOSSARY OF TERMS

2-D	-	Two-dimensional
3-D	-	Three-dimensional
4G	-	Fourth generation
ACM	-	Adaptive Coding and Modulation
ARMD	-	Assymetric Random Midpoint Displacement
CAMRa	-	Chilbolton Advanced Meteorological Radar
CEOS	-	Committee on Earth Observation Satellites
CFARR	-	Chilbolton Facility for Atmospheric and Radio Research
dB	-	Decibels
DNM	-	Dynamic Network Management
DRM	-	Dynamic Resource Management
DSD	-	Drop Size Distribution
DVB-RCS	-	Digital Video Broadcasting - Return Channel via Satellite
DVB-S2	-	Digital Video Broadcasting - Satellite - Second Generation
ECMWF	-	European Centre for Medium-Range Weather Forecasts
EUMETNET	-	European Meteorological Network Services
EUMETSAT	-	European Organisation for the Exploitation of Meteorological Satellites
EHF	-	Extremely High Frequency
EXCELL	-	Exponential CELL
FBfs	-	Fractional Brownian Fields
FMTs	-	Fade Mitigation Techniques
GBS	-	Global Broadcast Service
GHz	-	Giga Hertz
GINs	-	Global Integrated Networks
GOES	-	Geostationary Operational Environmental Satellite
HAPs	-	High Altitude Platforms
HRFNS	-	Hull Rain Fade Network Simulator

HYCELL	-	HYbrid CELL
ICAO	-	International Civil Aviation Organization
IPTV	-	Internet Protocol television
IR	-	Infrared
ISA	-	International Standard Atmosphere
ITU-R	-	International Telecommunication Union-Radio Section
JAXA	-	Japan Aerospace Exploration Agency
LAS	-	Local Average Subdivision
LEO	-	Low Earth Orbit
LMS	-	Land Mobile Satellite
MESO	-	Multi-community Environmental Storm Observatory
MIMO	-	Multiple-input and multiple-output
MPE	-	Multi-Sensor Precipitation Estimate
MPEF	-	Meteorological Product Extraction Facility
NASA	-	National Aeronautics and Space Administration
NCAR	-	National Center for Atmospheric Research
NCEP	-	National Centers for Environmental Prediction
NEXRAD	-	Next-Generation Radar
NGA	-	National Geospatial-Intelligence Agency
NOAA	-	National Oceanic and Atmospheric Administration
NWP	-	Numerical Weather Prediction
OFDM	-	Orthogonal frequency-division multiplexing
PSD	-	Physical Science Division
SATNEx	-	SATellite Network of EXperts
SHF	-	Super High Frequency
SISTAR	-	SImulator of the Space-Time behaviour of the Attenuation due to Rain
SRTM	-	Shuttle Radar Topography Mission
SSM/I	-	Special Sensor Microwave/Imager
THz	-	Tera Hertz

TRMM	-	Tropical Rainfall Measuring Mission
UAS	-	Unmanned Airborne Systems
UAVs	-	Unmanned Aerial Vehicles
UM	-	Unified Model
VHF	-	Very High Frequency
ZDI	-	Zero Degree Isotherm

CHAPTER 1 INTRODUCTION

Modern telecommunications systems use a wide variety of channels e.g. copper, fibre-optic and air-links. Wireless links are often faster and cheaper to set up as they do not require the disruption of installing a wire or fibre along the route. They also yield greater flexibility and mobility compared to fixed cables. Air-links also allow communications with, or via, elevated platforms such as satellites, airplanes, High Altitude Platforms (HAPs) and other places to which it would be impossible to install a physical connection. A large proportion of all communications is carried by radio waves along air-links. High capacity Super High Frequency (SHF) and Extremely High Frequency(EHF) radio links are integral to the backbone networks of all developed countries, and are even more important in developing countries with less legacy wired network. Communications via elevated platforms require both an uplink and downlink and so are, at a minimum, networks of at least two links. Currently there are no internationally recognized models to predict the performance of networks of two or more links.

High capacity communications systems require higher operating frequencies to provide the bandwidth. High capacity radio systems currently use the millimetre and microwave frequencies in the higher SHF and EHF bands. These links can be broadly characterised as terrestrial if both transmitter and receiver are near the ground or Earth-Space if one end is on a satellite. Intermediate categories exist where one end of the link is a High Altitude Platforms (HAPs) or an aircraft. Terrestrial links between fixed ground stations and copper-fibre networks form the backbone of telecommunications systems. However, satellite communications are increasingly important for both broadcast systems and as parts of Global Integrated Networks (GINs).

This is an attraction in developing countries that can roll-out telecommunications infrastructure quickly and cheaply. Mobile phone communications can be made

rapidly available in large cities using a base stations networked by microwave links. In remote places, broadband can be delivered via satellite. Apart from the sudden broadening in the services provided by the satellite, many private and government organizations, especially in United States and Europe, have made massive investments in the development of satellite communication systems based on the WTEC panel report on Global Satellite Communications Technology and Systems (www.wtec.org/pdf/satcom2.pdf). Furthermore, there is a market shift where business and consumers are more directly in contact with satellite service providers.

Although microwave links are cheaper and quicker to deploy than fixed wired services, the signals that travel between transmitter and receiver must propagate through the surrounding environment or channel. During propagation signals can be distorted or attenuated by a wide range of mechanisms (Chris Haslett, 2008; Crane, 1996). Other signals are received as interference to the wanted signal. When present in the channel, rain and other hydrometeors (sleet, fog, and cloud) will scatter and absorb radio waves. The specific attenuation due to hydrometeors is highly frequency dependent. For frequencies below 5 GHz, hydrometeor attenuation is small compared to signal impairment caused by other causes, for example multipath or ducting. Therefore, attenuation due to rain and other hydrometeors is not part of the system design and planning for communications between mobile base stations and handsets. However, the higher capacity links joining peripheral base stations to the wired network operate at higher frequencies and their availability is limited by hydrometeor fading. For most links operating above 10 GHz, hydrometeor fade is the dominant and limiting fade mechanism (Zhang, 2008; Chris Haslett, 2008; Crane, 1996).

National telecommunications regulators typically license fixed terrestrial links to operate at a power level aimed to yield a specific average annual availability; 99.99% for most links and 99.999% for critical links (Trevor Manning, 2009). A base power level is calculated given typical clear-sky path attenuation, calculated using diffraction models and knowledge of the path elevation profile, and estimated

interference from other systems. In addition, a fade margin is calculated from models of the hydrometeor fade that would be expected for 0.01% or 0.001% of an average year. The International Telecommunication Union-Radio Section (ITU-R) maintains a set of models for predicting average annual distributions of fade, with a one-minute integration time, on individual, terrestrial and Earth-Space links. These models are adequate for the regulation and coordination of terrestrial links and can be used to assign a fixed fade margin and estimate link budgets for Earth-Space links. The ITU-R also provides models of fade duration and fade slope for a ten-second integration time, principally used in the design of Fade Mitigation Techniques (FMTs). However, these ITU-R models are not sufficient for the design and optimisation of networks of radio links, even as simple as two links in route diverse or multi-hop configuration, which require a joint channel model with a temporal resolution of one-second or shorter.

The recently completed SATNEx (SATellite Network of EXperts) II (IST 027393) European Network of Excellence, and the ongoing IC0802 COST Action, have identified the urgent need for joint channel models for Global Integrated Networks (GINs) utilising terrestrial, satellite, unmanned airborne systems (UAS) and HAPs radio links in the Very High Frequency (VHF) to W bands. In particular, these models are necessary for the design and optimisation of proposed Land Mobile Satellite (LMS) systems at Ka and Ku bands and higher EHF frequencies (currently at L, S and C-band but quickly reaching capacity), see W. Zhuang (1997). Recent projects by the French space agency CNES (SWIMAX and SDMB) have identified these as the future for broadband and broadcast systems to mobile receivers in trains, planes and road vehicles. A draft report by the Electronic Communications Committee of CEPT (European Conference of Postal and Telecommunications Administrations) stresses the importance of proposed consumer systems delivering broadband, (Internet Protocol television) IPTV and multimedia applications to users, direct from satellite at Ka and Ku bands, (www.erodocdb.dk/docs/doc98/official/pdf/ECCRep152.pdf). These services will need to coexist with terrestrial services. Of particular concern is

the performance of the terrestrial networks linking ground stations to content providers, in conjunction with the satellite uplinks. These systems require adaptive FMTs and Dynamic Resource Management (DRM), see Callaghan (2008). Based on work reported in COST 255 and 280, various adaptation techniques have been included in standards Digital Video Broadcasting - Satellite - Second Generation (DVB-S2) and Digital Video Broadcasting - Return Channel via Satellite (DVB-RCS) such as up-link power control, reconfigurable antenna systems, and adaptive coding and modulation (ACM). All these dynamic adaptation techniques require simulation on channel models during their development and evaluation. The most important fade mechanisms for EHF on terrestrial or slant paths are scattering by rain and cloud droplets, absorption by atmospheric gases and scintillation. These fade mechanisms exhibit complex spatial and temporal correlations, due to their dependence upon the weather. Furthermore, it is necessary to be able to model a very wide range of scales i.e. from a radio beam Fresnel diameter to the width of a continent and from one-second fade variation to the life-time of a large weather system.

Joint channel simulators are vital for the design, evaluation and optimisation of these proposed systems. It is essential that sufficient diversity exists in terrestrial networks to ensure ground stations have access to content and that ground station diversity ensures content can be communicated to satellites. This will require meteorological nowcasting to predict link outage and to dynamically reconfigure networks. The development of fourth generation (4G) direct broadcast to mobile from satellites techniques, such as multiple-input and multiple-output (MIMO) Orthogonal frequency-division multiplexing (OFDM), will require adaptation to differential fade along alternate paths, see Liolis et al. (2007). There is likely to be considerable advantage in the application of ACM techniques developed for satellite communications to terrestrial networks. However, joint channel models are required to quantify the benefits on terrestrial networks.

System designers and radio planners face a common problem in forecasting or

predicting the effects of rain and other hydrometeors on telecommunication systems. Current existing models offer limited prediction of joint rain fade distribution on microwave links. At the moment, most designers rely on existing models such as from the ITU-R to predict statistics of hydrometeors events for an average year or average worst month.

A known method to generate simultaneous fade time-series for a heterogeneous networks of SHF and EHF radio links is to generate fine-scale, spatial-temporal weather fields and then to simulate the effects on each radio link Zhang (2008). The weather fields have come from a range of sources i.e. measured radar data, Numerical Weather Prediction (NWP) or stochastic simulations constrained by measured statistics.

One of the earliest systems was developed in Italy and is known as EXCELL; see (Bosisio and Riva, 1998; Paraboni et al., 2002). However, the EXCELL system assumes unrealistically smooth spatial-temporal variation of rain rate and its scope and resolution are poorly defined. The Hull Rain Fade Network Simulator (HRFNS), Paulson and Zhang (2009), is based on the downscaling of radar data, but is only applicable over squares of size 50 km in the southern UK. The University of Bath EHF SATCOM system, Hodges et al. (2003), combines numerical weather models with radar data to model satellite channels and is valid across the UK. It includes rain and cloud fade mechanisms as well as scintillation and absorption by atmospheric gases. Rain fields derived purely from statistical models of rain rate or log rain rate variation have been employed to model Earth-Space and terrestrial links (Callaghan, 2004; Gremont and Fillip, 2004). A new simulation tool is currently being developed by ONERA in France called SISTAR. The ONERA system utilises ERA-40 historical NWP data from European Centre for Mid Range Weather Forecast (ECMWF) and is applicable to satellite links, see Jeannin et al. (2009). However, the input ERA-40 data is very coarse and the downscaling techniques employed have not been verified. More of these will be discussed later in Chapter 4.

1.1 Brief description of GINSIM

As discussed in the earlier sections, joint fade time-series are necessary to evaluate and optimise the performance of a more complex radio networks and it can only be acquired through simulation of these links on fine spatial and temporal scale meteorological fields. This thesis describes the development of GINSIM, a network fade simulation tool and an extension to the previous HRFNS system. The new GINSIM is capable of simulating SHF and EHF radio links including terrestrial and Earth-Space links. Fine-scale rain fields are generated by numerically downscaling composite rain images produced by networks of radars. These fields are then transformed to specific attenuation fields and pseudo-integration along the link path can be performed to obtain the joint fade time-series. All other fade mechanisms (other than rain effects) can be added later into the system. The detail procedures of GINSIM will be explained later in Chapter 4. The following figure describes the block diagram of GINSIM.

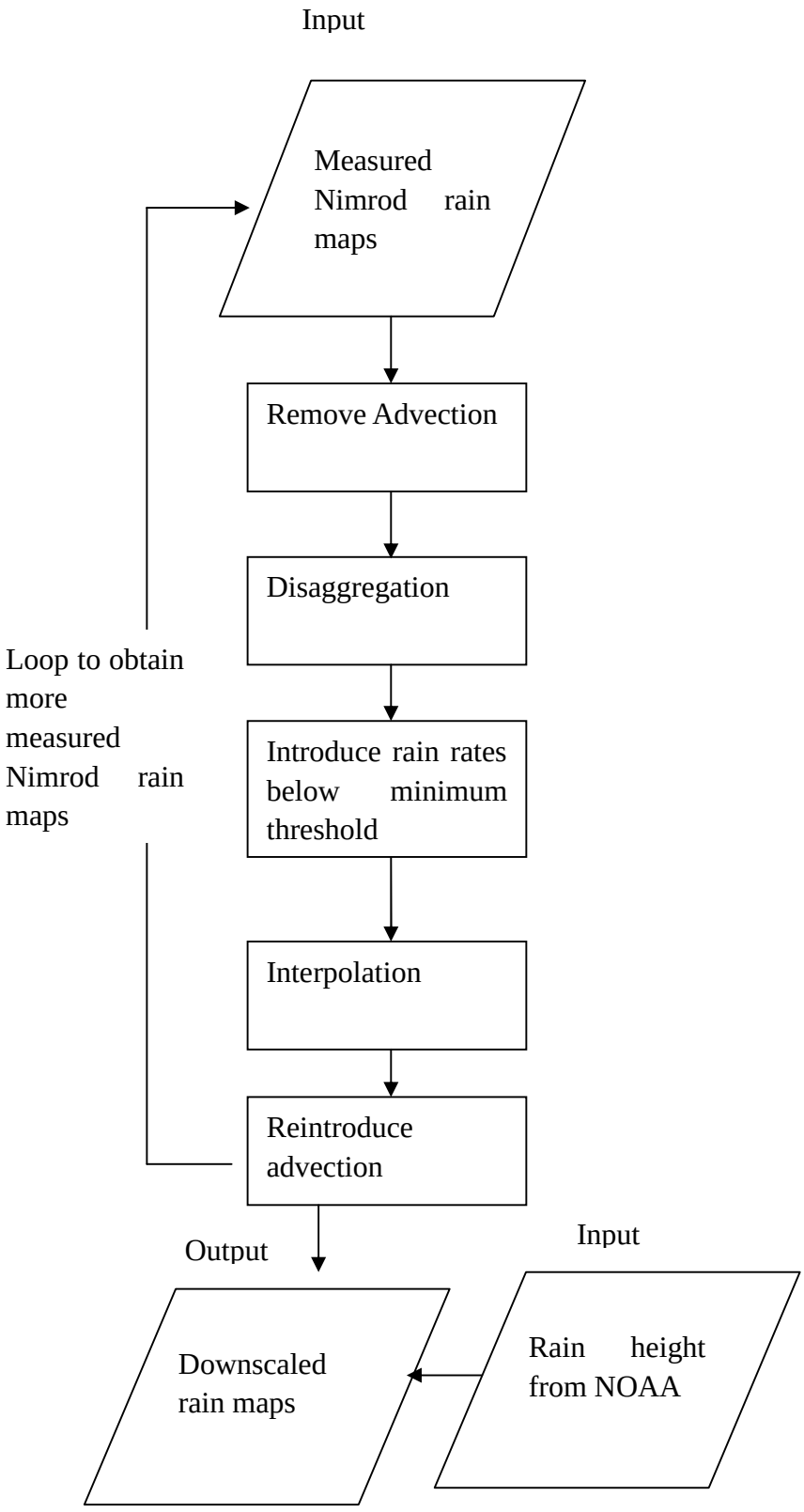

Figure 1.1: Block diagram of the GINSIM

1.2 Aims and objectives

The main aim of this research is to expand the capability of the previous HRFNS by adding new fade mechanisms, particularly attenuation due to sleet (wet snow), and the ability to simulate slant path links such as Earth-Space, Earth-HAPs and Earth-UAV. Sleet specific attenuation can be calculated using the Bacon-Tjelta sleet model, see Tjelta et al. (2005). Both the sleet fade calculation and the effective path length of slant path link rely on rain height parameter which can be extracted from NCEP/NCAR reanalysis dataset. The old HRFNS was based on rain fields measured by Chilbolton Advanced Meteorological Radar (CAMRa). The proposed system, GINSIM utilises rain maps from Nimrod and OPERA to expand the coverage to most of Europe.

The major objectives of this research:

1. Develop a joint channel rain fade simulation tool, based on algorithms developed for HRFNS, but using new datasets with European or global coverage,
2. Incorporate fading by wet snow (sleet),
3. Expand the current system to be able to simulate slant path links,
4. Validate the simulated results with ITU-R models,
5. Validate the simulated results with real radio links.

1.3 Thesis outline

The review of research undertaken throughout three years of study has been documented in this thesis. Chapter 1 provides an introduction, the aims and objectives and the research overview. Chapter 2 reviews hydrometeors fade mechanisms from the relevant ITU-R models.

Chapter 3 lists meteorological and other measurement datasets, including rain radar maps from Nimrod/OPERA and NCEP/NCAR reanalysis data, that can could be used

in the proposed simulator.

Chapter 4 details the downscaling algorithms applied to the meteorological data, including the disaggregation and interpolation techniques. Chapter 5 investigates the validation of downscaled rain radar and simulated radio networks against theoretical ITU-R models. Chapter 6 reports the validation and comparison between simulated radio networks and real links measurements.

Finally, Chapter 7 summarises and concludes the project. Suggestions of future work and recommendations are also provided in this chapter.

CHAPTER 2 MICROWAVE FADE MECHANISMS

Microwave telecommunication links, including terrestrial and Earth-Space satellite links operating at EHF band (30-300 GHz), offer the large bandwidth and high capacity required for applications such as multimedia services. The increasing number of users and the growing complexity of multimedia have driven a demand for capacity that has pressured regulators to explore higher frequency bands for larger bandwidth. However, most of the atmospheric fade mechanisms are frequency dependent, and higher frequencies are usually associated with higher losses. Rain attenuation is the dominant fade mechanism on fixed links operating above 10 GHz. Attenuation by other hydrometeors such as cloud, fog and sleet (wet snow), scintillation due to movement of the atmosphere, absorption by atmospheric gasses, and multipath effects such as ducting also contribute to fade distributions and may be the largest fade mechanism in specific circumstances and for short times. This chapter discusses these fade mechanisms, their effects on radio links and the relevant ITU-R models.

2.1 Formation of Cloud and Rainfall

A wide variety of hydrometeor particles exist in the atmosphere, mainly differing in shape, size and composition. They are made by complex processes such as ice nucleation, evaporation and sublimation, condensation, particle break-up and coalescence. Clouds exists in many forms including convective (Cumulus type of clouds), uniformly distributed layer (stratus) and thin layer clouds (cirrus) which can be located at altitudes above 5 km. Generally, clouds are formed in the troposphere when rising air containing water vapour cools to its dew point (the temperature at which the air becomes saturated). Water vapour condenses and freezes onto existing dust, salt and ice particles. Ice crystals within the cloud can fall into warmer layers and melt to become water droplets. These water droplets then will be large and dense enough and fall as rain drops.

Clouds are usually formed in a convective or stratiform type. Convective clouds are usually smaller, typically from hundreds of metres to several kilometres across and are often associated with thunderstorms. Convective clouds are formed when there are intense heating from the sun and an abundance of moist air. Stratiform clouds are typically larger, stably stratified and caused by broader layers of more slowly rising air. Stratiform cloud could range from 100 to 1000 km across. Figure 2.1 illustrates the formation for stratiform and convective clouds.

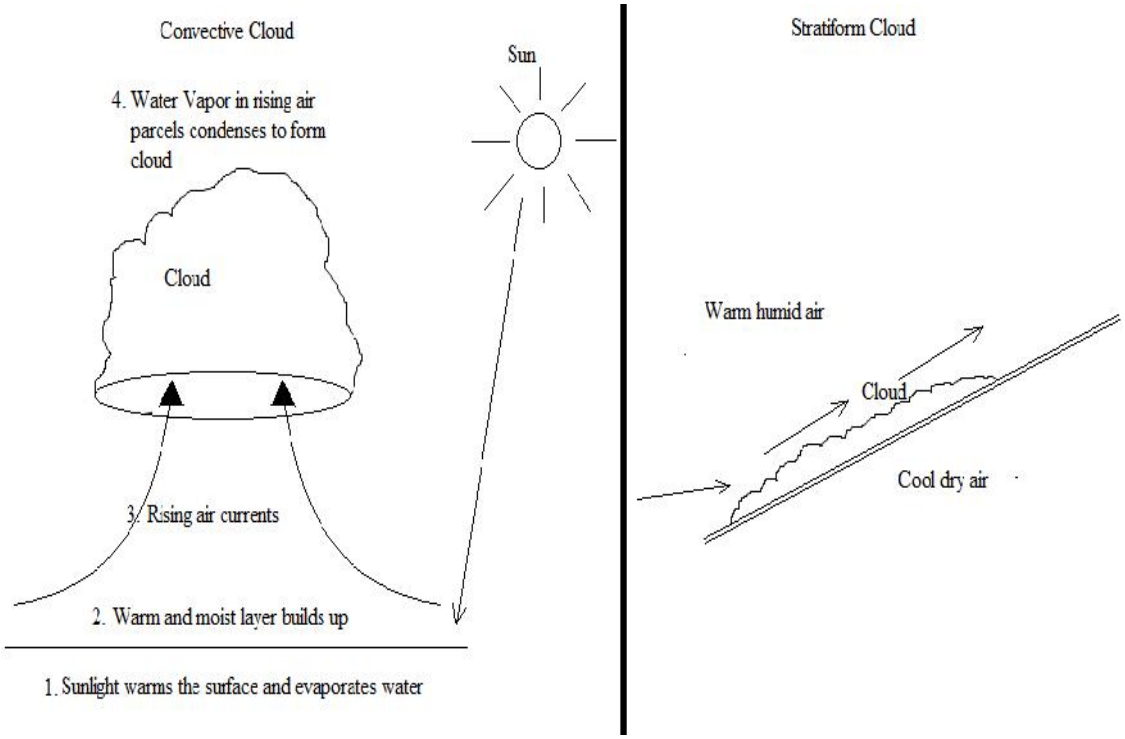

Figure 2.1: Convective and stratiform cloud formation. (The diagram was derived from www.weatherquestions.com/How_do_clouds_form.htm).

Generally, there are several types of rain events which are usually associated with cloud types; the convective rain, stratiform or frontal rain and orographic rainfall. Convective rain is usually heavy, from convective clouds and dominates in tropical regions. The rainfall rate for convective rain can be as high as 150 mm/hr for temperature regions and more than 200 mm/hr in tropical regions, for short periods of time. In the UK, rain event are often assumed to be convective when rain rates

exceeding 20 mm/hr last for more than a few minutes. Rainfall from stratiform cloud is usually light and contains a larger proportion of small raindrops. However, stratiform rain has larger coverage area in contrast to convective rain events, typically hundreds of kilometres across. Orographic rainfall is formed when a parcel of air containing water vapour collides with a mountain and is forced upwards. Orographic rain can lead to significantly different microclimates around large geographic features but is not important for most areas of the UK.

For temperate regions, the Bergeron process is the leading rainfall generating mechanism (Usman, 2005). The Bergeron process, also known as the ice crystal process, forms precipitation in cold clouds by the growth of ice crystals. Supercooled water droplets, as cold as -40°C, evaporate and the vapour sublimes onto ice crystals, making larger crystals. Water droplets can also collide with ice crystals and freeze. These ice crystals will melt into water droplets as they fall into warmer levels. This region is called melting layer and it is related to a radio term known as the rain height. In radar meteorology the melting layer is known as the bright band as it produces a strong return echo. The height of the melting later is strongly affected by temperature profile or lapse rate through the atmosphere and can vary depending on seasons and regions. Typically, the melting layer is at its maximum height during summer. Collision and coalescence processes are more important in rainfall formation in the tropical region. Cloud droplets which are carried by air currents will collide with other droplets forming larger drops until they become large enough to form raindrops. Not all droplets fall as rain since some evaporate before they reach the ground (Usman, 2005). Figure 2.2 illustrates the processes leading to the formation of rain within a cloud.

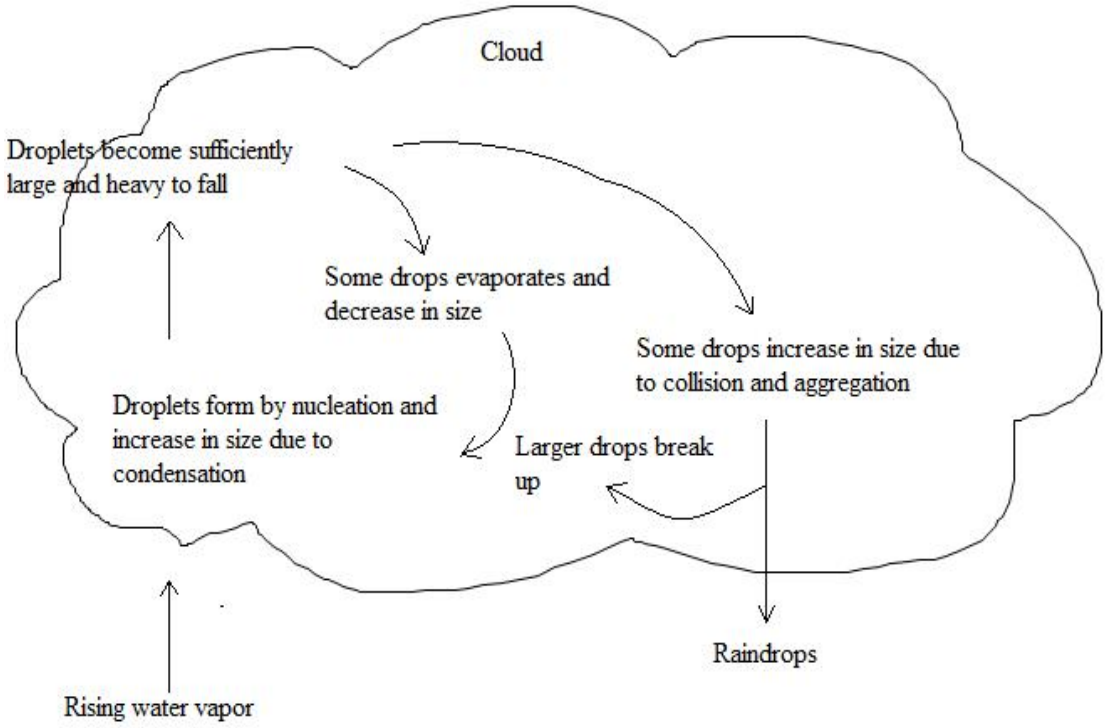

Figure 2.2: Rain formation within a cloud from Usman (2005)

2.2 Earth-Space Radio Communication System

Radio communications with satellites may use high frequencies as the path through the attenuating troposphere is often short. Due to the elevation of the link, interference is often less of a problem than with terrestrial links. In most of the commercial Earth-Space telecommunications, the satellites are located in geostationary orbit above the equator where the angular velocity of the satellite is equal to the rotation of Earth. The large orbit radius (approximately 36,000 kilometres) allows large areal coverage, without the ongoing expense of building and maintaining terrestrial networks. Except for at high latitudes, Earth-Space links do not require 'path clearance' like the terrestrial link to check if the signal will be blocked by tall obstacles (hills, mountains, buildings) since the Earth station only need point directly to the satellite. The most important parameter when dealing with hydrometeor fades on Earth-Space links is the rain height. The zero degree isotherm (ZDI) height (the altitude where the temperature is zero degrees Celsius) is closely related to rain height. Figure 2.3 illustrates the path geometry for an Earth-Space link.

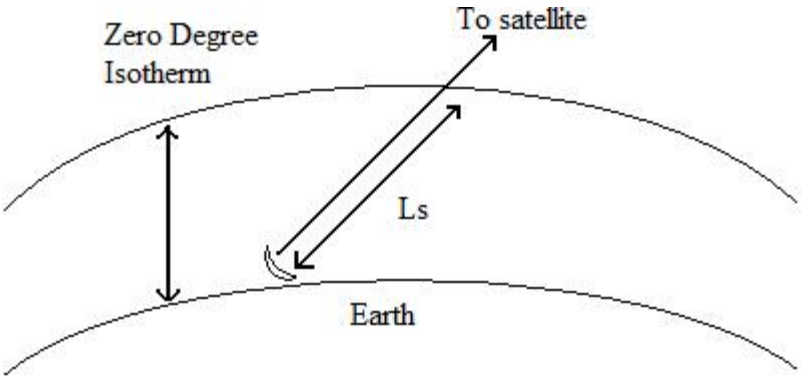

Figure 2.3: A geometry path for an Earth-Space link.

For a stratified, rainy atmosphere the Earth-Space path passes through three regions. Near the ground, rain will consist entirely of liquid particles and the specific attenuation will be close to that predicted by Rec. ITU-R P.838-3 (2005). Higher, in the melting layer, mixed phase particles will exist leading to specific attenuations many times that associated with rain rate of the equivalent intensity. Above the melting layer, all hydrometeors will be frozen and the specific attenuation at EHF frequencies is close to zero. The melting layer straddles the ZDI as super-cooled water particles exist above this level and partially melted mixed phase particles exist below. Rec. ITU-R P.618-10 (2009) includes the effects of the melting layer by assuming rain exists up to an altitude known as the rain height, assumed in Rec. ITU-R P.839-3 (2001) to be 360 m above the ZDI. Rain height can vary from near the ground level to 5 km depending on seasons and regions.

2.3 Absorption by Atmospheric Gasses

Water vapour and oxygen molecules in the atmosphere have resonant frequencies at which they strongly absorb radio waves, causing high attenuation. Absorption by atmospheric gasses depends upon the temperature and partial pressure of these gasses. Therefore their spatial and temporal variation is rather gradual. Rec. ITU-R 676-8 (2009) provides procedures to calculate losses due to absorption for radio waves as shown in Figure 2.4. Specific attenuation has been calculated using the model in Rec.

ITU-R P.676-8 (2009) for frequencies from 1 to 350 GHz using parameters for a standard atmosphere i.e. a temperature of 20 Celsius, pressure 1013 hPa, and water vapour density of 7.5 g/m^3. Rec. ITU-R P.676-8 (2009) writes the specific attenuation due to absorption by atmospheric gasses is written as:

$$¥ = ¥_o + ¥_w = 0.1820 f \ N''(f) \text{ dB/km} \tag{2.1}$$

where γo and γw are specific attenuations for dry air and water vapour respectively, f is the frequency in GHz and $N"(f)$ is the imaginary part of the frequency dependent complex refractivity.

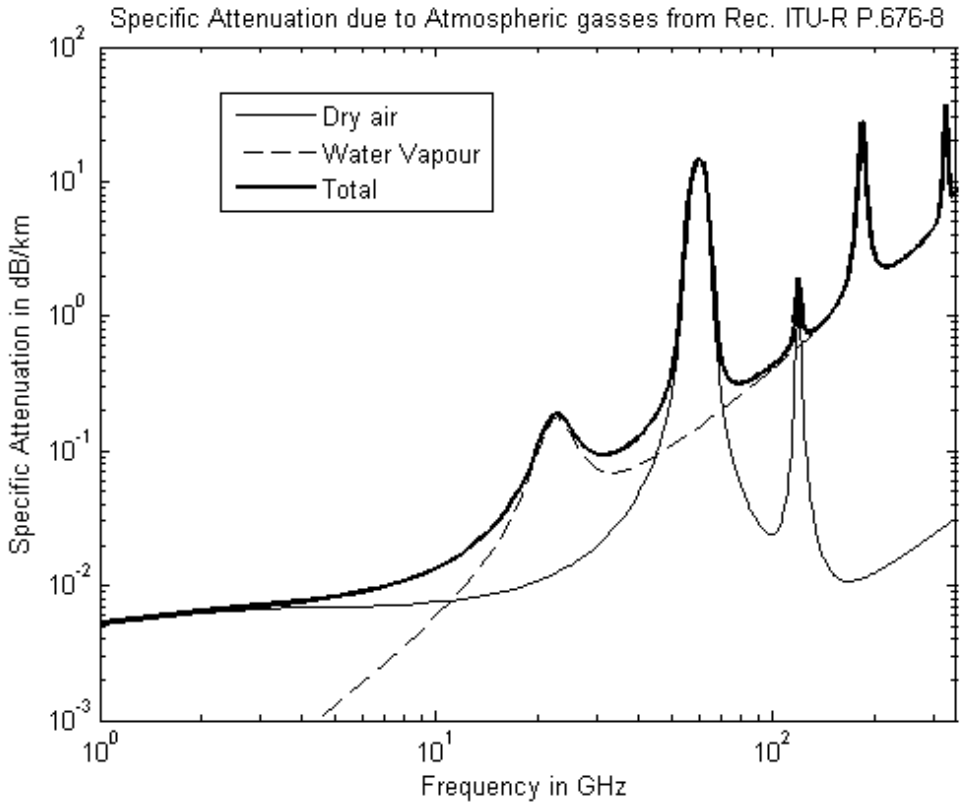

Figure 2.4: Specific attenuation due to Atmospheric gasses from Rec. ITU-R 676-8 (2009)

For most links the average and dynamic fading caused by atmospheric gasses is insignificant. For instance, for a radio link operating at 10 GHz, the total specific attenuation due to absorption is approximately 0.01 dB/km. On the other hand, the specific attenuation rises steadily beyond 20 GHz and at resonance peaks, for

example the oxygen line at 60 GHz, can reach values between 16 and 17 dB/km. Peaks of absorption within communications frequencies occur at approximately 22 GHz (for water vapour) and 60GHz (for oxygen). The frequency regions between these absorption peaks are called atmospheric windows. The frequencies in demand for use in long distance telecommunications and radar system design are in the window regions. Bands close to absorption peaks are available for ad-hoc, unlicensed use due to the short reuse distance. As the frequency windows become congested, radio designers are forced to consider higher frequencies. Beyond 60GHz, the absorption loss for oxygen is decreasing but the absorption for water vapour steadily increases and becomes more complicated with stronger water vapour lines occurring at 183, 325 and 380 GHz (Liebe, 1989). For radio links operating at frequencies at beyond 350 GHz, the atmospheric absorption loss can be more significant than rain fading, Paulson (2005). For instance, specific attenuation for atmospheric absorption can be at 1000 dB/km at 1THz. Low margin systems operating close to absorption lines can experience slow variation in fade margin due to changes in temperature and pressure and this can lead to outages at lower rain rates than would be otherwise expected.

2.4 Rain Parameters, Scattering and Attenuation

Scattering and absorption by rain and other hydrometeors (wet snow, hail) is the dynamic fade mechanism leading to the largest prolonged fading on most millimetric telecommunications links. Attenuation due to rain is negligible at frequencies below 5 GHz. However, above 10 GHz, losses due to rain can cause outages and it is the factor that limits availability of these links. Scattering by rain can increase interference by scattering unwanted signal into a receiver, as well as reduce the power of the wanted signal. Raindrops have a similar size to the millimetre radio wavelength in the EHF band. For instance, the wavelength for 38 GHz radio signal is around 8 mm while the diameters for raindrops are usually from 1 or few mm to 10 mm (Usman, 2005). Specific attenuation of rain on microwave links depends on various

parameters including the rain drop size distribution (DSD), raindrop shape and rain rate.

2.4.1 Rain Scattering

Rain drops scatter and absorb the incident radio wave energy. Rayleigh scattering is an approximate theory that describes scattering when the hydrometeor particle is much smaller than the wavelength of the radio wave. According to Rayleigh scattering, the energy of the incident radio wave is scattered with a radiation pattern similar to that of a dipole and the amount of energy that is scattered is proportional to D^3/λ, where D is the diameter of the particle and ^{a} is the wavelength. If the hydrometeor particles are of a similar size to the wavelength then the more complicated Mie scattering model is used. Mie scattering is only applicable to spherical objects and so becomes increasingly inaccurate for larger rain drops and is not applicable to most sleet particles. Mie scattering predicts larger peaks in the forward and backwards scattering directions than Rayleigh scattering. The Rayleigh scattering model can be used for most cases of rain scattering effects on microwave links. Figure 2.5 illustrates the radiation pattern predicted by Rayleigh and Mie scattering models.

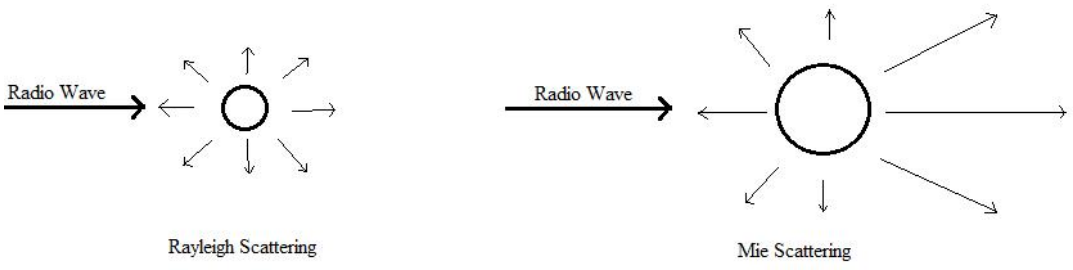

Figure 2.5: Energy scattering pattern of Rayleigh and Mie.

2.4.2 Raindrop Size Distribution (DSD)

The distribution of different sizes of raindrop has been studied and modeled since the beginning of 1940s, (Law and Parson, 1943; Marshall and Palmer, 1948). Initially a crude measurement of DSD was performed using flour pallet or bloating paper methods. Since then, more advance equipment has been designed and built for DSD measurement, such as the well known drop impact disdrometer by Joss & Waldvogel (1977). A disdrometer with impact sensor served as a basis for drop sizing instruments where vertical momentum of an impacting drop is transformed into an electrical pulse whose amplitude is a function of the drop diameter. One such example of a disdrometer is the Distromet Joss Waldvogel Impact Disdrometer RD-69, installed at Chilbolton and Sparsholt and operated by the Chilbolton Facility for Atmospheric and Radio Research (CFARR). Recently, an optical disdrometer, (Lempio G. E. et al., 2007) was presented where the main working principles for such equipment is the light extinction of precipitation particles passing through a cylindrical sensitive volume of 120 mm length and 22 mm diameter. The electronic signal caused by a precipitation particle is proportional to its cross-sectional area.

The DSD, $N(D)dD$ is the number of raindrops per unit volume where the diameter of the equivalent volume spherical drop is between D and $D+dD$. The DSD is related to rain rate by the fall-speed as a function of D. The shape of the DSD is often assumed to be exponential (Marshall and Palmer, 1948, Waldvogel, 1974) or a Gamma function (Ulbrich, 1983). Both distributions have exponential large drop tails but differ in the proportion of small drops. Some of the variation in the size of the small drop distribution is due to systematic measurement errors associated with the instruments used to measure the distribution. The uncertainty in the number of large drops is always large due to the low numbers measured leading to large sampling uncertainty.

The exponential distribution DSD from Marshall and Palmer is given by:

$$N(D) = N_0 \exp(-\Lambda D) \tag{2.2}$$

where N_0 is a Marshall-Palmer scale parameter and found to be approximately 8000 $mm^{-1}m^{-3}$. The value of Λ is given by:

$$\Lambda = 4.1R^{-0.21} \tag{2.3}$$

where R is rainfall rate in mm/hr.

It is usually assumed that for sufficiently large sample volumes, exponential DSD models are adequate. As the sample volume becomes small, usually for ground based instruments and short integration times, then the Gamma distribution often provides a better fit. The Gamma-type distribution is known to adequately model the DSD variation and is given by:

$$N(D) = N_0 D^m \exp(-\Lambda D) \tag{2.4}$$

Λ is given by:

$$\Lambda = \frac{3.67 + m}{D_0} \tag{2.5}$$

where D_0 is the mean diameter.

The value of m, the order of the Gamma distribution varies within a range of -1 to 10. From the equation above, when m is 0, the distribution is a Marshall-Palmer type exponential distribution. When m is increases, the number of drop concentration decreases and when m is decreases, the number of drop concentration increases as shown in Figure 2.6. Note that for positive m the concentration of small drops goes to

zero as drop diameter goes to zero. The values of *m* can be related to a particular rain event type. Values of *m* correspond to convective ($0 \leq m \leq 1$), stratiform ($m > 2$) and orographic ($m < 0$) (Usman, 2005).

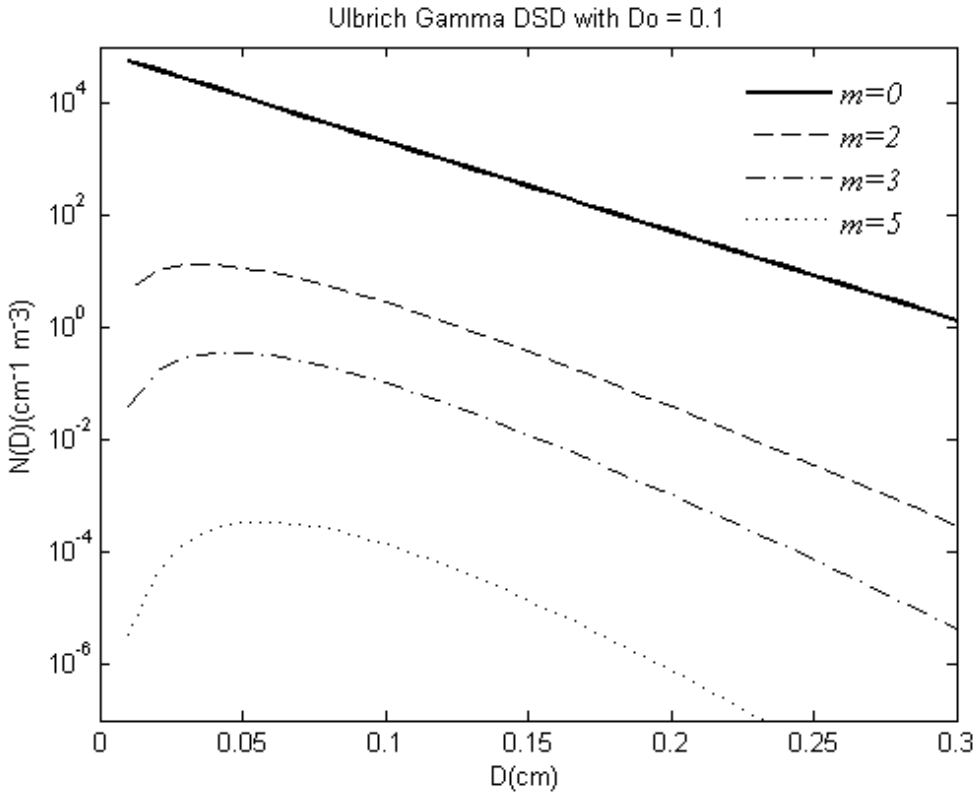

Figure 2.6: Ulbrich Gamma DSD model with *m* variation. D_0 is assumed to be 0.1 cm and N_0 is 80000 $cm^{-1}m^{-3}$.

For the same rain rate, variation in the DSD can lead to variation in the predicted microwave specific attenuation by a factor of two, more or less than the average value. At higher EHF frequencies, this uncertainty grows due to the increasing importance of smaller drops. At millimetric frequencies, the uncertainty is large due to variation in the number of large drops. Rayleigh scattering predicts a scattering cross-section proportional to the diameter raised to the sixth power. At frequencies for which Rayleigh scattering is appropriate, a single 10 mm drop scatters as much as a million 1 mm drops while having only a thousandth of the water volume. As the first Fresnel zone for many links is of the order of a metre across, specific attenuation is expected to vary along the link around the ITU-R value associated with the rain

rate. However, the uncertainty in link fade due to this variation is expected to be reduced by integration of specific attenuation along the link path. Because of this, using the specific attenuation predicted by Rec. ITU-R P.838-3 (2005) is expected to be adequate in most cases.

2.4.3 Rain Drop Shape and Canting Angle

Small rain drops around 1 mm in diameter are spherical due to surface tension. However, shapes and sizes of larger raindrops gradually change due to hydrodynamic forces experienced when they are descending in free fall, as illustrated in Figure 2.7. The diagram was based on Usman (2005) evolution of rain drops and sizes.

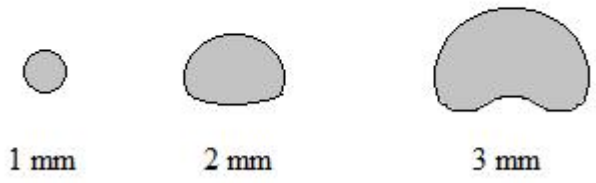

Figure 2.7: Evolution of rain drops with radius lengths in mm.

The distribution of raindrop sizes reflects the very complicated collision, break-up and evaporation processes occurring in the air column. The combination of water circulation within the drop, and drag due to air flowing around the drop as it falls, tends to flatten the base of larger raindrops turning them into oblate spheroids. As the raindrop diameter further increases, the base becomes concave (Zhang, 2008). When the radius increases to 5 mm or more, the drop balloons and breaks-up into a random number of smaller drops. The entire evolution process will start again for new small raindrops. Convective rain event such as thunderstorms generally have a wider range of raindrop sizes compared to the stratiform type of rain event.

For scattering calculations, it is common to view the shape of rain drop as oblate

spheroids. One of the earliest studies of the shapes of raindrops was performed by Pruppacher and Beard (1970). The experiment was performed by observing water drops suspended in a vertical wind tunnel. They have shown that water drops falling at terminal velocity were deformed into approximate oblate spheroids. They have discovered that water drops with diameters in the range 1 to 4 mm have a linear correlation between the axial ratios and drop size leading to the following equation:

$$\frac{b}{a} = 1.03 - 0.62D \tag{2.6}$$

where b and a are major and minor axis length of the water drop respectively and D is the diameter of the volume equivalent spherical drop. This expression is only known to work for diameters larger than 1 mm, (Usman, 2005). Equation (2.6) was later theoretically verified by the numerical evaluation of the balance of forces acting on a drop falling under gravity, (Pruppacher and Pitter, 1971). The rain drop shape model of Pruppacher-Pitter is a well known and accepted model by scientific communities for the calculation of microwave attenuation by rain. Several other models were suggested later to refine the linear expression of Pruppacher-Pitter including Morrison and Cross (1971), Beard and Chuang (1987) and Goddard and Cherry (1984).

Linearly polarized radio waves propagating through a rain event suffer phase shift and differential attenuation due to the vertical-horizontal asymmetry of the non-spherical large raindrops. However, for a given fade depth, differential attenuation and phase shift decrease as frequency is increased because the more spherical smaller rain drops make a larger contribution to the total attenuation (Barclay, 2003).

Rain drops are known to be canting if the rain drop axis symmetry is not vertical. This is commonly caused by vertical wind shear near the ground. Canting angles affect radio links by transferring some energy between horizontally and vertically polarized waves. The fading effect due to canting angle is considered insignificant in

contrast to variation in drop size (Usman, 2005).

2.4.4 Rain rate

Specific attenuation can be calculated from the DSD and a drop shape model. However, the disdrometers required to measure DSD are still relatively rare and instruments to measure drop shape are even less common. Specific attenuation is more commonly associated with rain rate as this is a parameter that is widely measured and much is known of its statistics. Rain rate, or rain intensity, is measured in units of millimetres per hour (mm/hr) and vast databases of rain rate measurements exists spanning hundreds of years and many thousands of locations. Specific attenuation is usually modeled as a power-law function of rain rate. This simple power-law combines all the complications of the scattering fields produced by all the drops of different shapes and their arrangement in space. Although rain rate is the most common parameter used for estimating specific attenuation, it is far from the best. Rain kinetic energy is much closer to specific attenuation, in terms of DSD moments, and can be measured by many instruments. Similarly, the transformation of radar reflectivity into a rain rate and then into a specific attenuation is effectively a frequency scaling and the derived specific attenuation may be more accurate than the intermediate rain rate.

The most important meteorological statistic when planning a radio system is the rainfall rate exceeded for 0.01% or 0.001% of the time, $R_{0.01\%}$ and $R_{0.001\%}$. These rain rates are highly geographical dependent. For temperate regions, $R_{0.01\%}$ can be around 30 mm/hr while for arid regions it is only few mm/hr. For tropical regions that experience monsoon seasons, the $R_{0.01\%}$ can be as large as 150 mm/hr. Normally, radio engineers will design a terrestrial fixed link to have 99.99% availability in an average year, and to fail when it experiences rain rates higher than $R_{0.01\%}$.

Several procedures exist to estimate the statistics of rain rate in a particular region. Empirically, rain rate statistics can be directly measured using a rain gauge and/or

rain radar. A rain gauge is a device utilised by hydrologists and meteorologists to quantify the amount of liquid precipitation over a set period of time. Rain radar is a type of weather radar that can be used to locate and estimate precipitation or rain. Statistics of rain rate can also be found in Rec. ITU-R P.837-5 (2007), or in the Global Crane model (Crane, 1996). Rain parameters are known to exhibit long term correlations and large year-to-year variability. Anecdotally, ten years of rain data is required to estimate the average annual rain rate exceeded 0.01% of the time to the precision needed for radio planning. The Rec. ITU-R P.837-5 (2007) model provides the annual distribution of rainfall rate with an integration time of 1 minute for the entire globe, derived from numerical weather prediction, but recommends the use of locally measured rain rates if available. Figure 2.8 illustrates an example of a rain rate distribution from Rec. ITU-R P.837-5 (2007), which shows the 0.01% of the exceeded level is around 25 mm/hr at Chilbolton, UK, at approximately 53 degrees north in latitude.

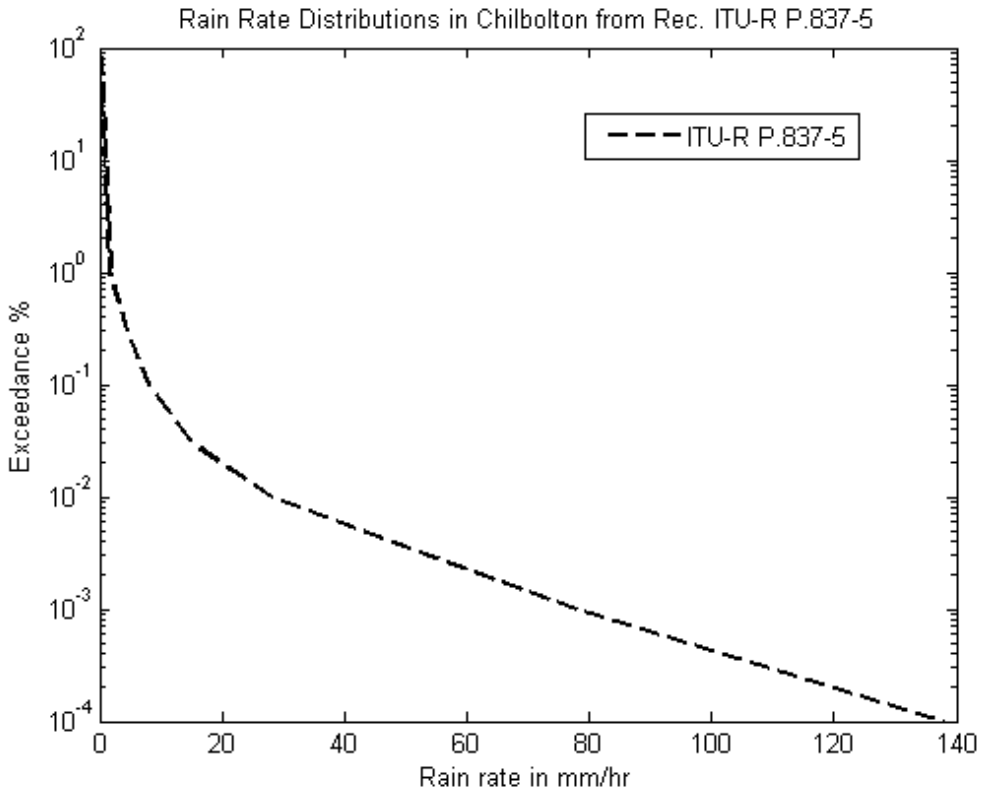

Figure 2.8 Rain rate annual distribution for Chilbolton from Rec. ITU-R P.837-5 (2007)

2.4.5 Specific Attenuation of rain

Rec. ITU-R P.838-3 (2005) provides the international recognized model to calculate specific attenuation of rain from the rain rate. The specific attenuation, γ_R (dB/km) is obtained from the rain rate R (mm/hr) using the power law relationship:

$$\gamma_R = kR^{\alpha} \tag{2.7}$$

where k and α are frequency and polarization dependent coefficients. The coefficients can be determined using the following equations:

$$\log_{10} k = \sum_{j=1}^{4} a_j \exp\left[-\left(\frac{\log_{10} f - b_j}{c_j}\right)^2\right] + m_k \log_{10} f + c_k \tag{2.8}$$

$$\alpha = \sum_{j=1}^{5} a_j \exp\left[-\left(\frac{\log_{10} f - b_j}{c_j}\right)^2\right] + m_\alpha \log_{10} f + c_\alpha \tag{2.9}$$

where f is the frequency in the range 1 to 1000 GHz. Values for the constants required to calculate k and α are provided by Rec. ITU-R P.838-3 (2005). Specific attenuation increases with frequency and rain rate as illustrated in Figure 2.9.

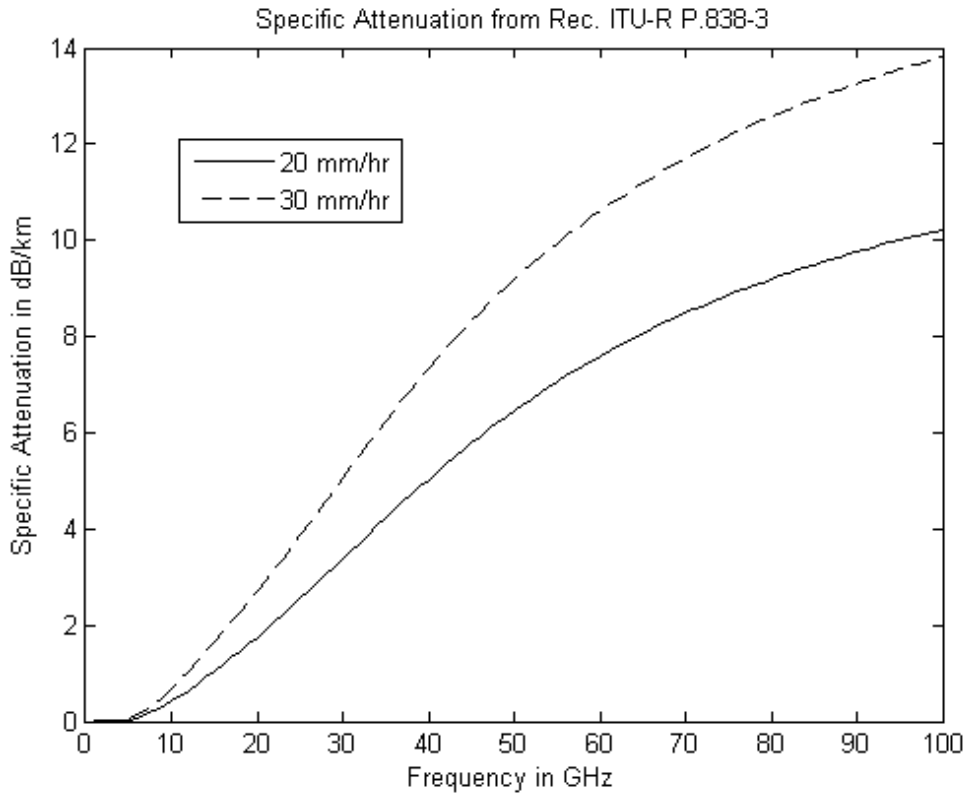

Figure 2.9: Specific Attenuation of 20 and 30 mm/hr for different frequencies from Rec. ITU-R P.838-3 (2005)

2.4.6 Rain Attenuation

Rain attenuation is defined as signal loss in dB at the receiver due to rain events. Calculation of rain attenuation for a microwave link requires integration of the specific attenuation along the link's path. Annual statistics of rain attenuation can be determined empirically by monitoring links. However, along with equipment effects, fading mechanisms other than rain scatter such as absorption by atmospheric gasses, scintillation, multipath, scattering by water drops on the antenna and interference/noise, will be present in the measurement and therefore it may not be impossible to identify just the fading due to rain. When planning a link, well established models, such as the Rec. ITU-R P.530-13 (2009) for terrestrial links and Rec. ITU-R P.618-10 (2009) for Earth-Space links, can be used to predict the average annual distribution of one-minute fading due to rain and other processes.

Rec. ITU-R P.530-13 (2009) predicts the rain attenuation that will be exceeded for 0.01% of an average year from $R_{0.01\%}$ and link parameters using the following steps:

1. Estimate $R_{0.01\%}$ using Rec. ITU-R P.837-5 (2007) or from locally measured data.
2. Determine the associated specific attenuation γ_R exceeded for 0.01% of the time using Rec. ITU-R P.838-3 (2005).
3. Determine the effective path length, $d_{eff} = r \times d$ using the following equations from Rec. ITU-R P.530-13 (2009):

   $$r = \frac{1}{1 + d / d_0} \tag{2.10}$$

   Where d is the actual length of a radio link in kilometres and r is the path reduction factor. This term is necessary to translate the point specific attenuation into a path averaged value.

   For rain rate ≤ 100 mm/h:

   $$d_0 = 35\ e^{-0.015\ R_{0.01}} \tag{2.11}$$

   For rain rate > 100 mm/hr, the $R_{0.01}$ value will be 100 mm/hr.
4. Finally, multiply the effective path length with the specific attenuation to estimate the rain attenuation at 0.01% exceeded level, $A_{0.01}$

   $$A_{0.01} = \gamma_R\ d_{eff} = \gamma_R\ dr \qquad \text{dB} \tag{2.12}$$

Figure 2.10 demonstrates the annual rain fade statistics calculated using Rec. ITU-R P.530-13 (2009) for a $R_{0.01\%}$ rain rate of 30 mm/hr and for terrestrial 38 GHz links of various lengths. Longer paths experience more rain attenuation as more of the link experiences fading.

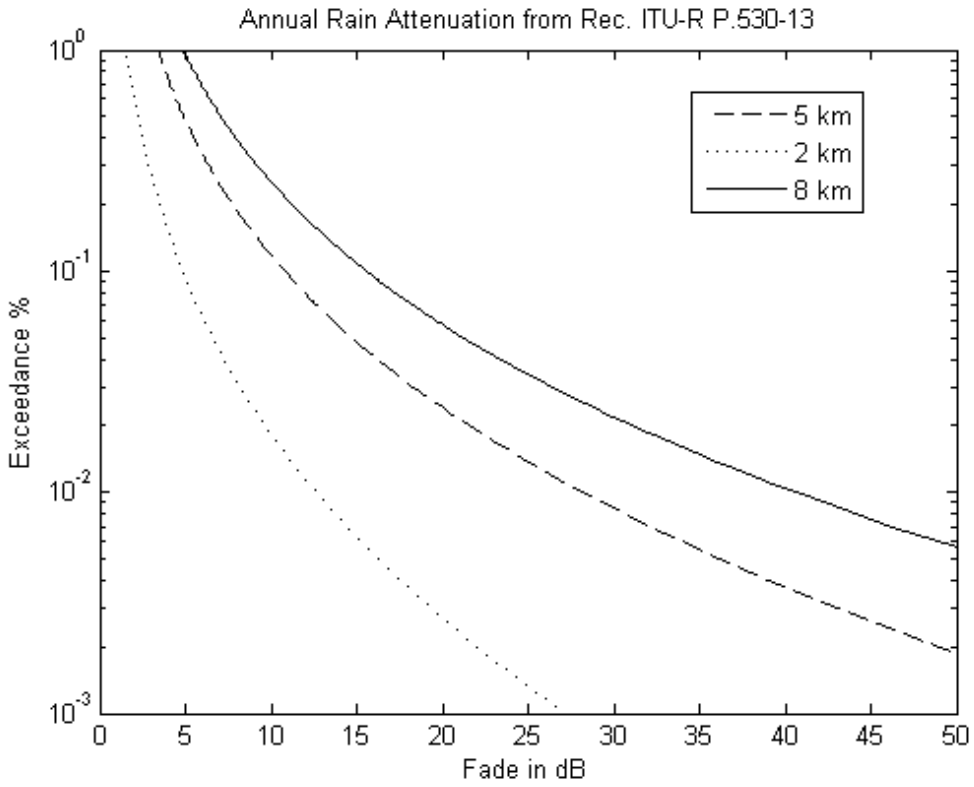

Figure 2.10: Annual Rain Attenuation distribution from Rec. ITU-R P.530-13 (2009)

Similarly, rain attenuation distributions can be derived from Crane's model. Unlike the ITU-R models which utilises the path reduction factor, Crane takes into account the variation of rain rates along a horizontal path. There are three versions of Crane's model. The first version was the Global Crane model developed in 1980. In 1982, Crane developed a 2-component Crane model that used a path integrated technique. Crane further refined his model in 1989 to include spatial correlation and statistical variations of rain within a cell. All of these models are included in his book, (Crane, 1996). However, there are some disputes in terms of reliability and performance between ITU-R and Crane's models. William Myer (1999) concluded that it is not clear which model is better than the other especially at higher rain rates. Both the ITU-R and Crane's models use differently globally defined rainfall zones or rain rate maps.

The calculation of rain attenuation for Earth-Space link using Rec. ITU-R P.618-10 (2009) is similar. Earth-Space links experience rain fading from the ground station up

to an altitude known as the rain height. Rec. ITU-R P.839-3 (2001) assumes that the average annual rain height is 360 m above the average annual zero-degree isotherm (ZDI) height. Both horizontal and vertical path reduction factors are introduced to account for the spatial variability of specific attenuation.

When a melting layer exists, an Earth-Space link will pass through it, albeit for a relative short distance. This is in contrast to terrestrial links, which only pass through the melting layer when the ZDI is near the ground, but then often the whole link is in the melting layer. The effects of the melting layer on Earth-Space links is introduced by the 360 m offset between the ZDI and the rain height. Currently there are no models for shorter slant paths that may terminate within the melting layer, such as links between ground and Unmanned Aerial Vehicles (UAVs).

.

2.5 Sleet Attenuation

Sleet particles are a mixture of ice, liquid water and air. In a stratified atmosphere, they can exist from about 500 m above the ZDI to approximately 1000 m below. In convective events they can exists throughout the rain column. It has been established that sleet or wet snow attenuates radio waves many times more than rain of the equivalent intensity, see (Tjelta et al, 2005).

There are many reports of outages on terrestrial links due to sleet or wet snow in the past 50 years. Takada and Nakamura published a report in 1966 where an experimental, 14.6 km radio link operating at 11 GHz experienced six times higher attenuation due to sleet than would be expected for the same precipitation rate of liquid water, (Takada and Nakamura, 1966). Link monitoring experiments carried out by Rutherford Appleton Laboratory identified sleet as the major cause of unexpected outages on links in both the southern UK, (Thurai and Woodroffe, 1997), and in Scotland, (Walden et al, 2003).

Currently, the most reliable model to predict average annual excess attenuation due to

sleet on terrestrial links is the Bacon-Tjelta sleet model (Tjelta et al, 2005) which utilizes global maps and a-priori information to calculate the quantity of sleet and establish a mean specific attenuation profile to acquire excess fade in the melting layer region. The model assumes a Gaussian distribution of rain heights and a fixed formula for the melting layer excess specific attenuation as a function of the position in the melting layer.

Excess attenuation due to sleet will vary with altitude relative to the rain height as illustrated in Figure 2.11. The sleet multiplication factor is the specific attenuation due to sleet divided by the specific attenuation due to the equivalent rain rate. On average, sleet will cause a maximum attenuation about 3.6 times higher than the specific attenuation due to the equivalent rain rate, approximately 300 m below the rain height. At altitudes more than a kilometre below the rain height, the multiplication factor approaches 1 as most particles have then melted into water. For heights that are closer to the rain height, the multiplication factor approaches zero as most particles are ice which has a very low specific attenuation.

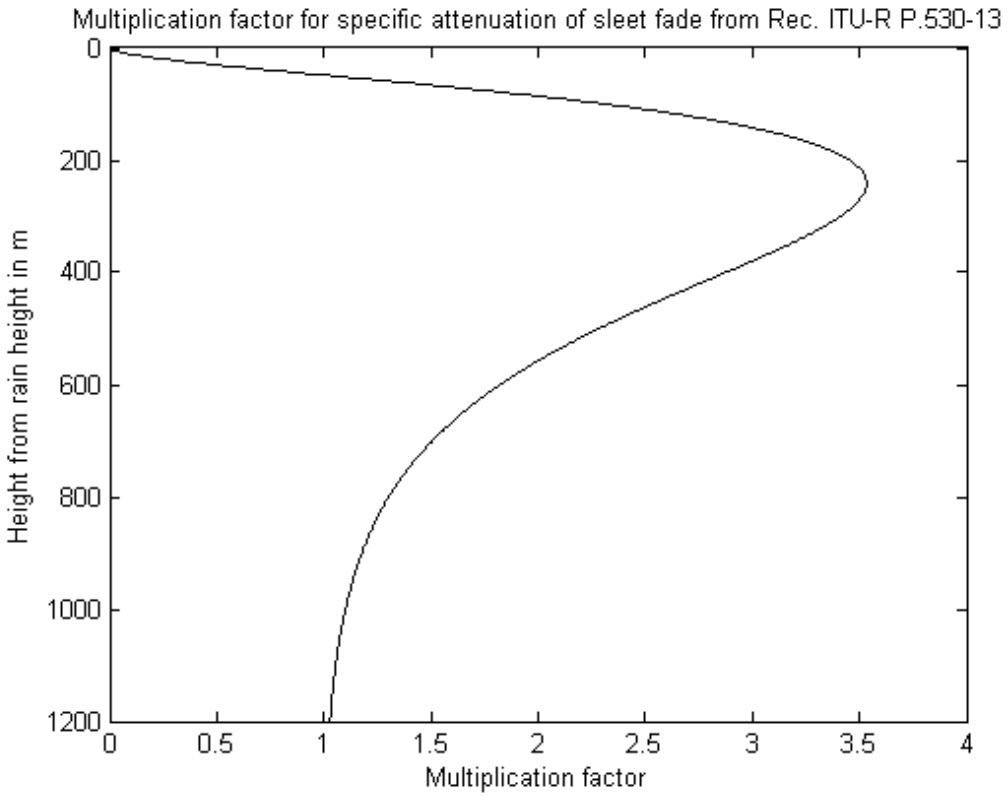

Figure 2.11: Sleet fade multiplication factor for specific attenuation of rain from Rec. ITU-R P.530-13 (2009)

Equation 2.13 is the model of the sleet multiplication factor provided by Rec. ITU-R P.530-13 (2009):

$$\Gamma(\Delta h) = \begin{cases} 0 & 0 < \Delta h \\ \dfrac{4\left(1 - e^{\Delta h / 70}\right)^2}{\left(1 + \left(1 - e^{-(\Delta h / 600)^2}\right)^2 \left(4\left(1 - e^{\Delta h / 70}\right)^2 - 1\right)\right)} & -1200 \leq \Delta h \leq 0 \\ 1 & \Delta h < -1200 \end{cases} \qquad (2.13)$$

where $\Gamma(\Delta h)$ is the multiplication factor and Δh is the altitude relative to the rain height in metres.

2.6 Cloud Attenuation

Rain events are usually associated with cloud although cloud has a larger spatial coverage. Cloud consists of water or ice particles with a diameter generally less than 0.01 cm and can occur across a wide range of altitudes and in a wide variety of shapes. Cloud attenuations are usually small, typically a few dB for Earth-space links operating below 100 GHz. However, cloud attenuation can be crucial at higher EHF frequencies since cloud particles are an order of magnitude smaller than rain drops. Cloud is not as dynamic as rain in space and time and often they are present when it is not raining. However, this will still be detrimental for satellite links since the duration of the cloud in an area will be longer than rain events, hence the period of cloud attenuation will be longer than rain fade. The different types of clouds including cumulus, cumunolimbus, stratus and nimbostratus have variable cloud liquid water content and fade which further complicates the problem of predicting cloud fade (Dissanayake et al, 2001). Rec. ITU-R P.840-4 (2009) provides guidelines to model and calculate cloud attenuation. According to the ITU recommendations, the Rayleigh approximation is applicable for frequencies below 200 GHz. Like fog, it is usual to link cloud specific attenuation to the volumetric liquid water content. The specific attenuation within a cloud can be written as:

$$\gamma_C = K_l M \quad \text{dB/km} \tag{2.14}$$

where:

γ_C : specific attenuation (dB/km) within the cloud,

K_l : specific attenuation coefficient ((dB/km)/(g/m^3)) and

M : liquid water density in the cloud or fog (g/m^3).

The coefficient K_l may be derived from a mathematical model based on Rayleigh scattering, which uses a double-Debye model for the dielectric permittivity $\varepsilon(f)$ of water and it is valid for frequencies up to 1 THz.

Chapter 2 summary

Microwave links suffer fading due to a range of mechanisms including absorption by atmospheric gasses and scattering by hydrometeors such as cloud drops, sleet and rain. Scattering by sleet and rain generally cause the largest protracted fades for radio links operating above 10 GHz, and limit the availability of these links. The specific attenuation of a hydrometeor-filled atmosphere may be related to the equivalent rain rate. The internationally recognised model Rec. ITU-R P.838-3 (2005) links rain rate to an average specific attenuation. In practice, specific attenuations vary considerably around the Rec. ITU-R P.838-3 (2005) value to variation in particle phase, drop size distributions, drop shapes and canting angles. In later chapters I introduce a rain fade simulation method for heterogeneous networks where the hydrometeor fade experienced by a link is estimated by pseudo-integration of the specific attenuation along the link path. The Rec. ITU-R P.838-3 (2005) value is used, multiplied by the Rec. ITU-R P.530-13 (2009) sleet multiplication factor. It is expected that averaging of specific attenuation along the link, and over many events, will yield the correct long-term statistics of hydrometeor fading.

CHAPTER 3 METEOROLOGICAL MEASUREMENTS

A range of meteorological input data is necessary for the simulator. At millimetre wave frequencies, terrestrial links are short, from 10 km down to a few hundred metres, but rain specific attenuation is high and so fine-scale spatial-temporal rain fields are vital. For the simulation of slant paths it is necessary to produce fields of rain and possibly cloud density, at a range of altitudes. The previous HRFNS system used Chilbolton Radar Interference Experiment (CRIE) rain maps as coarse-scale input data, but these data is only cover a 52^{o} arc with a range of 60 km, centered on Chilbolton in the southern UK. The proposed simulator requires measurement datasets that can cover a large part of Europe or are global as part of the development for network simulator applicable at global scale, and so a new source of input data is needed. This chapter catalogues the datasets relevant for GINSIM and discusses the techniques used for parameter estimation. Meteorological datasets other than rainfall that can be useful for GINSIM and these will also be discussed.

At a minimum, three parameter datasets are required for the GINSIM development: topography, rain height and rain field. This will be described on section 4.3 in Chapter 4. These parameters should be provided on a sufficiently fine sampling interval to allow for numerical downscaling to the scales required for channel simulation. Topography is time-invariant and available from several sources. Rain height needs to be deduced from zero degree isotherm height. This varies slowly in space and can be provided by several NWP model databases. Rain fields are the most difficult parameter due to their spatial and temporal variability. Additionally, rain parameters are notoriously difficult to estimate remotely.

3.1 Rainfall Measurements

Forecasting or estimating spatial and temporal distributions of rain events remains one of the most challenges issue for meteorological services. A range of instruments

exist to measure rainfall including rain gauges, weather radars, aircraft and satellites. Rain gauges provide direct measurement of rainfall rates but lack spatial coverage due to the small collection area for each rain gauge and low gauge densities. Rain gauges are completely absent in some areas such as over the sea where analysts have to use weather radars or measurements from satellites to estimate rainfall rates. Rain gauges are usually used as “ground truth” in order to compare, calibrate and verify other remote measurement techniques such as from radars and satellites. Meteorological radars utilise an echo-sounding system to estimate hydrometeor parameters. Polar or cross-polar radar reflectivity can be related to parameters of the drop-size-distribution and derived parameters such as rain rate. Rain radars can provide wide spatial coverage and high spatial and temporal resolution. However, the surface-based weather radars only cover some parts of the world (Western Europe, Japan and North America). In addition, many effects such as ground clutter, variation of raindrop size distribution and bright band reflections may lead to inaccurate rain parameter estimation.

Measuring weather parameters, including rainfall rate, from sensors on board satellites is becoming increasingly important as this method can yield global coverage relatively economically. Satellite observations suffer a fundamental limitation as they observe weather from above. Often parameters near the ground, such as rain rate, need to be estimated from measurements of cloud top parameters. These estimates may suffer very large prediction uncertainties and some have low temporal and spatial resolutions. Weather satellites are usually fitted with radiometers that can measure emissions from the Earth’s surfaces and cloud tops. Increasingly weather satellites have been equipped with rainfall radars, i.e. the Tropical Rainfall Measuring Mission (TRMM). Other satellites such as the National Oceanic and Atmospheric Administration (NOAA)’s Geostationary Operational Environmental Satellite (GOES) rely on measuring the infrared (IR) visible radiation emission from Earth to estimate rainfall rate, (Scofield and Kuligowski, 2003).

3.1.1 Rain Gauges

A rain gauge is a device mainly used by hydrologists or meteorologists to estimate the amount of precipitation over a set period of time. The use of rain gauges can be dated back to ancient Greece. The Egyptian nilometer provided a time-series of the size of Nile inundations spanning 5000 years (www.waterhistory.org/histories/cairo/). The world's first standardize rain gauge was invented in 1890 by George James Symons, one of the members of British meteorological society.

Rain gauges are still considered to be the most dependable tool to accurately estimate rainfall intensity in a particular location and are often used as point measurements. The calculation of rainfall rate using standard rain gauges is performed by dividing the volume of water collected by the area of catchment area (commonly a funnel) and the collection period. Gauges may be heated to melt snow collected in the funnel. A range of methods exists to automatically measure the volume of collected water including weighing, drop counting or tipping bucket mechanisms. Over the last decade, wide ranges of optical devices have come to dominate the market.

Tipping bucket rain gauges operate by using a funnel to collect and direct the collected rainfall to a seesaw like container. The lever tips when the amount of water collected reaches the pre-set volume, sending an electrical signal for recording, and dumps all the collected water. Drop counting gauges perform in a similar fashion. Precipitation is collected in a sump that over flows producing equil-sized drops. These drops are detected optically. Since tipping bucket and drop counting rain gauge physically measure the collected precipitation in small quanta, they may produce errors in extremes of rain rate. They suffer the same problems of funnel collection efficiency as manual gauges.

Weighing rain gauges operate by measuring the changes of the collected water's mass. A major advantage is the ability to measure the accumulation of non-liquid

hydrometeors e.g. hail and snow. They may also provide a more accurate reading of intense rain events compared to tipping bucket or drop counting rain gauges.

Rain gauges have many limitations and require constant maintenance. Rain gauge funnels distort the wind field in their vicinity and this can change the amount of precipitation at the point of measurement. This is a particular problem when measuring light rain in high winds. Ice that collects in the funnel, either ice that falls as hydrometeors or due to freezing of the funnel, can block the funnel and cause no rain to be detected for long periods. When this ice melts, all the collected water can suddenly flow into the measurement container or system. Heating the funnel reduces this problem but also causes evaporation in the funnel and reduces the accuracy of light rain measurements. Obtaining rain data, especially during intense storms can be difficult due to wind extremes. Birds often sit on the funnel edge and defecate into the funnel causing blockages. Spiders and insects may build nests in the funnel or measurement system, also causing blockages. Dust, pollen and soil can also block systems. Additionally, it is difficult to find suitable sites for rain gauges, particularly in urban areas. These sites need to be secure from interference by people and other animals. They also need to be in open areas where the microclimate is not effected by nearby buildings or trees.

Even though rain gauge provides direct rainfall rate measurement, compared to radar which estimate rainfall rate by relating precipitation to some remotely sensed quantity, a single rain gauge has poor spatial coverage and only indicates rainfall intensity at a small local area. Smith et al. (1994, 1996) have shown that rain radar can performs better than a network of rain gauges in terms of depicting the intensity and spatial extent of heavy precipitation. Rain radars avoid some of the problems associated with wind extremes and the mechanical limitation of automatic rain gauges during heavy precipitation events, (Groisman and Legates, 1994) and (Peck, 1997).

3.1.2 Weather Radar

Radar (Radio Detection and Ranging) was first developed in United Kingdom in 1935 by a meteorologist named Robert Watson-Watt. At first, radar was not intended to observe precipitation echoes but to detect aircraft. At that time, weather echoes detected by radars were treated as unwanted signals or noise. Shortly after the world war two, scientists become more interested in studying weather phenomenon.

Radar operates as an echo-sounding system where it transmits and receives the returned echo as illustrated in Figure 3.1.

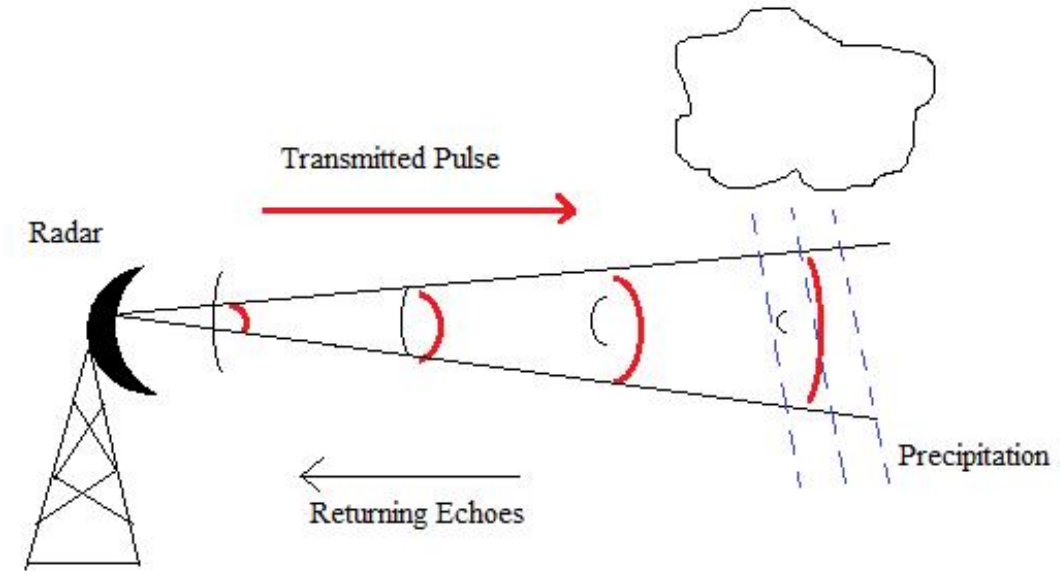

Figure 3.1: Basic diagram of an echo-sounding system for radar.

The radar transmits pulses of electromagnetic waves in a narrow beam for a very short period of time: Chilbolton's CAMRa radar has a pulse length of 0.5 microseconds. Some of the transmitted energy is reflected back to the radar when the transmitted beam collides with atmospheric precipitation. The radar collects the reflected energy until reflections are too small to measure before transmitting a new pulse. For radars operated by the UK Meteorological Office, the reading or listening time of the reflected energy is usually around 3300 microseconds. Figure 3.2 illustrates the internal working of Nimrod rain radar.

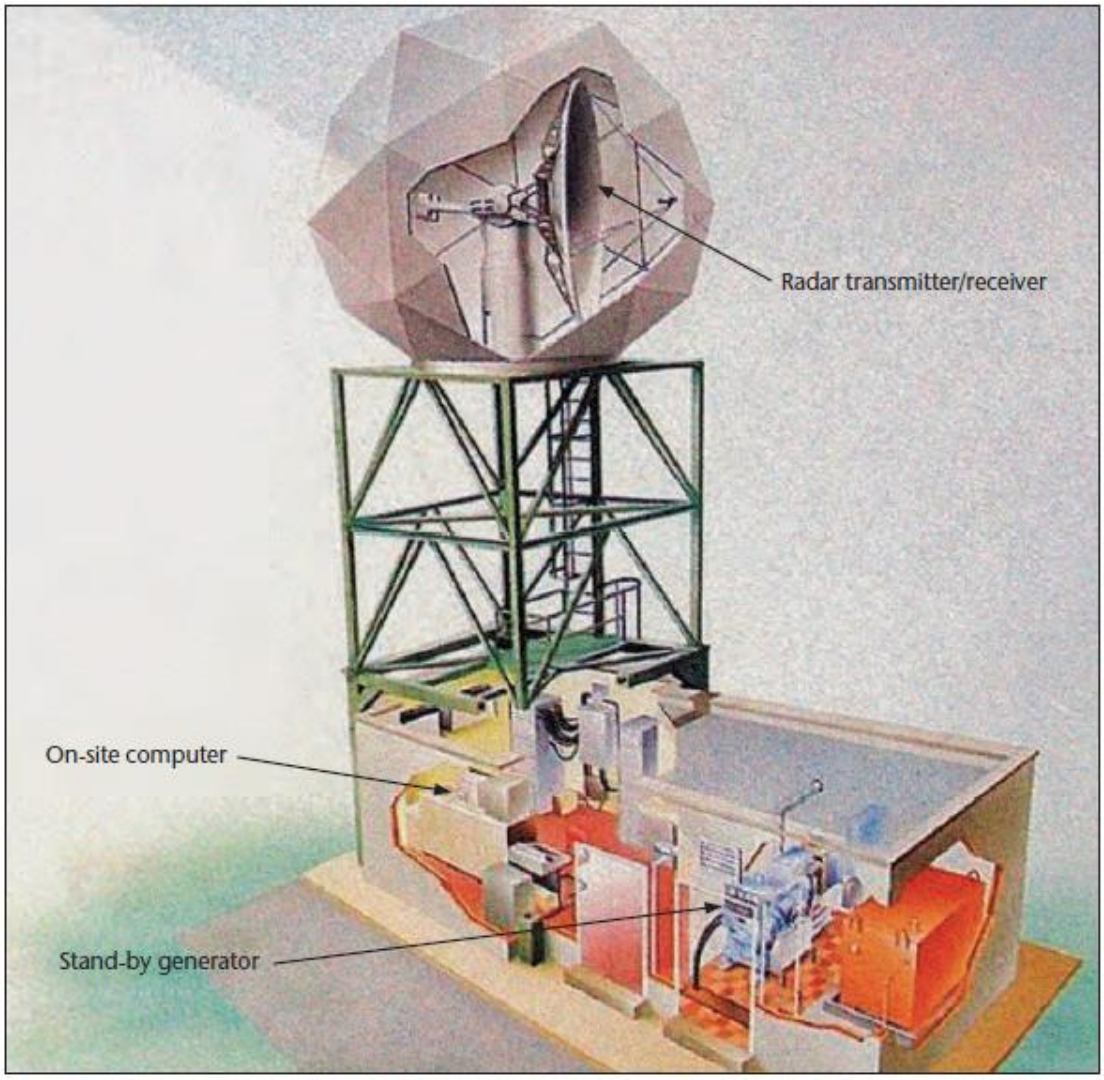

Figure 3.2: Internal working of a Nimrod rain radar. (Courtesy of UK Meteorological Office)

Typically, the beam width of modern radars is around 1^{o}. The distance from the radar to precipitation or other targets can be derived from the time taken for pulses to travel back and forth between radar and the targets. The reflected energy collected by the radar antenna is much weaker than the transmitted pulses mainly due to free-space loss, atmospheric scatterings and absorptions. The equation for reflected power collected by the radar, (Skolnik, 2002), is given by:

$$P_r = \frac{P_t G^2 \mathrm{a}^2 \pm}{(4®)^3 r^4} \tag{3.1}$$

P_r is the received power, P_t is the transmitted power, G represents antenna gain, a is the wavelength, $\pm$ is the backscattering cross section of the target and r is the distance between the radar and target. Based from the equation in (1), all the constant parameters of the radar equation can be merged into a coefficient C:

$$\overline{P_r} = \frac{CZ}{r^2} \tag{3.2}$$

where $\overline{P_r}$ is the averaged received power for precipitation illuminated by the radar and Z is the radar reflectivity usually expressed in dBZ: $\mathrm{dBZ} = 10\log(Z)$. Equation (3.2) shows that the received power $\overline{P_r}$ from a volume of precipitation is inversely proportional to r^2 (Patra, 2001) due to the increasing spread of the radar beam. The conversion of radar reflectivity Z to precipitation rate R in mm/hr can be made using a Z-R relationship, $Z = aR^b$, where a and b are parameters that can be obtained using regression analysis. Numerous Z-R relationships exist for different rain types, radars and climate regions. Battan (1973) has listed 69 different Z-R relationships derived from different climate regions by several researchers. Some of the variation in Z-R relationships is due to the mix of rain types and DSD in the region of the radar (Cluckie and Rico-Ramirez, 2004). A well known Z-R relationship equation is derived from the Marshall-Palmer DSD formula:

$$Z = 200\,R^{1.6} \tag{3.3}$$

The UK's Meteorological Office's Nimrod radars use this equation to estimate precipitation rate, (Harrison et al., 2000). A formula to relate $\sum D^6$ and rain rate R was given by Usman (2005) and Patra (2001):

$$Z = \frac{1}{\Delta V}\sum_{\Delta v} D^6 = aR^b = 200R^{1.6} \tag{3.4}$$

$$\Delta V = ® \frac{h}{2}(r\overline{}{2})(r\frac{¤}{2}) \tag{3.5}$$

where ΔV is the volume illuminated at any instant, D is the diameter of the water droplet, h is the pulse length, ¤ and ¯ represent vertical and horizontal beam widths of an antenna.

The most conventional form of radar is the single polarised radar which transmits and receives pulses using the same linearly polarised antenna, either horizontally or vertically polarisation. More advance radars such as dual polarised and Doppler radars can extract more or different measurement parameters.

Doppler radar is commonly used to obtain information on the direction and speed of falling hydrometeors. Doppler radar operates by measuring the Fourier power spectrum of the reflected energy. The Doppler effect increases the frequency of the reflected energy when the scatterer is moving towards the radar. Similarly, targets moving away from the radar reflect at a lower frequency. The power spectrum may be interpreted as the radial velocity mix within the sample volume.

Dual polarisation radars measure the horizontal and vertical polarised components of reflected radio waves. Typically, rain drops are either spherical for small drops or oblate spheroid for large drops (Pruppacher and Pitter, 1971). Large rain drops tend to have larger horizontal cross-section area than vertical and their radar reflectivity of horizontally polarised waves tends to be higher than for vertically polarised. The difference in polar reflectivity allows the radar to estimate the mixture or large and small drops. A ratio of reflected horizontal and vertical power in decibels, known as the differential reflectivity, may be written:

$$Z_{DR} = 10\log(\frac{Z_H}{Z_V}) \tag{3.6}$$

where Z_V and Z_H are the reflectivity of a vertically and horizontally polarised pulse. Larger positive values of Z_{DR} indicate the presence of large oblate raindrops and are associated with heavy rain.

Radars can operate in different frequency bands, depending on the application. Table 3.3 shows the different frequency bands with its wavelength and application based from Multi-community Environmental Storm Observatory (MESO)'s website (w8lrk.org/article/RadarTutorial.pdf) and from Usman (2005).

.

Frequency (GHz)	**Wavelength (cm)**	**Band**	**Application**
30	1	K	Cloud
10	3	X	Precipitation
6	5	C	Precipitation
3	10	S	Precipitation
1	30	L	Precipitation

Table 3.3: Operating Bands for Radar with its relevant frequency and wavelength.

Raindrops have typical diameters from 1 to 10 mm. The wavelengths used to measure rain are a trade-off between getting sufficient reflection from the raindrops and the loss of reflected power due to absorption and scattering by other particles. Most of the current weather radars utilise S-Band with a frequency of 3GHz to estimate precipitation. However, over the last decade, the use of C-Band and X-Band has become increasingly important for weather radars to estimate precipitation. Higher frequency bands for radar have more precise rainfall estimation but may suffer larger atmospheric attenuations (Usman, 2005). Radars operating at K-Band are highly sensitive to extremely small or light precipitation and thus can be used to estimate cloud density.

The deployment of weather radar to estimate precipitation addresses the lack of spatial coverage when using a rain gauge network. Furthermore, radar provides rainfall information in near-real time whereas it may take some time to collect data from a gauge network. However, the translation from radar-measured reflectivity into rainfall rate can be challenging and may produce estimation errors due to various reasons including reflection from non-liquid hydrometeors and non-meteorological factors such as beam block, ground clutter and spurious echoes. Differences in calibration between radars also lead to estimation error where a difference of 1 dBZ in calibration can lead to 17% difference in rain rate, (Hunter, 1996). Precipitation located at extreme long range from radar may not be fully representative of the actual rainfall near the surface due to Earth's curvature and the increasing elevation of beam with the distance from radar. At long ranges the radar beam may be above the precipitation or rainfall may evaporate at lower levels beneath the radar beam, and so precipitation is underestimated or often undetected, (Hunter, 1996; Kitchen and Jackson, 1993; Smith et al., 1996). In addition, bright band (melting layer) effects may lead to overestimation of rainfall rates when the radar beam reflects off the melting layer, (Kitchen and Jackson, 1993; Smith et al., 1996). Furthermore, the relationship between radar reflectivity and rain rate can vary widely and the use of simple *Z-R* relationships, $Z = aR^b$ may lead to estimation errors up to 100 %, (Usman, 2005).

Various methodologies have been suggested and employed to address these issues including vertical profile adjustment, comparing with the previous or adjacent radar scans to find radar faults and verification with other sources of measurements such as rain gauges or even communications links.

3.1.3 Meteorological Satellites

Meteorological or weather satellites are equipped with passive or active sensors to detect radiation emission from Earth's surface and atmosphere while orbiting at low

Earth orbit or polar orbit (Nimbus) and at geostationary orbit (GOES, METEOSAT). These satellites can be uses to measure or estimate various meteorological fields including cloud and precipitation. Generally, rainfall rate estimation from satellite can be divided into two categories, infrared (IR) and microwave-based precipitation estimates. Both of these measurements have a very in-direct relation between surface precipitation and the measured satellite signal.

The IR-based satellites, such as NOAA's GOES, estimate rainfall rate by measuring the radiance or brightness temperatures of the cloud-top in the infrared (IR) frequency spectrum from geostationary orbit in which the temperature of the cloud top is related to cloud-top height for optically thick clouds below the tropopause. This relationship assumes that the cloud height is related to cloud thickness and colder clouds are more likely to produce precipitation than warmer clouds. This method may only work for convective events where cloud top parameters are more closely related to surface rainfall, but will be problematic for warm top stratiform clouds (where surface rain rates are often underestimated because of the relatively warm cloud tops) and for non-precipitation cirrus clouds since they have low brightness temperature, (Scofield and Kuligowski, 2003). Even if this method could work with convective clouds, the amount of precipitation produced is strongly dependent on the stage in the life cycle of the convective event. Despite of this, IR-based satellites usually provide high spatial and temporal resolution data. For example, GOES and METEOSAT both yield 4 km spatial resolution rainfall rates, every 15 minutes for GOES and 30 minutes for METEOSAT.

The use of microwave-based satellite measurements is a more direct method to estimate rainfall rates than IR-based measurements. These instruments estimate rainfall rate by measuring the absorption of microwave radiation by liquid water or on the scattering by ice particles within the microwave spectrum, (Scofield and Kuligowski, 2003). However, it is usual for microwave instruments to have poorer spatial resolution than its IR-based counterpart. Resolution is typically insufficient to

determine small scale precipitation events. Furthermore, the long revisit times of the Low Earth Orbit (LEO) satellites that carry these instruments lead to significant sampling errors for accumulated rainfall estimation (Ebert et. al, 1998).

Estimation of rainfall rates from satellites offer considerable advantages over radar and rain gauge networks since it can provide crucial rainfall information in regions where data from radar and rain gauges are not available, such as over oceans. In addition, they do not have the spatial inconsistencies that radars have such as changes in radar beam height and the different calibrations between radars. However, the relationship between satellite-measured radiance and surface rainfall rates is less robust than the relationship between ground based radar reflectivity and rainfall rates. Therefore, rainfall estimation results from these satellites must not be considered as a replacement for radars and rain gauges but as a complement, (Scofield and Kuligowski, 2003). Both the IR and microwave-based satellite instruments can be combined (known as blending) to expand their applications and increase accuracy. One such example algorithm is the Multi-sensor Precipitation Estimate (MPE). The MPE regularly uses rain gauge or radars for validation purposes. Recent weather satellite systems, such as the Tropical Rainfall Measuring Mission or TRMM, have been equipped with precipitation radar (Scofield and Kuligowski, 2003; Usman, 2005). Systems such as the TRMM radar are a new alternative to IR and microwave-based satellite precipitation estimation.

TRMM is a joint venture between National Aeronautics and Space Administration (NASA) and Japan Aerospace Exploration Agency (JAXA) and it is the first weather satellite utilising precipitation radar to estimate rainfall in the tropical regions The TRMM satellite is equipped with multiple sensors and instruments including TRMM Microwave Imager (TMI), precipitation radar, visible and infra-red sensors, and a lightning detector. The TRMM satellite is able to provide vertical profiles of rain and snow from the surface up to 12 miles in height and offers average rainfall over 5^{o} x 5^{o} (for low resolution) and 0.5^{o} x 0.5^{o} (for high resolution) areas with a monthly rainfall

rate. The TRMM project is highly ambitious since it offers rainfall estimation over a large coverage area. However even the high resolution data are not adequate for radio propagation simulation (Usman, 2005) due to the low temporal resolution. With the improving sensor technology and algorithms, satellite borne rainfall radars, such as those used by TRMM, may soon be able to provide the finer resolutions necessary for radio network simulation. Figure 3.4 illustrates the wide variety of weather satellites operated by different agencies/countries and in different orbits including the geostationary and polar orbit.

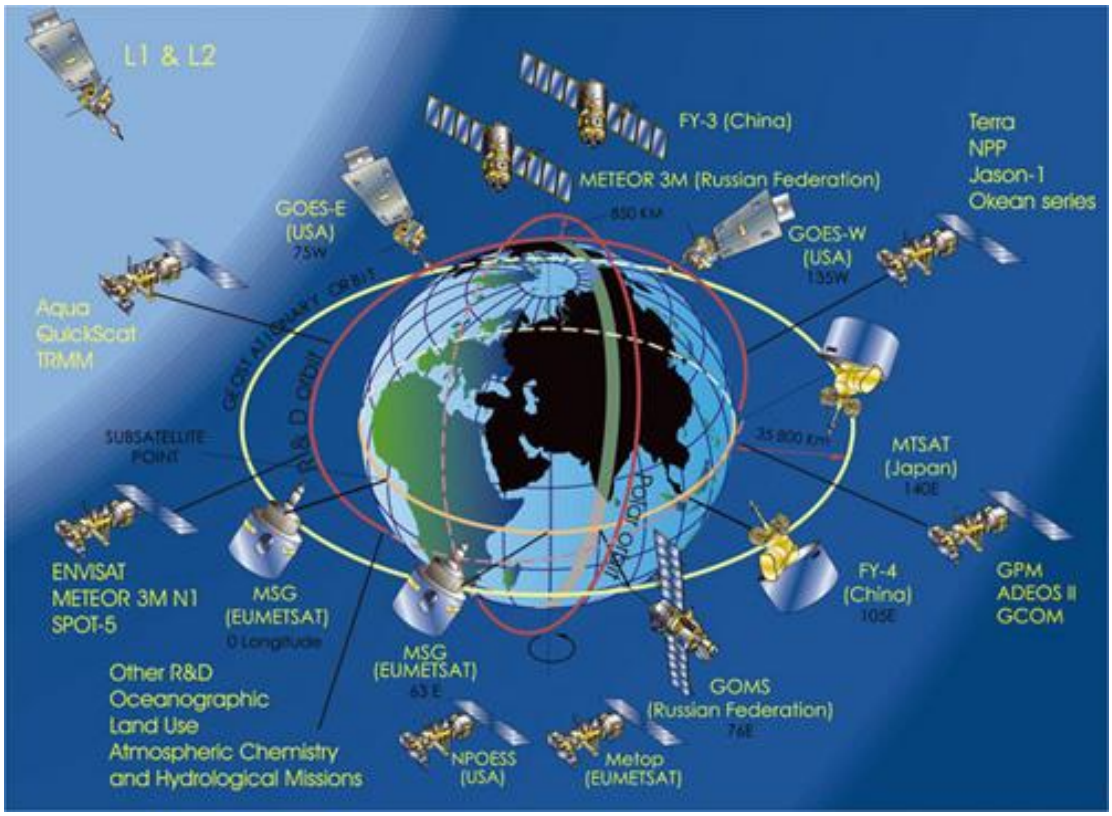

Figure 3.4: Weather satellites from various countries and agencies. (Taken from Earth Observation Handbook by Committee on Earth Observation Satellites (CEOS), www.eohandbook.com/eohb05/ceos/part2_6.html)

3.2 Meteorological Measurement Datasets

This section discusses the range of meteorological measurement datasets that are produced by different measurement sources including rain gauge, weather radar and

satellite. Some of these datasets can be applied to or assist GINSIM and this will be explained later in the following sections.

3.2.1 Chilbolton Drop-Counting and Tipping-Bucket Rain Gauge

British Atmospheric Data Centre (BADC) archives the Chilbolton drop-counting and tipping-bucket rain gauge data. The drop-counting gauges were developed by the staff at Chilbolton Observatory (www.stfc.ac.uk/chilbolton). Tipping-bucket gauges are common, the UK Environment Agency operates a network of 1300 such gauges, but they offer poor rain rate resolution compared to drop-counting gauges. The drop-counting rain gauge collects the rainwater in the 150 cm^2 funnel which channels water into a sump that produces equil-sized drops. These drops are counted as they pass through an optical sensor and the number observed in each 10 second period is recorded. Each drop corresponds to an accumulation of 0.004 mm, compared to 0.2 mm per tip for a standard Environment Agency tipping-bucket gauge. For this research, the rain gauge data was used not as a part of the GINSIM's main operations but for verification with the results. The rain gauges operate routinely at Chilbolton Observatory, UK (51.1445°N, 1.4370°W) and Sparsholt, UK (51.0879°N, 1.3914°W).

3.2.2 Chilbolton Advance Weather Radar (CAMRa)

The Chilbolton Advance Meteorological Radar (CAMRa) operated by Rutherford Appleton Laboratory and located at Chilbolton Observatory in Hampshire in the southern UK, is the largest fully steerable meteorological radar in the world. CAMRa operates at 3 GHz and its large antenna offers an extremely narrow beam resulting in increased resolution: at 100 km from the radar, the resolution of a 0.25 degree beam width is 400 metres. CAMRa has dual polarization capability which makes it possible to determine the shape and orientation of cloud and precipitation particles, (Chilbolton Radar Website, www.stfc.ac.uk/Chilbolton/24821.aspx).

The CAMRa weather radar was used in the Chilbolton Radar Interference Experiment (CRIE) which operated for two years 1987-1989 to measure rain over the Southern UK. The CRIE was designed mainly for examination and development of rain scatter interference models as part of the COST 210 project (COST 210, 1991). This dataset provides rain information with a very high spatial resolution, 300 m diameter voxels, and temporal sampling time, 10 minute return time. However, the experiment operated on a 9 day out of 27 duty cycle and only provides information for the area around Chilbolton. The previous HRFNS, (Zhang, 2008) is based on these data. The downscaling algorithms developed for this dataset are applicable over spatial and temporal scales up to tens of kilometres and minutes.

3.2.3 Nimrod and OPERA

The UK Meteorological Office operates the Nimrod network of 15 C-Band rain radars operating at 5.4 GHz. Composite measurements of instantaneous rain rate over 1, 2 and 5 km voxels, spanning UK and neighboring European countries including northern of France, are produced with a 5 or 15 minute sample period. These data span 1999 to the present, with the higher resolutions (1km spatial resolution) available since 2004. Currently, the British Atmospheric Data Centre (BADC) archives single-site and composite Nimrod rain maps. Figure 3.5 shows a typical composite Nimrod rain map.

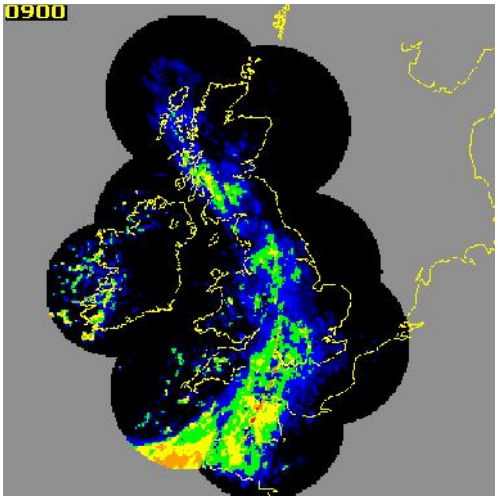

Figure 3.5: Nimrod rain map covering the whole UK and part of Europe. (Courtesy of BADC)

Each Nimrod site has a computer system that can perform aerial elevation control and digital signal processing. These raw data then sent to Radarnet IV Central Processing at Exeter for various corrections and calibrations, including correction for attenuation by intervening rain, correction to range attenuation, elimination of ground clutter, conversion of radar reflectivity to rainfall rates and conversion from raw polar cells to National Grid Cartesian Cell. Rain gauges are used as ground truth as part of the main quality checking method for Nimrod's rainfall rate scans.

Each rain radar vertically scans the area between four to eight low elevation angles (commonly between 0.5 and 4 degrees depending on the surrounding hills) every 5 minutes to ensure the best rainfall rates estimation on the surface. The radars provide scans with ranges up to approximately 75 km (for 1 and 2 km spatial resolution) and 255 km (for 5 km resolution).

The European Meteorological Network Services (EUMETNET) is currently managing OPERA, a project that aims to integrate Nimrod with a large number of continental European radars into a network that will provide these data spanning Europe. Limited OPERA composite data is now available for research purposes. OPERA data was to be generally available from 2011 but has suffered delays due to

difficulties maintaining consistency across national boundaries. Figure 3.6 shows a typical OPERA composite rain map over Europe.

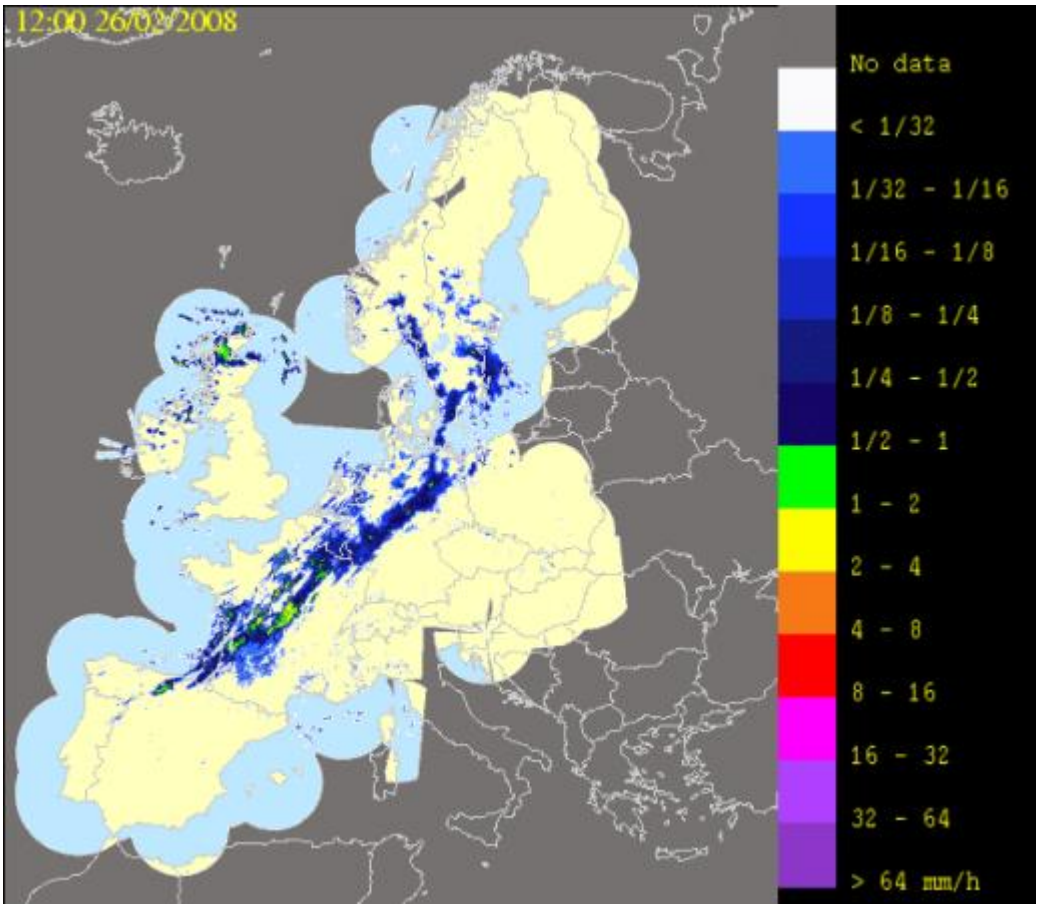

Figure 3.6: OPERA rain maps covering most of Europe. (Courtesy of EUMETNET)

3.2.4 Multi-Sensor Precipitation Estimate (MPE)

Although Nimrod and OPERA data will provide a basis for UK and European network simulation, the development of a global simulation tool requires consistent data with a global span. This is far more likely to be achieved by satellite Earth observation systems than by combining national radar networks. The European Organisation for the Exploitation of Meteorological Satellites (EUMETSAT) is an intergovernmental organisation that operates a constellation of METEOSAT Earth observation satellites and publishes a wide range of derived datasets. The MPE dataset yields global rain rates integrated across 3 km pixels with a 5 minute sample period. Cloud information is provided with 9 km pixels and hourly sampling. The

EUMETSAT's MPE integrates the IR channel data from METEOSAT satellites and Special Sensor Microwave/Imager (SSM/I) microwave data from US-DMP satellites in the re-processing branch of its Meteorological Product Extraction Facility (MPEF) to estimate precipitation rate.

3.2.5 NCEP/NCAR Reanalysis datasets

The NCEP/NCAR Reanalysis datasets provides various parameters (including geo-potential height, air temperature, vector wind) of the Earth's atmosphere over a global 2.5^{o} grid at 6 hour intervals from 1948 to the present, calculated at 17 pressure levels ranging from 1000 mBar to 10 mBar. The global grid has 73 latitudes and 144 longitudes. Reanalysis datasets are produced by assimilating climate observations taken from various sources including satellites, ships, weather radars and ground stations and using the same climate model throughout the entire reanalysis period. The product is a joint collaboration between National Centers for Environmental Prediction (NCEP) and the National Center for Atmospheric Research (NCAR). The data is available from NOAA's Earth System Research Laboratory and NCEP. Figure 3.7 demonstrates the global map of geo potential heights for 1000 mBar pressure level, extracted from NCEP/NCAR Reanalysis I data that are archived by NOAA's Physical Science Division (PSD) (www.esrl.noaa.gov/psd).

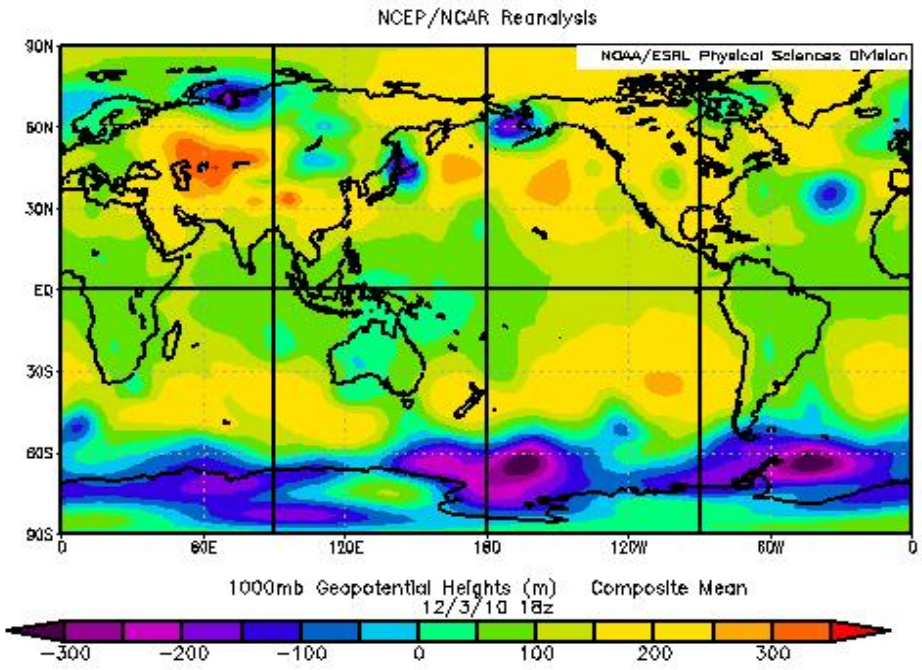

Figure 3.7: Geo potential Hei**g**hts of 1000 mBar pressure level. (Courtesy of NOAA)

The NCEP/NCAR Reanalysis I data provide information (specifically the geo-potential height and air temperature as a function of pressure levels) that allows the estimation of rain height. This is important when calculating the fade experienced by slant paths and for the implementation of the Bacon-Tjelta sleet model for terrestrial microwave links.

3.2.6 Shuttle Radar Topography Mission (SRTM)

The Shuttle Radar Topography Mission (SRTM) is an international research effort spearheaded by the National Geospatial-Intelligence Agency (NGA) and NASA in obtaining digital elevation models on a near-global scale to generate the most complete high-resolution digital topographic database of Earth to date.

SRTM consisted of a specially modified radar system that flew onboard the Space Shuttle Endeavour during an 11-day mission in February of 2000, completing 176

orbits. A key SRTM technology was radar interferometry, which compared two radar images or signals taken at slightly different angles. This mission used single-pass interferometry, which acquired two signals at the same time by using two different radar antennas. An antenna located on board the space shuttle collected one dataset and the other dataset was collected by an antenna located at the end of a 60-metres mast that extended from the shuttle. Differences between the two signals allowed for the calculation of surface elevation. The elevation models derived from the SRTM data are used in Geographic Information Systems or other application software. The spatial resolution for the SRTM datasets is 1 arc-second, approximately 30 metres, for area within United States of America and 3 arc-second, approximately 90 metres, for the rest of the world. Figure 3.8 illustrates a sample image of SRTM in the southern UK, extracted from Consortium for Spatial Information's website (www.cgiar-csi.org) which archives SRTM's global topography map with 90 metres spatial resolution. Each of the pixels in this data contains specific information on height in metres above sea level.

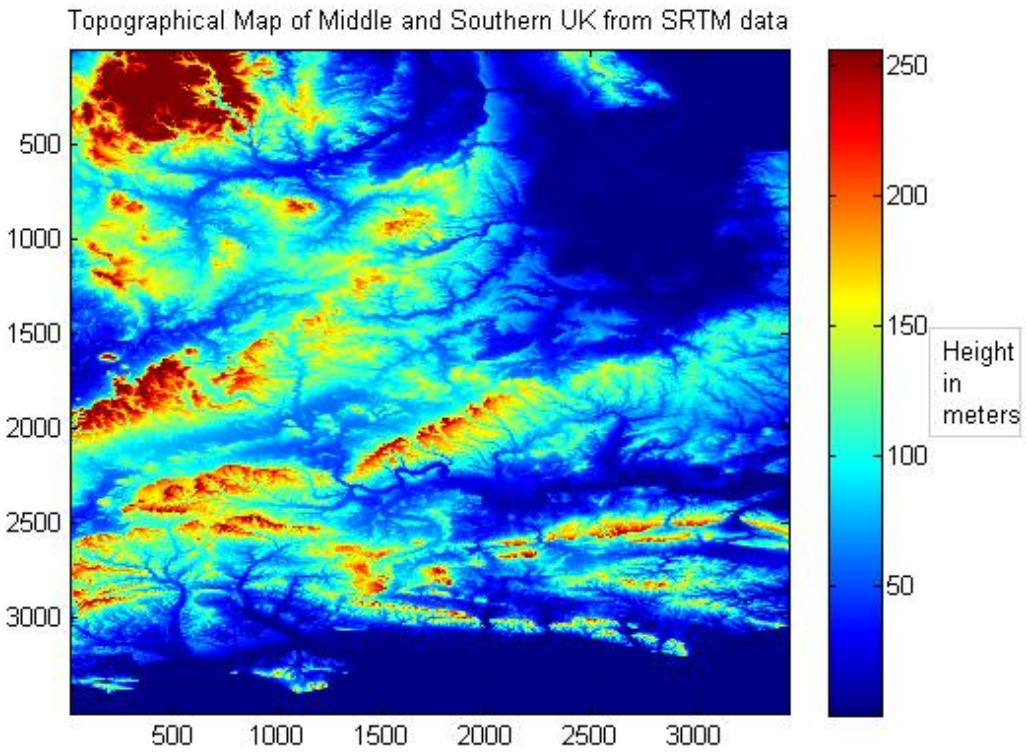

Figure 3.8: SRTM topographical map of the southern UK.

The variations of the Earth's surface height constraint the melting layer height and the altitude of ground stations. The SRTM can be incorporated into the GINSIM simulator to increase its accuracy in calculating sleet attenuation in the melting layer for both terrestrial and Earth-Space links. It is possible to use this map to produce a path profile of wanted and interference paths. For microwave links, the map can be used to check that the wanted path has adequate clearance. It will be desirable for interference path to be obstructed by terrain features. Rec. ITU-R P.452-14 (2009) uses path profiles generated by the terrain map in order to estimate the likely strength of any interfering signal.

Chapter 3 Summary

There exists a range of estimated precipitation datasets derived from measurements of ground based and space instruments. Rain gauges are often used as "ground truth" since they measure rainfall directly, but with poor spatial coverage. Rain gauges are often used for verification or calibration of indirect rainfall estimates. Rainfall estimation from satellites offer wider coverage than ground based radars but their measurements are less reliable and require further developments before they can truly replace radars. Currently, weather radar provides sufficient spatial and temporal resolution, suitable for GINSIM development for radio network simulation across Europe, even though it faces some challenges including spurious echoes, beam block, different calibration with adjacent radars and the variable relationship between radar reflectivity and the actual precipitation. Nonetheless, rain radars are still reliable and widely used by meteorologists and even as part of verification process for satellite-based precipitation estimation such as MPE. In addition, radar has finer spatial and temporal resolutions than measurements from weather satellites.

Nimrod/OPERA rain maps have been identified as suitable inputs for GINSIM. Although Nimrod uses single polarisation radar, unlike the dual polarisation CAMRa,

its wider coverage of the whole UK (Nimrod) and most of Europe (OPERA) give them a significant advantage for GINSIM. NCEP/NCAR Reanalysis I data provide crucial information to calculate rain height for slant path and the integration of Bacon-Tjelta sleet model. Furthermore, the global coverage and easy access for NCEP/NCAR Reanalysis I data make it ideal for GINSIM development.

CHAPTER 4 NETWORK FADE SIMULATION

As discussed earlier in Chapter 1 and 2, microwave links including terrestrial and Earth-Space links operating above 10 GHz, experience losses or fade due to absorption and scattering by liquid and mixed-phase hydrometeors in the atmosphere (rain, sleet, fog, wet snow and cloud). Hydrometeor fade exhibits complex spatial and temporal correlations, due to its dependence upon the atmospheric circulations. The Radio Section of the International Telecommunication Union (ITU-R) archives a large number of propagation models in the P recommendations. These models are generally utilised for predicting average annual, one-minute, fade distributions for individual Earth-Space and terrestrial links. Second order statistics including fade duration and slope are also provided in the ITU-R models. These models are sufficient to determine fixed fade margins for those individual links but are of little use in the design and optimisation of Fade Mitigation Techniques (FMTs) and Dynamic Network Management (DNM) of a more complex radio networks. For these tasks it is necessary to have models capable of predicting joint channel time-series of fade, often at a time resolution considerable shorter than one-minute.

One of the known methods of producing joint hydrometeor fade time-series with correct auto and cross-covariance is to simulate the fade on link networks superimposed on specific attenuation fields derived from realistic hydrometeor fields. This method has been used by Bosisio and Riva (1998), Hodges et al. (2003), Callaghan (2004), Gremont and Filip (2004), Paulson and Zhang (2009) and Jeannin et al. (2009). The variety of systems indicates that the network fade simulation is an active area of research. This chapter focuses on the principles of network fade simulation tools, development of Hull's GINSIM and descriptions of other tools.

4.1 General Procedures for Network Fade Simulation

Network fade simulation tools provide the joint hydrometeor fade time-series for a

heterogeneous network of EHF radio links by producing fine-scale, spatial - temporal hydrometeor fields and then overlaying radio networks to simulate the effects on any number of individual links. In general, network fade simulation involves some or all of the following processes:

1) Produce or obtain the coarse scale meteorological data
2) Downscale the coarse scale data to scales similar to Fresnel zones
3) Transform the downscaled fields into specific attenuation fields.
4) Perform pseudo-integration of all specific attenuations along the radio link's path to obtain time-series of attenuations.
5) Downscale the attenuation time-series.
6) Add other fade mechanisms to produce total attenuation.

Rain fields are the most dynamic of meteorological events and exhibit considerable variation in both time and space. Measuring rain intensity fields has fundamental difficulties and is prone to both systematic and random errors whether measurement is performed by networks of gauges or radar, either hosted on the ground or on satellites.

The fade experienced by a radio link is determined by the scattering and absorption within a volume roughly defined by the first Fresnel zone. Meteorological scatterers, such as hydrometeors (raindrops, ice pellets, hail, and complex mixed-phase particles) exhibit considerable spatial and temporal variation. Typically, smaller integration volumes yield more extremes of parameter variation i.e. one-minute rain rates are typically less smoothed that hourly rain rates. For channel fade simulators to yield variation with the correct distribution and variation, they need to be based on parameter fields with integration volumes similar in size to Fresnel zone diameters. These scales are typically tens to hundreds of metres, depending upon the frequency and path length. The following equation described the calculation for the radius of the first Fresnel zone:

$$r = 8.657\sqrt{\frac{D}{f}} \tag{4.1}$$

where r is the radius in meters, D is the total distance in kilometers, f is the frequency operation of the link in gigahertz

Currently there exist no meteorological databases of measured rain fields with the required spatial and temporal resolutions suitable for radio network simulation. Rain gauges can provide point rain rates recorded with integration times as short as 10 seconds. However, rain gauges are usually widely separated. Radars can provide instantaneous measurement of rain rates over large areas, albeit with the added complication of estimating rain parameters from radar reflectivity. It is generally uneconomic to operate rain gauge networks to provide similar spatial coverage and resolution to that provided by radars. Weather radars hosted on satellites can offer global coverage but often provide low spatial resolution and may have irregular temporal sampling. The rain rate estimated provided by satellite based radars suffer the same problems as estimates derived from ground based radars with the added complication that surface rain rates are estimated from above the weather system. Numerical Weather Prediction and reanalysis datasets (with assimilated data from a wide range of meteorological measurements) provide wider coverage than radars and rain gauges but they are based on global grids with extremely low spatial and temporal resolution.

Rain fields with high resolutions can be obtained using numerical methods to stochastically introduce finer-scale variation into the coarse-scale datasets. These downscaling processes rely upon statistical models for parameter variation valid over the range from coarse to fine-scale. The downscaling of meteorological fields is an active area of research as indicated with numerous simulators by different researchers. Downscaling relies upon constraining statistics of variation that span the range of scales from coarse to fine. A range of statistical models have been proposed for the variation of rain parameters. Across scales where one physical process

dominates there is a possibility of a single simple statistical model. However, over the range of scales between radio link Fresnel zones and typical radar resolution, it is likely that more than one process dominates. Various spatial break-points between models have been proposed associated with the scale of rain cells and the spacing between cells in clusters, see (Veneziano and Bras, 1996). Fine-scale spatial-temporal datasets are required not just for statistical model development but also for the verification of downscaled rain fields. Numerous scaling models, both simple and multi-scaling, have been proposed to describe the spatial and temporal variation of rain parameters. Over wide scale ranges models generally assume multi-scaling behaviour; see (Lovejoy and Schertzer, 1995). Similar statistics for non-liquid hydrometeors e.g. snow and wet snow (sleet), have barely been addressed despite the importance of these particles in microwave scattering, (Tjelta et al., 2005). Once *a priori* variation constraining statistics have been identified, numerical downscaling algorithms may be used to introduce the fine scale variation onto coarse scale, measured fields.

The combination of spatial and temporal downscaling of meteorological fields remains an unsolved problem although approximations have been suggested, (Deidda, 2000) and (Paulson and Zhang, 2009). Meteorological measurement can produce spatial-temporal averages or intermittent samples, and so both disaggregation and interpolation algorithms are required. For example, radars yield radar reflectivity averaged over a volume defined by the radar beam width, the scan rate, the integration time and the range gates; but is also a sample in time as a scanning radar will only return to that volume once per scan cycle. The downscaling of radar data requires both the interpolation and disaggregation of measurements and these processes are fundamentally different.

The transformation of rain rates into specific attenuations can be done using Rec. ITU-R P.838-3 (2005). This is an approximation, as specific attenuation is known to vary by a factor of two or more for the same rain rate due to variations in drop size

distribution, (Shkarofski, 1979). However, this variation is assumed to be reduced to negligible by the averaging effect of pseudo-integration along the link path. Fading due to other non-liquid hydrometeors, such as sleet, can be introduced into network simulation tools using Bacon-Tjelta sleet model, (Tjelta et al., 2005) and (Tjelta and Bacon, 2010) if the rain height is known. Rec. ITU-R P.530-13 (2009) has incorporated Bacon-Tjelta sleet model in its recommendations to calculate sleet fade. However, this procedure relies on many assumptions. The method assumes horizontal stratification of the atmosphere which is generally not true for convective events. The vertical variation of specific attenuation amplification factor was derived from an average over a small number of measurements made at a single location. It is likely to vary by a large factor between individual events.

The pseudo-integration of specific attenuation along the path of a radio link is also an approximation as it ignores the effects of multi-path and refraction. Currently it is unrealistic to downscale the coarse scale meteorological fields to a size of the first Fresnel zone with 1 second sampling time as such procedure requires astronomically high computational resources while introducing insignificant amounts of variation. An alternative method is to downscale the attenuation time series after the fields have been downscaled to an intermediate scale (larger than Fresnel zones) and the pseudo-integration process. This procedure requires less computational resources. However, the process is still in its infancy and only ad-hoc methods have been suggested, see Jeannin et al. (2009). The *a priori* statistics of temporal attenuation variation, which need to be conserved by the downscaling process, depend upon many geometric, climatic and radio parameters and have not been catalogued. Due to the number of unknowns, the computationally optimal distribution of effort between pre and post pseudo-integration downscaling has not been investigated.

Fading by other meteorological effects may be introduced into simulations. Absorption by atmospheric gasses, which is determined by temperature, humidity and pressure, can be introduced into specific attenuation fields using Rec. ITU-R P.676-8

(2009). It has been suggested that turbulence indices could be used to predict scintillation amplitudes, see Tatarski (1961). Most existing systems do not attempt to include either of the mechanisms as both are considered insignificant compared to hydrometeor fade.

4.2 Different approaches for Network Fade Simulation

Taxonomy of network fade simulation tools can be defined by the methods used to produce the rain fields. Fine scales of rain fields can be produced by statistical models of rain cell parameters, purely statistical models of spatial temporal rain rate variation or derived from meteorological radar networks and NWP systems.

4.2.1 Rain Cell models

Fine scale rain fields can be produced by aggregating multiple rain cells. Rain cells are often defined as regions where the rain rate exceeds a given threshold. Generally, rain cells have been modeled as circular or elliptical. Rain cell models assume rain rate variation within the cells to be constant (cylindrical), Gaussian or an exponentially decline from the centre of the cell. Few parameters are required to establish rain-cell profile including radius of the rain cell and the maximum rain intensity at the center of the cell, see (Paraboni et al., 2002). The constant rain-cell profile is frequently used for hydrological modeling purposes, Wheater et al. (2000). However, models based on constant rain-cell profiles do not reproduce second order statistics of rain fade, especially for the covariance of rain fade on two links, Zhang (2008). Smoother variation of rain rate within a cell could yield better results for second order statistics. The exponential and Gaussian methods introduce continuous smooth variation of rain intensity within a cell with the highest rain rate value at the center point of the cell.

The best known rain cell models are the EXCELL model (Capsoni et al., 1987), the

enhanced version of the EXCELL model or MultiEXCELL (Luini and Capsoni, 2011) and HYCELL model (Féral et al., 2003a&b). EXCELL, and the latter derived HYCELL, models are based on the joint statistics of parameters describing rain cell shape and intensity. These joint distributions were derived from databases of rain radar derived rain fields, (Bosisio and Riva, 1998; Paraboni et al., 2002). The EXCELL and HYCELL methods claim global application, although there are few published comparisons with real measurements. This claim relies upon the global application of rain cell parameter statistics measured in France and Italy.

The EXCELL or (EXponential CELL) was first presented in 1987 by Capsoni (Capsoni et al., 1987). The model based on the three dimensional S-Band meteorological radar scans for rainfall rates measured at Spino d'Adda near Milan. The measurements were carried out in 1980 from April to October. In this model, rain cells were identified when the rain rate exceeded a 5 mm/hr threshold and only with an area greater than 5 km^2 as smaller rain cells would introduce excessive quantitasation error to the system. The model is based on the distribution of cells; characterised by an exponential profile of the rain rate. However, the EXCELL system assumes unrealistically smooth spatial variation of rain rate and its scope and resolution are poorly defined.

MultiEXCELL, a new rain cell model inspired by EXCELL, offers several advantages over to its predecessor including the ability to generate complete rain fields by simulating the natural rain cells' aggregative processes that have been observed in the rain fields derived by the weather radar at Spino d'Adda. MultiEXCELL also claims to have global applicability and it also includes a methodology that utilises ECMWF ERA-40 data. Figure 4.1 shows the example of rain fields produced by the MultiEXCELL model simulating the site diversity of two Earth-Space links represented by the red arrows, (www.dei.polimi.it).

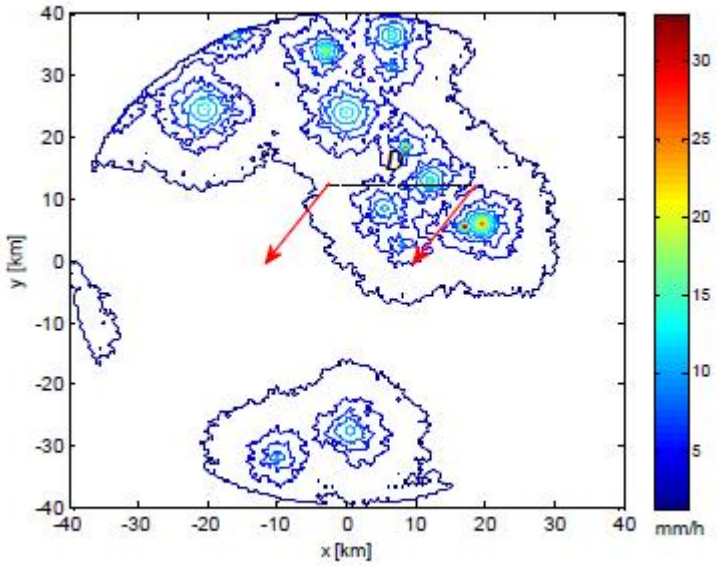

Figure 4.1 Sample images of rain fields produced by MultiEXCELL

The HYCELL or (HYbrid CELL) model was based on rain cells identified from radar observations in Bordeaux (South-Western France, near the ocean) and Karlsruhe (South-Western Germany, in the continental region). HYCELL utilises a hybrid distribution of the rain rate profile (Exponential and Gaussian distributions). The HYCELL model uses Gaussian profiles to describe convective type of precipitation and exponential profiles for stratiform events with low rain rate down to 1 mm/hr. The model uses elliptical rain cells with major axis, minor axes and the orientation angle as its parameters. According to the author, the model is well suited for describing the spatial variability of rain rate at small scales up to few tens of kilometres. However, the model assumes that rain cells are uniformly distributed over an area. The rain rate profiles are unrealistically smooth as are the contours. The authors have even tried to deface the contour lines by introducing noise to the field in order to produce more realistic rain cell shapes with a similar fractal dimension to measured rain cells. These models have experienced incremental improvement over several decades.

4.2.2 Statistical Rain Rate Variation Models

Early spatial-temporal rain simulators aimed to reproduce observed statistics such as point distributions of rain rate, covariance structure and intermittency. The early simulators were primarily designed for hydrological purposes and for the calibration of satellite measurements, and so the scales and resolutions are much larger than Fresnel zones. However, radio engineers and other researchers are now increasingly more interested in second order statistics describing high-resolution rain rate variation in both time and space, and so researchers are now developing spatial-temporal statistical models that can produce rain fields with scales near to Fresnel zones. These models can generate rain fields with more realistic shapes of rain events compared to EXCELL and HYCELL models. Often these models are divided into those with exponential correlations, often based on Markov models, and simple or multi-scaling models with power-law correlation tails, see (Lovejoy and Schertzer, 1995). One of the earliest simulation models was developed by Bell (1987). The simulation method could generate time-series of rain rates defined on a grid.

A range of spatial-temporal statistical models can be used to generate entirely synthetic rain rate fields. These models typically assume a specific form for the autocovariance or spectral density; often exponential or power law. One of these assumptions, combined with the assumption of stationarity and Gaussian or log-Normal distribution, allows rain fields to be generated. Rain fields derived purely from statistical models of rain rate or log rain rate variation have been employed to model Earth-Space and terrestrial links (Callaghan, 2004; Gremont and Filip, 2004).

At Rutherford Appleton Laboratory (RAL) and Portsmouth, fully numerical models developed by Callaghan (2004) have been used produce rain fields based on Voss's algorithms (Voss, 1985) to simulate fractional Brownian motion in two dimensional. The output of this simulator is a mono-fractal log rain rate field. The method assumes that log rain rate, where raining, is a stationary, fractional Gaussian process with a

Hurst coefficient of 1/3. The assumption that log rain rate is simple-scaling leads to multi-scaling rain rate variation. This model was first proposed by Paulson (Paulson, 2002), where it was found to be a good model for temporal variation of rain intensity derived from optical rain gauge and for spatial-temporal variation of stratiform rain rate measured using the Chilbolton, CAMRa radar. Figure 4.2 shows the sample image of a stratiform type of rain field produce by the simulator (www.port.ac.uk/research/telecoms/pdfs/filetodownload,26495,en.pdf).

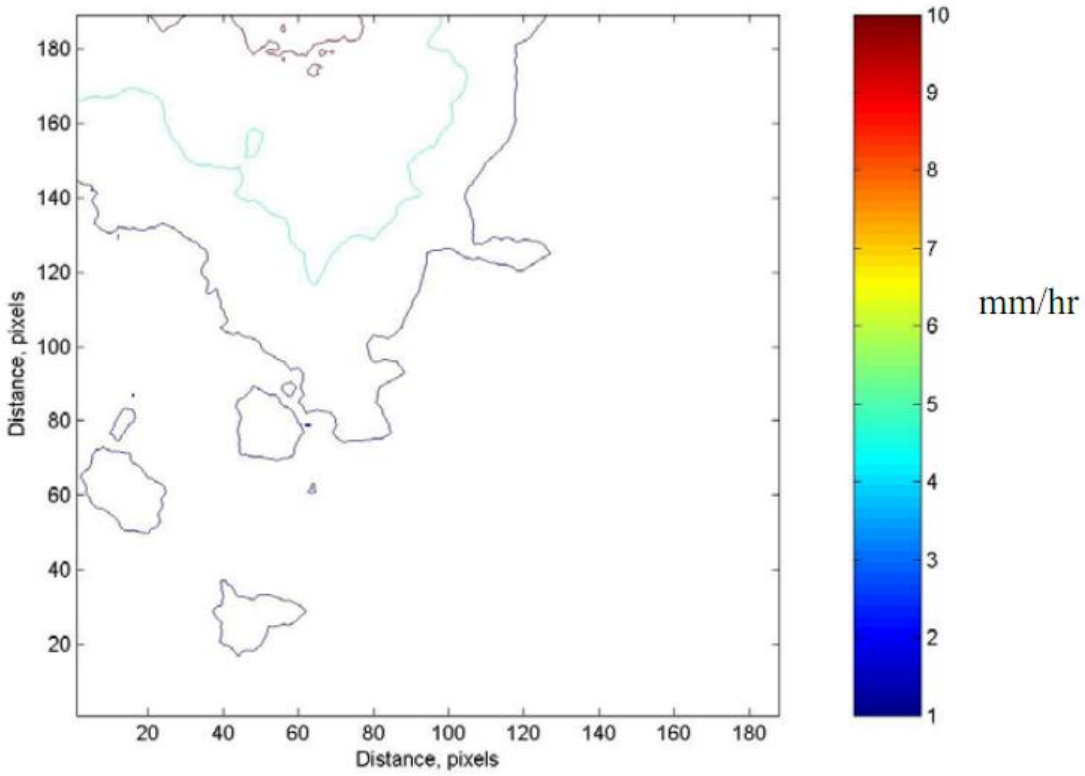

Figure 4.2: Example simulation of a stratiform event type of precipitation

Gremont and Filip (2004) at the University of Portsmouth have developed a spatial-temporal rain attenuation model and since then has been applied to two dimensional channel simulation tool to generate joint fade time-series. The model is based on generalisation of a stochastic dynamic Maseng Bakken model (Maseng and Bakken, 1981) and has been extended to two arbitrarily correlated satellite links at two different carrier frequencies. This paper assumed log rain rate fields to be Gaussian with an exponential or empirical correlation structure. The correlation lag is a linear

combination of separation in time and space and is consistent with Taylor's hypothesis (Taylor, 1938). Rain specific attenuations along the path are assumed to be homogeneous up to rain height. The statistical model is capable of producing consistent first and second order statistics such as the rain attenuation's power spectral density, dual location site diversity system, fade slopes, rain attenuation's frequency scaling factor and fade duration based on Markov chain. It is claimed that the proposed model is applicable to metropolitan areas with a 60 km diameter and with all types of radio networks. It is applicable to the statistical analysis of rain attenuation and the modeling of site diversity systems. A simulation tool based on this model has been developed at the University of Portsmouth. The simulator is able to produce joint fade time-series for terrestrial and Earth-Space links which can be crucial for the design of FMTs. Rain advection is assumed to be linear in the simulation and the not-raining regions have been introduced by a thresholding technique.

4.2.3 Downscaling NWP or Meteorological Data

Several systems are based on the downscaling of NWP or meteorological data to generate fine scale rain fields. Some of these systems use the same statistical models of variations as the methods described in the earlier section 4.1.2.

4.2.3a SISTAR

The French aerospace laboratory, ONERA, is also developing a simulation tool called SISTAR (SImulator of the Space-Time behaviour of the Attenuation due to Rain) for Earth-Space links. Its ultimate goal is to produce fine scale rain fields for radio network simulation with 1 second sampling time and with global applicability. The system starts with ERA-40 historical reanalysis data from ECMWF with global span but relies upon numerical downscaling of these data from very large grid squares and integration times, see Jeannin et al. (2009).

The ERA-40 database yields a large number of parameters including the 6-hour rain accumulations over 2.5^o x 2.5^o regions and the wind vector at a range of pressure levels. SISTAR downscales the rain accumulations to 0.01^o x 0.01^o regions over periods of 0.1 hours. Disaggregation is achieved by modeling the fine-scale rain field as a lognormal process with a given, empirical, double exponential auto covariance.

The disaggregated rain field is advected with the ERA-40 wind field at the 700 hPa to yield time-series. The fade on slant paths is estimated by pseudo-integration of the specific attenuation associated with the interpolated-dissagregated-advected rain field along a path from the receiver to the -2^o C isotherm (provided by the ERA-40 database). The resulting fade time-series are sampled every 6 minutes (0.1 hours) and these are stochastically interpolated to yield a 1 Hz sample rate.

The ONERA method is very ambitious and has a number of fundamental limitations. The distribution of rain rates over each ERA-40 pixel is made to be lognormal. However, Zhang (2008) reported rain rates over regions of a similar size to often have multimodal distributions due to the mix of event types.

The spatial-temporal disaggregation is performed with a rather ad-hoc method that initially yields spatially disaggregated fields of indeterminate temporal accumulation, and then interpolates between these fields separated by 6-hours. No point temporal autocovariancies imposed. The double exponential spatial autocovariance decays faster than the power-law form consistent with the more accepted simple-scaling or multifractal models of rain rate variation, see Paulson and Zhang (2009). In addition, the ERA-40 datasets spatial and temporal resolutions are too coarse to be downscaled with the downscaling algorithms developed for HRFNS and GINSIM, and may miss out many important rain events.

4.2.3b SATCOM

Researchers at the University of Bath, Hodges et al. (2003) have developed the EHF

SATCOM system using numerical weather models, forecast data and rain radar data for deriving attenuation time-series on fixed satellite and terrestrial links. The system includes rain and cloud fade mechanisms as well as scintillation and absorption by atmospheric gases. The performance of this technique depends on the insertion of the short interval temporal properties (varying typically over 1 second to 15 minutes) that are statistically independent between stations. This allowed the system to generate maps of attenuations with spatial resolution of a few kilometres and temporal resolution of a few seconds. The UK Meteorological Office's Unified Model (UM) and Nimrod C-Band rain radar network was used to acquire meteorological inputs for SATCOM, see Hodges et al. (2003). The UM is a NWP model and provides the basis for the calculation of background fading effects (water vapour absorption, scintillation and cloud losses). For rain fade, the model uses Nimrod rain radar data as these have higher spatial and temporal resolutions compared to the current UM model.

4.2.3c Hull Rain Fade Network Simulator (HRFNS) and GINSIM

The Hull Rain Fade Network Simulator (HRFNS), Paulson and Zhang (2008), is a heterogeneous network simulation tool capable of producing joint rain fade time-series for arbitrary networks of terrestrial SHF and EHF links. Over the last three years, GINSIM has been developed from HRFNS as the application has been extended to include slant paths including Earth-Space links and links to Unmanned Airborne Vehicles (UAVs) and High Altitude Platforms (HAPs). Vertical variation of specific attenuation has been introduced using the Bacon-Tjelta sleet model used in Rec. ITU-R P.530-13 (2009), and rain heights derived NOAA NCEP/NCAR Reanalysis I data, Kalnay et al. (1996).

The rain data used in the development of GINSIM has been obtained from the UK Meteorological Office Nimrod rain radar network, but the use of equivalent data produced by the OPERA project (www.knmi.nl/opera) would extend the area over

which the system could be used to most of Europe. Nimrod and OPERA composite rain field images have a 1 km spatial resolution and 5 minutes sample time. The numerical downscaling processes employed by both GINSIM and HRFNS are described in detail in Paulson and Zhang (2009) and Zhang (2008).

Paulson (2004) have suggested that the downscaling techniques from the HRFNS can be applied to input datasets with sample times as long as 20 minutes and spatial voxels up to 30 km. Nimrod and OPERA derived rain fields have spatial and temporal resolutions within this range and so are appropriate input data sets for a network simulator. A simulator based on these datasets would be applicable anywhere in the UK or Europe respectively.

4.3 Downscaling and network simulation processes for GINSIM

The downscaling techniques developed for the HRFNS and GINSIM produced numerically enhanced time-series of rain radar images from the Chilbolton Radar Interference Experiment (CRIE), measured as part of the European COST 210 project (1991). Techniques that can preserve a mixture of measured and *a priori* known statistics have been implemented for downscaling and interpolating measured rain fields such as the CRIE. GINSIM downscales a selected region of coarse scale rain fields from Nimrod and OPERA composite time-series to produce much finer resolution spatial and temporal rain fields.

Currently, the simulation processes in GINSIM for radio networks can be summarised by the following steps (further knowledge on these steps will be explain later in the relevant subsections in this chapter):

1. Estimate and remove the advection between consecutive pairs of composite images.
2. Disaggregate the coarse scale rain fields.
3. Interpolate log rain rate into no-rain regions using Minimum Bending Energy

algorithm.

5. Interpolate scans using ARMD algorithm.
6. Re-introduce advection.
7. Transform the downscaled rain rate fields to specific attenuation fields.
8. Implementing rain height for Earth-Space links and the integration of Bacon-Tjelta sleet model.
9. Perform pseudo-integration of specific attenuation along the path of links.

The simulation of a network involves several steps. First the area spanned by the network of interest is identified and a coarse, rain-map time-series for this area is extracted from Nimrod or OPERA data. Advection of rain events are measured and removed between two consecutive rain scans. For areas of diameter less than a few hundred kilometres, advection is usually well modeled as a linear translation. For larger areas or more complex advection, more complex translations can be used. The translation is identified by maximization of the cross-covariance between consecutive composites. For complex advection, cross-covariance is maximised for different sub-regions and the advection vector is smoothly interpolated between region centres. Each 2-D spatial rain map is disaggregated to smaller integration volumes using a multiplicative cascade algorithm. Interpolation between scans uses a simple-scaling log rain rate model that requires log rain rates in regions with no rain. These extremely low rain rates are introduced using Minimum Bending Energy interpolation algorithms (Zhang, 2008). Then the 3-D spatial-temporal data volume between each consecutive pair of scans is interpolated to finer temporal sampling and the advection is reintroduced. Once the fine spatial-temporal rain field data is calculated, the microwave network can be overlaid and the joint fade time-series calculated by pseudo integration of the specific attenuation along each link path. The specific attenuation is calculated using the power-law of Rec. ITU-R P.838-3 (2005) and the Bacon-Tjelta sleet model that has been incorporated into Rec. ITU-R P.530-13 (2009). The sleet model introduces a specific attenuation amplification factor that allows for the mixed-phase hydrometeor types in the melting layer. For slant paths,

the altitude of each segment of the path is calculated from the link geometry. The sleet model reduces the specific attenuation to zero when the link altitude is more than 360 m above the zero-degree isotherm. This altitude is obtained from NOAA NCEP/NCAR reanalysis data. The fade calculation using this method is equally applicable to terrestrial, Earth-Space and shorter slant paths such as those to HAPs or UASs.

4.3.1 Disaggregation

Finer-scale spatial variation is introduced into the Nimrod data using a multiplicative cascade algorithm and constrained by multi-scaling exponents measured on CRIE data and extrapolated from the smallest measured scale i.e. from voxels of diameter 300 m down to 30 m. Lilley et al. (2006) have proposed that the multi-scaling exponents are applicable down to sub-metre scales. Disaggregation (i.e. refining existing samples to smaller integration volumes) is achieved using the log-Poisson multiplicative cascade algorithm of Deidda (1999), designed to reproduce measured multi-scaling statistics, Paulson and Zhang (2007). For the GINSIM system, the Nimrod / OPERA rain fields are disaggregated from 1 km to 125 metres.

According to Zhang (2008), the disaggregation of an instantaneous spatial average cannot be done in separation from the disaggregation of other samples made near in time. For instance, two measured radar rain rates separated by only a few seconds could not be disaggregated independently, since the fine-scale variation would be correlated. Therefore, they need to be adequately separated in time. Independent disaggregation will be acceptable if the spatial integration volume is small relative to the temporal sampling interval. In general, the disaggregation will be valid as long as $\Delta x / Dx << \Delta t / Dt$ where Δx and Δt are the spatial and temporal sampling respectively while Dx and Dt are the spatial and temporal decorrelation distances.
Figure 4.3 demonstrates before and aftermath of a Nimrod rain rate field that have gone through the disaggregation process.

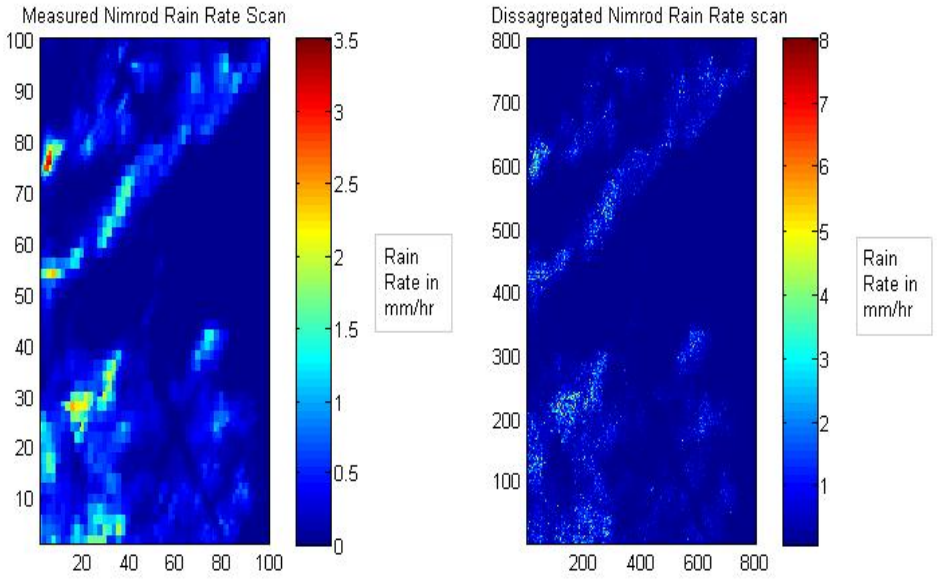

Figure 4.3: Before and after the disaggregation process of a rain rate field

4.3.2 Interpolation

The temporal interpolation algorithms are based on an underlying statistical rain model that assumes spatial-temporal log rain rate fields, when raining, are well approximated by homogeneous, isotropic, fractional Brownian fields with a Hurst coefficient of 1/3; (Paulson, 2002; Callaghan, 2004). This model has been derived and verified over the scales of interest, by analysis of Chilbolton rapid response rain gauge and CAMRa radar data. The model has been used for the interpolation of rain gauge data, Paulson (2004). In HRFNS and GINSIM, the interpolation (i.e. introduction of new samples with the same spatial-temporal averaging at new points in space-time) is achieved by ARMD (Assymetric Random Midpoint Displacement) by Zhang (2008), a variant of the Local Average Subdivision (LAS) algorithm of Fenton and Vanmarcke (1990). In GINSIM, Nimrod / OPERA rain data are interpolated to 18.75 seconds from 5 minute sampling time. This is equivalent to introducing 15 new rain fields between each pair of disaggregated composite images. Figure 4.4 illustrates the general diagram on interpolated scans produced between two consecutive measured scans.

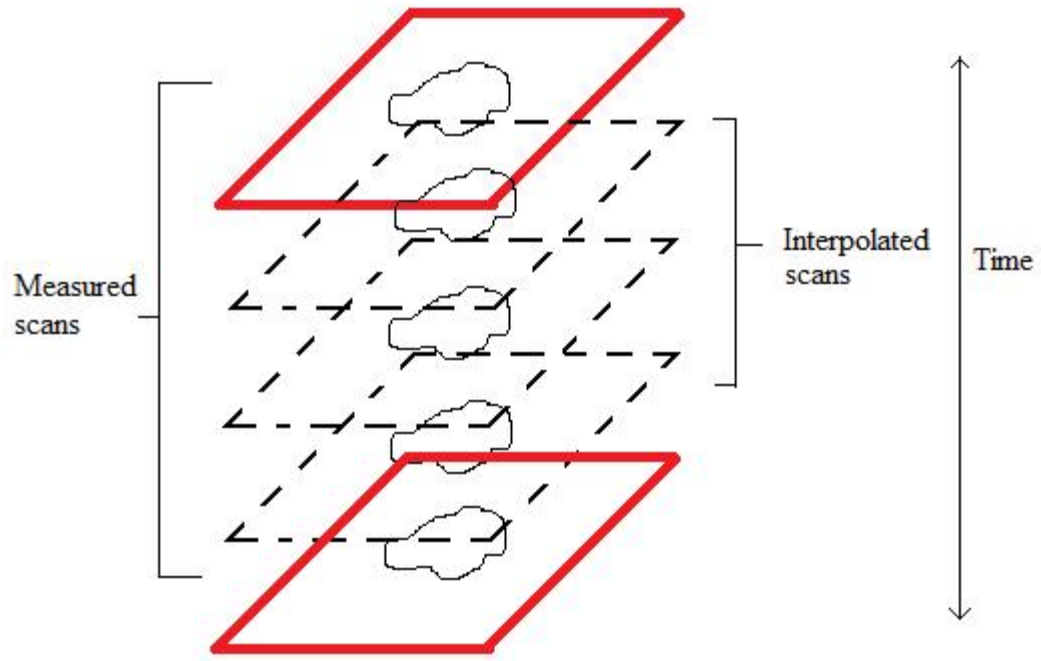

Figure 4.4: Basic diagram of the interpolation process (time domain)

4.3.3 Extrapolation into Low Rain Rate Regions

Measured log rain rate fields and numerically generated FBfs (Fractional Brownian Fields) have considerable differences in terms of marginal distribution due to intermittency of real rain (real rain events are finite in degree and separated by long intervals without rain and so zero rain rates is always present). Threshold of 0.05 mm/hr has been set to represent no rain rate region but this will inflates rain rates near the edges of rain events resulting new events being numerically generated in a region of no rain. Before interpolation, zero rain rates need to be replaced by very low rain rates that conserve the covariance of log rain rate near the edges of rain events. This is achieved by using a Minimum Bending Energy interpolation algorithm (Zhang, 2008), constrained by the non-zero rain rates, to replace zero-rain rate regions with very low rain rates. This process creates plausible decay of rain rates at the edges of rain events. These values are required by the ARMD algorithm use to create new rain fields between measured fields.

4.3.4 Advection

Before interpolation between consecutive disaggregated rain fields, advection needs to be removed. Advection is the movement of the rain fields horizontally by the ambient wind. The statistical models of rain rate variation used to constrain interpolation are only applicable to advection less rain fields. Therefore, advection is removed before interpolation and then reintroduced afterwards.

Zhang (2008) has developed a method to measure and remove advection for CRIE rain data assuming a linear translation between radar scans and using a concept of Taylor's frozen storm hypothesis (Taylor, 1938) . According to Taylor, the temporal statistics of rain at a fixed location as equivalent to the spatial statistics measured along a line parallel with advection, assuming that the rain variation is mainly determined by advection while the evolutionary effects are insignificant, hence Taylor's algorithm also known as the frozen storm model. Taylor's frozen storm hypothesis assumes that the spatial-temporal rain field may be estimated as a fixed spatial field moving with a stable velocity. The speed of the rain fields being advected was calculated by searching the linear displacement that will maximise the correlation between two successive scans. Currently, GINSIM apply the same method to measure and remove advection in a small selected area in Nimrod and OPERA rain data. However, this method is not reliable to be used for larger area i.e. whole of UK since larger region with such size certainly has multiple advections travelling at different speeds or directions.

4.3.5 Transforming to Specific Attenuation Fields and Pseudo-integration

The downscaled rain rate fields are transformed into specific attenuation fields using the power-law relationship between specific attenuation, γ_R (dB/km) and rain rate R (mm/hr) in Rec. ITU-R P.838-3(2003). Radio links can then be overlaid on the downscaled rain fields to extract points of specific attenuations along the links. Figure

4.5 demonstrates the process of overlaying a radio link on a matrix with each pixel experiencing a specific rain rate. Each rain rate is converted into a specific attenuation at the frequency of interest, the specific attenuations are interpolated to equil-spaced points along the link path using bi-linear interpolation (part of or the extension of linear interpolation between two variables on a regular grid) or the 2-D data interpolation (the "*interp2*" function from Matlab). The array of specific attenuations can be numerically integrated to obtain the total attenuation either through a simple summation or using a more advance numerical integration method such as Simpson's rule.

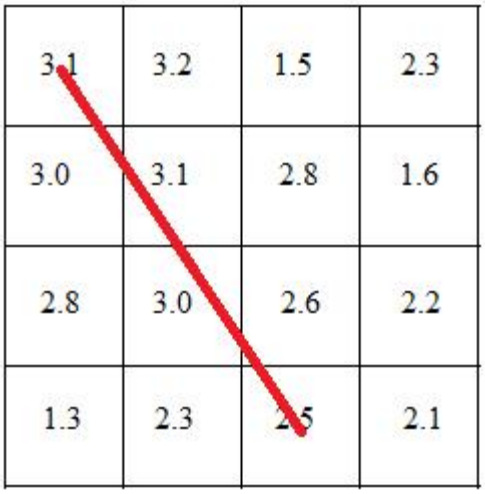

Figure 4.5: Diagram of a radio link (red) superimposed on a matrix with rain rates

4.3.6 Rain Height model

As discussed earlier in the Chapter 2, rain height (height between the surface and altitude where all hydrometeors are frozen) is a crucial parameter to simulate slant paths such as Earth-Space radio links, and implementation of the Bacon-Tjelta sleet model. The altitude of rain height is strongly determined by the temperature profile or lapse rate (the rate of decrease of atmospheric temperature with increase in altitude) in the troposphere region and is given by:

$$¥ = -\frac{dT}{dz} \tag{4.2}$$

Where ¥ is the lapse rate in units of temperature divided by units of altitude, *T* is the temperature and *z* is the altitude. The air temperature typically decreases linearly with the increasing altitude from the surface until it reaches a tropopause line (approximately 10 km from surface) in the atmosphere. Various average values of lapse rate exist. Angot performed the earliest known study in 1892, which concluded that the average value is around 5.5^{o}C/km. Currently, the average global value of lapse rate defined by the International Civil Aviation Organization (ICAO) as part of International Standard Atmosphere (ISA) model is 6.5^{o}C/km. However, the actual lapse rate varies depending on seasons, regions and moisture content of the air. The average value of the lapse rate is a rough approximation and unsuitable for more precise studies. Therefore, a more sophisticated method is required to determine rain height, Christian Roland (2002).

In GINSIM, rain height can be established from NCEP/NCAR Reanalysis I data from NOAA. As discussed in Chapter 3, the dataset provides various atmospheric parameters at global grids including geo-potential height and temperature for 17 different pressure levels ranging from 1000 to 10 mb. These parameters provide the basis for a ZDI calculation that can allows the estimation of rain height. Figure 4.6 illustrates the calculation of ZDI based on the reanalysis data from NOAA.

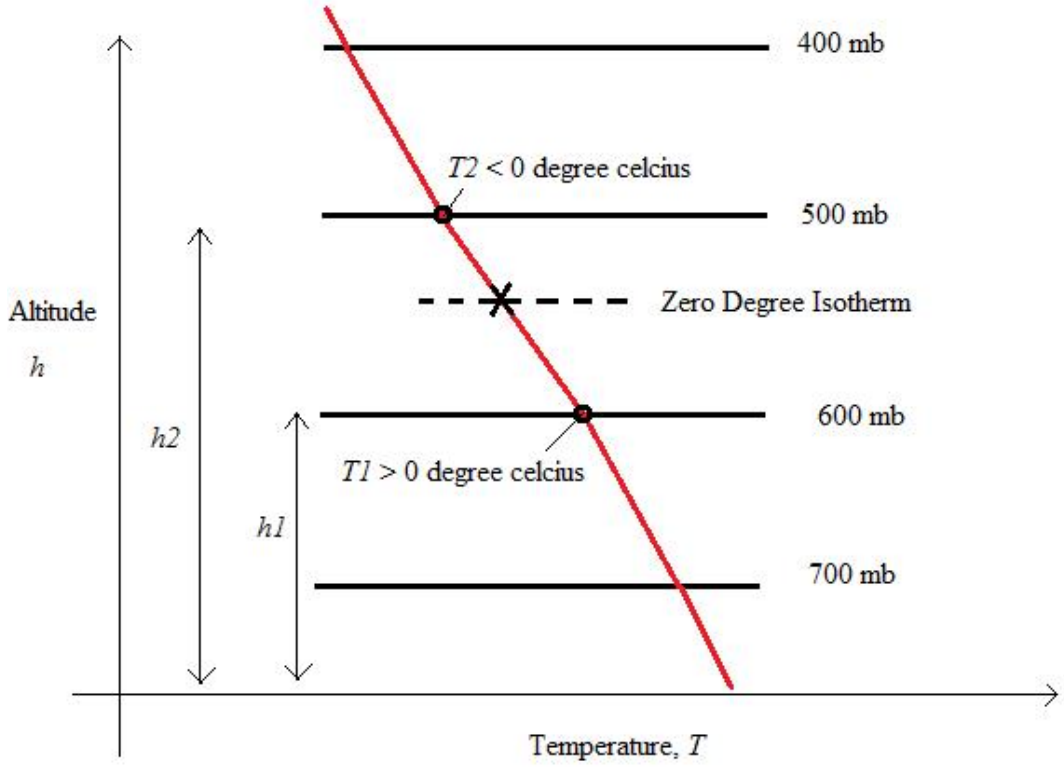

Figure 4.6: General diagram to calculate ZDI for rain height

Two parameters are used for the ZDI height calculation, the air temperature and the geo-potential height or altitude, both as a function of pressure level. The ZDI height is calculated by linear interpolation between the two lowest temperature-height points decreasing through zero Celsius with increasing altitude. Diaz et al. (2003) conclude that the reanalysis data can reliably predict ZDI height, even over mountainous areas, over the period 1958 to the present. Figure 4.7 shows the average annual ZDI height variation, calculated at 6-hour sample intervals and averaged over 30 years from 1980 till 2009 for the Southern UK. The ZDI is consistent with the average global lapse rate of 6.5^{o}/km. In winter the ZDI height minimum occurs around 1 km, consistent with a ground temperature of 6^{o} and constrained by the ground. In summer when the ground temperatures are typically 20^{o} the ZDI height is around 3 km.

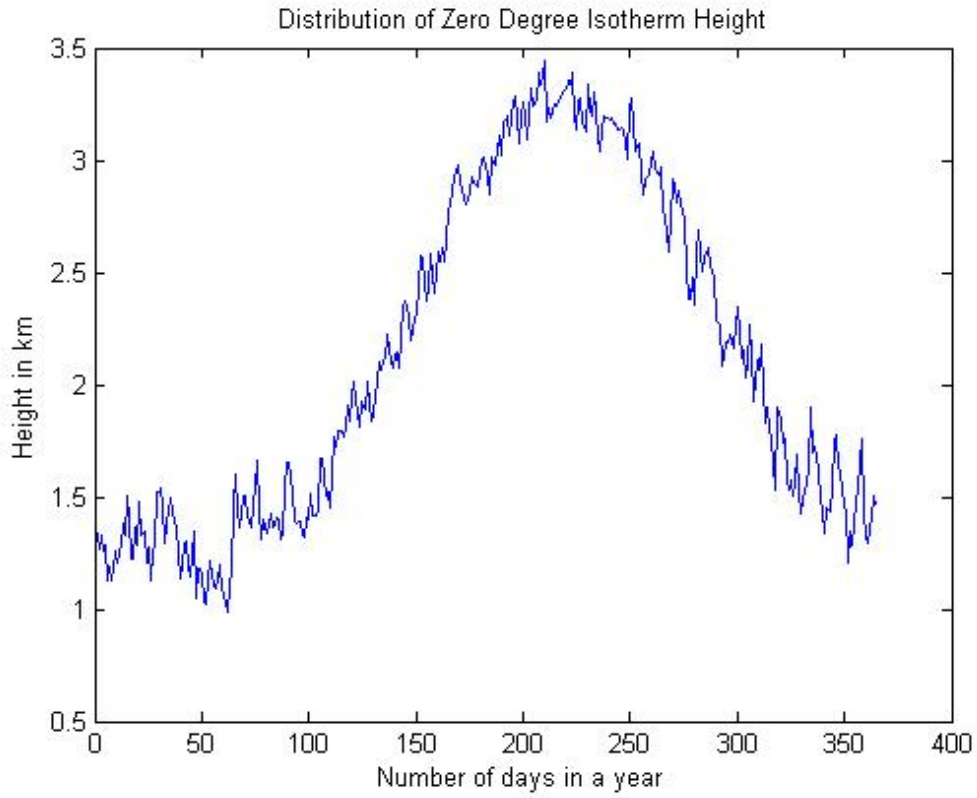

Figure 4.7: ZDI heights in a year (30-year average)

Average annual rain height assumed to be 360 metres above average annual ZDI height, by Rec. ITU-R P.839-3(2001). I assume the same relationship holds for six-hour averages. This is a coarse assumption that will often not be true in practice, particularly in the presence of convective events. However, it was the most expedient assumption at the time and a simplification worth investigating. The obtained rain height can then be used to establish slant paths and for the integration of Bacon-Tjelta sleet model for all types of radio links. In GINSIM, vertical rain rate variation along the column from surface to rain height is assumed to be constant, although in reality this may not be true. However, based on weather radar observations by Goldhirsh and Katz (1979), on average, the rain intensity did not significantly vary with height between the surface and the base of the bright band or melting layer. Crane (1996) has used this evidence to justify his assumption that specific attenuation may be modeled as being constant from the surface to rain height.

As discussed earlier in Chapter 2, the amplification factor for attenuation by wet

snow, relative to the equivalent rain, given by the Bacon-Tjelta sleet model will vary with height relative to the rain height as shown in Figure 2.11 in chapter 2. Wet snow can attenuate more than four times more than the equivalent rain. For slant paths, links are divided into segments with rain rates and different altitudes. These altitudes can then be used to extract amplification factors for specific attenuation from Bacon-Tjelta sleet model as illustrated in a diagram in Figure 4.8.

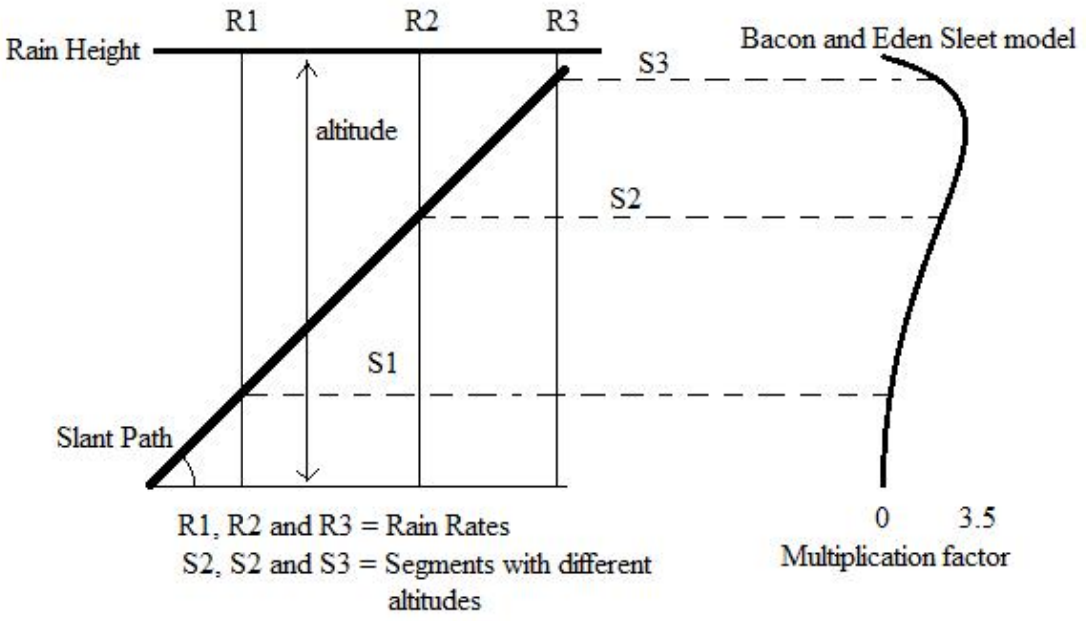

Figure 4.8: General diagram of the implementation of Bacon-Tjelta sleet model for a slant path

The rain height model in GINSIM assumes horizontal stratification of atmosphere when it is raining which may hold true for stratiform types of precipitation but certainly not for convective events where the mixed phase hydrometeors may exist in the entire column of the rain event. This can be problematic for GINSIM to properly simulate radio links in regions with high occurrence of convective precipitations. Furthermore, convective events produce more critical attenuations than stratiform events which can significantly affect the fade distribution statistics.

Chapter 4 Summary

A known common method of producing joint hydrometeor fade time-series with correct auto and cross-covariance, is to simulate the fade on link networks superimposed on specific attenuation fields derived from realistic hydrometeor fields. Often, network fade simulators operate by obtaining coarse meteorological data, numerically downscale to higher resolution, transform the fields to specific attenuation and perform the pseudo-integration along link paths to obtain attenuation time series. There are generally three different sources of coarse-scale rain fields including the rain cell models, purely statistical models of spatial temporal rain rate variation and models derived from meteorological radar networks and NWP. Interpolation and disaggregation algorithms applicable to Nimrod and OPERA rain composite data have been described. These algorithms have been used to downscale coarse scale Nimrod / OPERA data from 1 km to 125 metres spatially and 5 minutes to 18.75 seconds temporally. The Nimrod / OPERA data could be downscaled further with smaller spatial and temporal scales but that process will require astronomical computer resources and currently our equipments are unable to do so. Section 6.2.2 in Chapter 6 describes the effects of different spatial and temporal scales to the annual fade distribution. In GINSIM, the application has been extended to include slant path simulation such as Earth-Space links and sleet attenuation calculation. This is done by using rain height as the parameter that can be calculated using the geo-potential heights and air temperature as functions of pressure levels from NOAA's NCEP/NCAR Reanalysis I data.

CHAPTER 5 VALIDATION WITH ITU-R MODELS

The simulation tool can be subjected to a wide range of validation tests. These can be divided into testing the statistics of the downscaled rain fields and of derived rain fade time-series. The whole theme about validation in this chapter and the next chapter is about testing the simulator whether it can produce the desired final output results that are consistent with theoretical models and measured links. As the downscaling process does not aim to reproduce the fine-scale fields that actually existed during the simulation interval, only the statistics of rain fields and fade time-series can be compared. ITU-R provides prediction methods for first order statistics i.e. distributions of average annual parameters. The ITU-R also provides limited models of second order statistics i.e. fade durations and fade slope. In this chapter, the simulation output will be compared with the theoretical ITU-R models.

5.0 Experimental setup

The following comparisons are based on three calendar years of Nimrod data, 2004 to 2006, spanning a 36 km square region centred on Chilbolton Observatory (51° 8.1’ N, 1° 26.2’ W). These data have been downscaled from a spatial integration area diameter of 1 km to 125 m. The original 5 minute sampling interval has been interpolated to 18.75 seconds. The downscaled dataset was used to simulate a range of terrestrial and Earth-Space links. In this chapter, downscaled Nimrod rain data and simulated terrestrial and Earth-Space links are compared to the ITU-R models including the rain rate, terrestrial (with and without sleet) and Earth-Space link. The validation process with ITU-R models are divided into two parts, the first order statistic (annual distribution of rain rate and fade) and the second order statistics (fade duration and slope). For the first order comparisons, the simulated outputs is calculated with rain rate of 29 mm/hr at 0.01% and it is expected to be consistent with the ITU-R models especially at higher probability level and probably deviate at lower exceedance level at 0.001%. For the second order statistics comparisons, the

simulated outputs are expected to be consistent and with the ITU-R models at different attenuation threshold levels. The word “consistent” in the validation sections simply means that the output results are in similar shape or patterns and at satisfactory scale with the models (in Chapter 5) or the measured links (in Chapter 6).

5.1 Validation of Rain Rate Distribution

In this section, three years of downscaled Nimrod rain data centered on Chilbolton are compared to Rec. ITU-R P.837-5 (2007) predicted average annual rain rate distributions. The downscaled data is also compared to the measured Nimrod data and rain gauge data. Figure 5.1 compares the rain intensity distributions derived from the Nimrod data, the downscaled data, Rec. ITU-R P.837-5 (2007) and from Rapid Response Drop Counting rain gauges, collected from the same years as the Nimrod data, sited at Chilbolton Observatory and a near-by site at Sparsholt. The Rec. ITU-R P.837-5 (2007) distribution is calculated using the 0.01% exceeded rain rate derived from the downscaled Nimrod data of 29.0 mm/hr. This result demonstrates that the downscaling process produces rain fields with a plausible distribution. Disaggregation has increased the probability of higher rain rates, as is expected for smaller integration volumes.

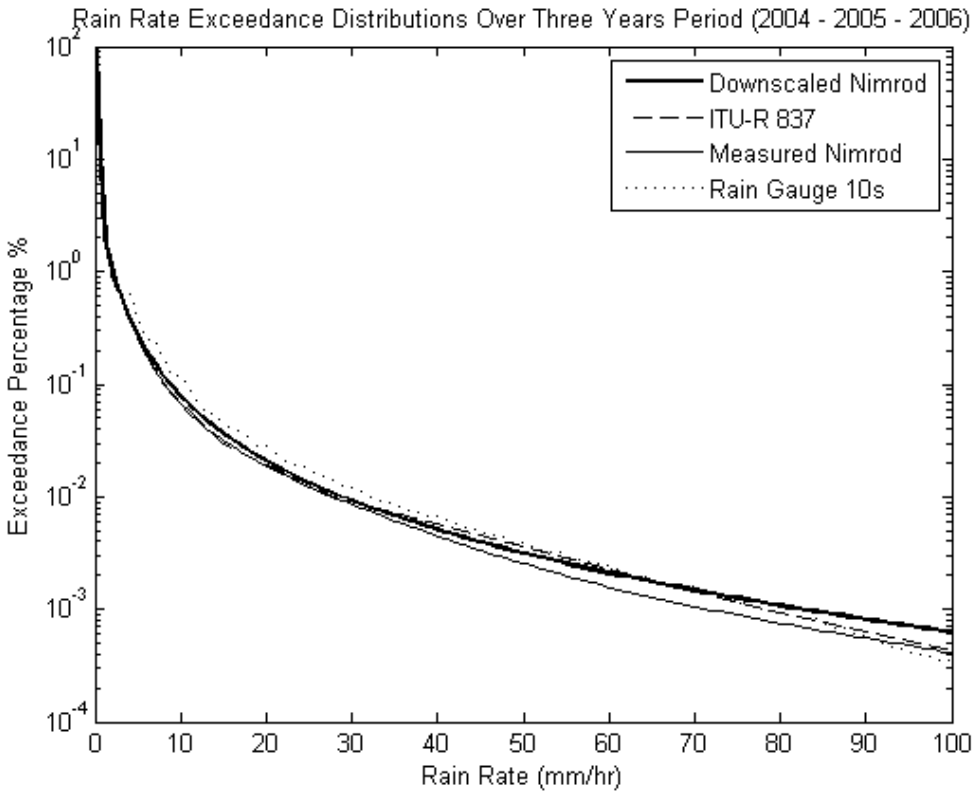

Figure 5.1: Comparisons of rain rate exceedance distributions derived from direct measurement and from Nimrod data over the three calendar years 2004 to 2006

Averaging over the three years of data obscures the year-to-year variation. Figure 5.2 shows the three years separately and illustrates a factor of two variations in the annual 0.01% exceeded rain rate. The large variations between the three years of measured Nimrod are consistent with the statistics archived in UK Meteorological Office's rainfall accumulation database (www.metoffice.gov.uk/climate/uk/anomacts/) where there are more rain accumulation was recorded in 2006, particularly in the southern of UK, compared to 2005 (the least) and 2004. This pattern is reflected in the Nimrod data, both before and after downscaling.

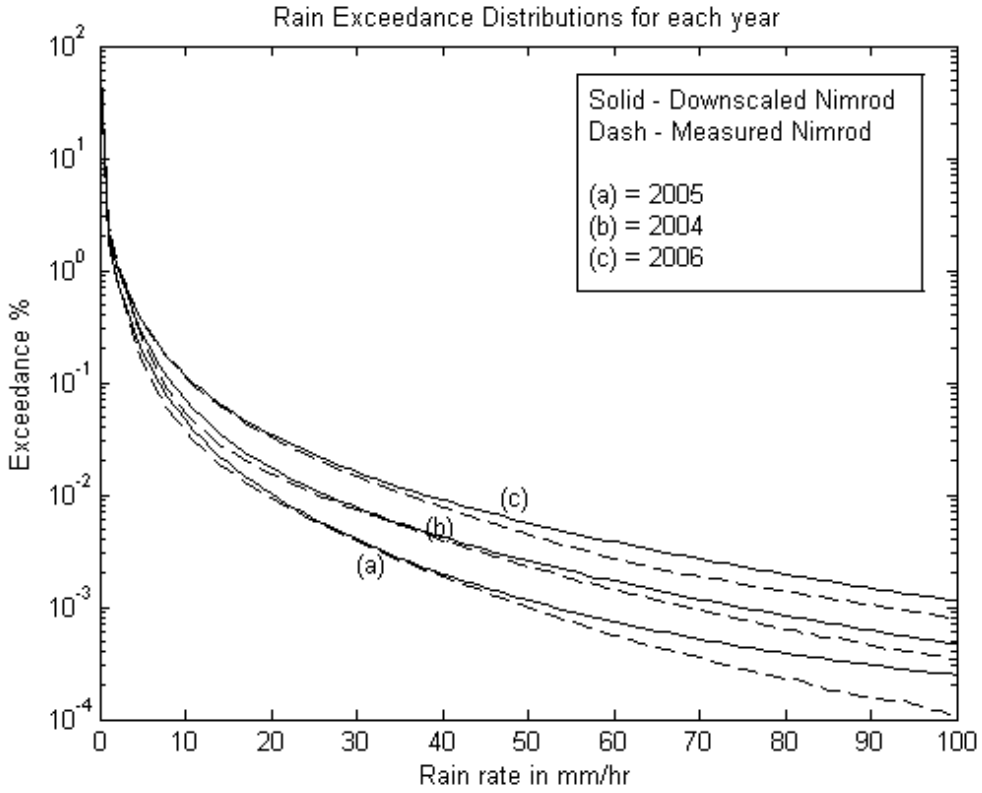

Figure 5.2: Annual rain exceedance distributions for the original and downscaled Nimrod-derived rain fields for the three calendar years 2004 to 2006

5.2 Validation of First Order Statistics for Annual Hydrometeor Fade

A large number of vertically polarised, 38 GHz, zero-elevation, terrestrial links, of length 5 km and 8 km; have been simulated. For each link length, all possible positions within the 36 km square orientated north-south and east-west (horizontal and vertical orientations), are simulated and each yields a fade time-series. With this technique, thousands of links from all the north-south and east-west orientations within the rain map can be simulated at a time. These links are then averaged to produce an annual fade distribution for a particular radio link. The links are assumed to be at an altitude of 600 m, to illustrate the effects of the melting layer, despite the land surface being at an altitude of 100 m. The hydrometeor fade distributions illustrated in Figure 5.3 are calculated by averaging over all these link time-series. Each fade time-series can be simulated with and without using Bacon-Tjelta sleet model (Tjelta et. al., 2005) which has been included in Rec. ITU-R P.530-13 (2009).

When the sleet model is not used, all hydrometeors are as assumed to be liquid rain. Alternatively, the zero-degree isotherm height can be assimilated from NOAA data and the effects of mixed phase hydrometeors included. Figure 5.3 illustrates the distributions of fade, with and without allowing for sleet, calculated by simulation over the three years. These are compared with the average annual distributions provided by Rec. ITU-R P.530-13 (2009), with and without the sleet correction. The rain rate exceeded 0.01% of the time used in the P.530 model is the 29.0 mm/hr extracted from the downscaled Nimrod dataset. Figure 5.3 shows very clear agreement between simulated distributions and ITU-R models, both with and without sleet. The variation is certainly within that expected given the year-to-year variation illustrated in Figure 5.2.

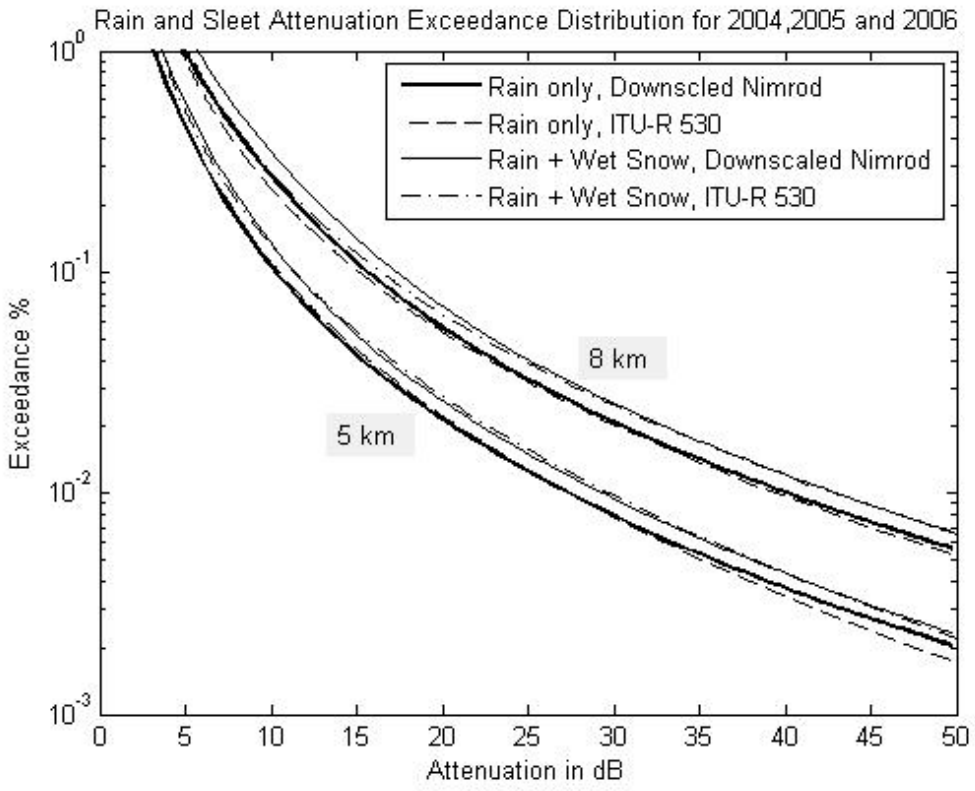

Figure 5.3: Distributions of annual hydrometeor fade for 38 GHz, terrestrial links of length 5 km and 8 km, as predicted by Rec. ITU-R P.530-13 (2009) and produced by simulation. Distributions are illustrated with and without allowing for extra fading due to wet snow.

The same simulation process was followed to calculate the hydrometeor fade distribution for a Ka band uplink to a geostationary satellite. The link uses circular polarisation at 27.5 GHz and operates at an elevation angle of 28°. Figure 5.4 illustrates the fade distribution calculated over the three year simulation period compared to the hydrometeor fade prediction of Rec. ITU-R P.618-10. Given the year-to-year variation observed over the three years, the differences between the distributions at time percentages above 0.01% are within expected bounds. The observed 0.01% exceeded rain rate is an input parameter into the P.618 model and so the good agreement at 0.01% is expected. The deviation at lower time percentages could be an inconsistency between the terrestrial and Earth-Space models P.530 and P.618, as the terrestrial link distributions were much closer at these time percentages. Alternatively, the deviation could be due to a feature of the small number of extreme events that determine the fade at these low time percentages e.g. the events could have greater rain height that the long-term mean.

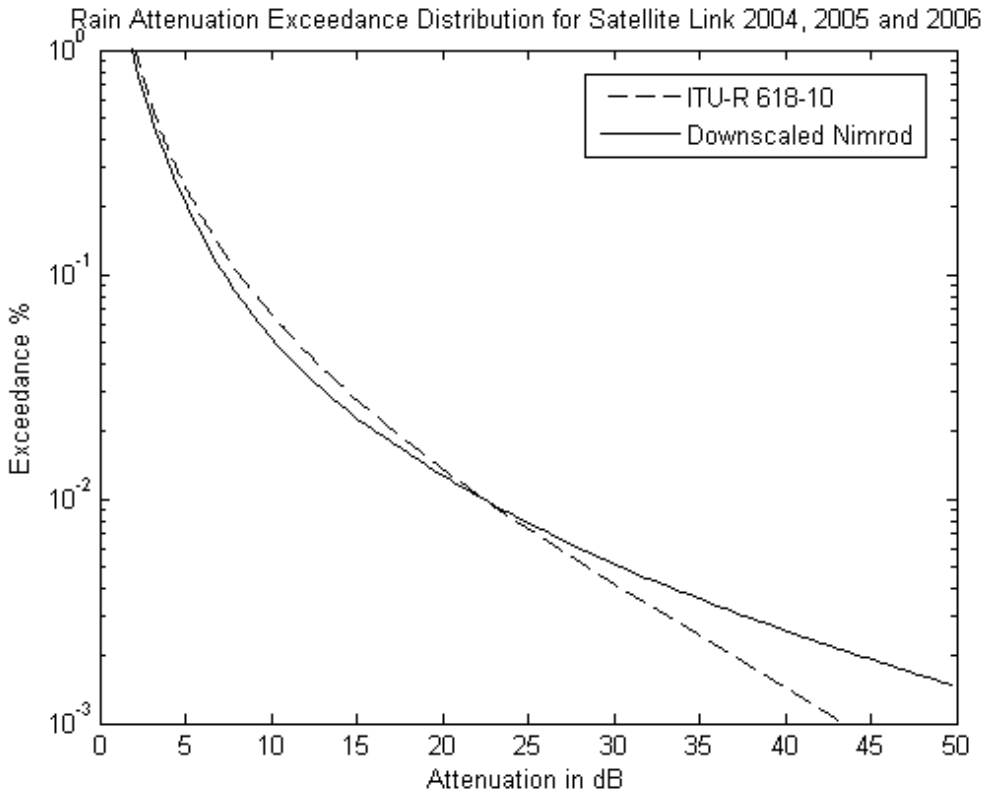

Figure 5.4: Annual distributions of hydrometeor fade for a Ka band uplink to a geostationary satellite from a Chilbolton ground station. Comparisons are between

Rec. ITU-R 618-10 (2009) and the simulation result over the three calendar years 2004 to 2006.

5.3 Validation of Second Order Statistics for Hydrometeor Fade

Optimisation of radio system capacity, quality and reliability require second order statistics such as fade duration and fade slope as stated in ITU Recommendations P.1623-1(2003). These are essential inputs for the design and optimisation of FMTs. The proposed simulator can produce joint time-series of fade for arbitrary networks and so can provide a wide variety of summary statistics.

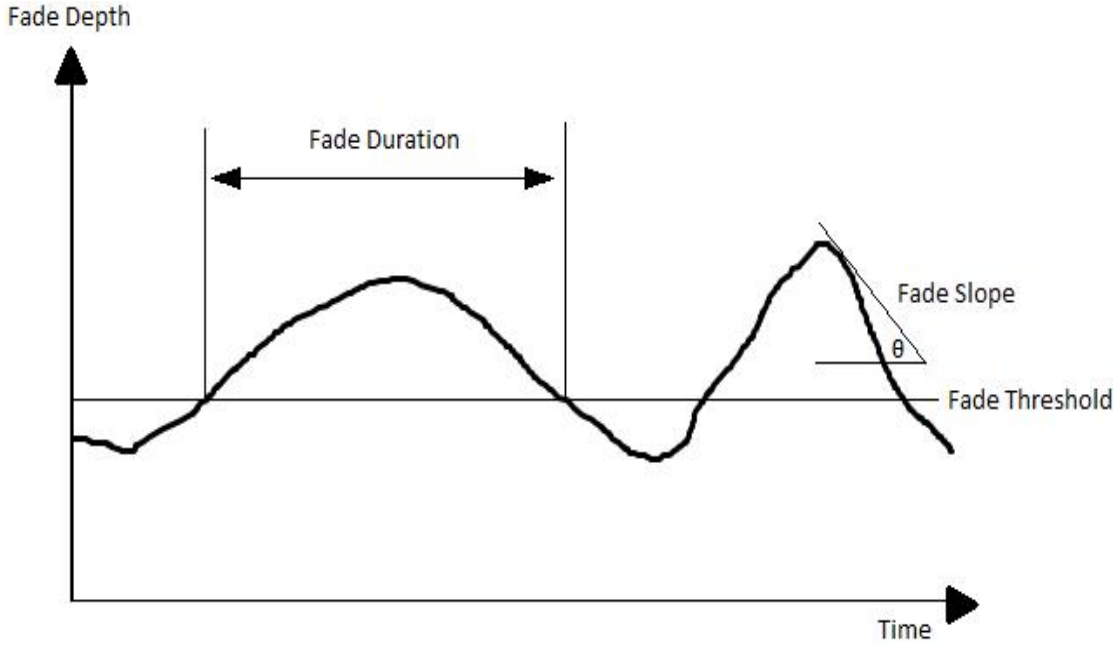

Figure 5.5: Illustrations of Fade Duration and Fade Slope

5.3.1 Fade Duration

Fade duration is defined as the time period that fade exceeds a given attenuation threshold. According to the ITU Recommendations P.1623-1(2003), the distribution of fade durations yields important information on system outage and unavailability and is one of the vital parameters which determine the choice of forward error correction codes and modulation schemes for satellite communication systems.

ITU Recommendations P.1623-1 (2003) provides a prediction model for the average annual distribution of fade durations for Earth-Space links. The fade duration model consists of a log-normal distribution for long fades and a power-law function for short fades and is valid for durations longer than one second. Currently, the fade duration model in the ITU-R can only be applied to Earth-Space links operating between 10 to 50 GHz with elevation angles between 5^{o} to 60^{o}. Figure 5.6 illustrates the simulated fade duration distributions for a Ka band (27.5 GHz), London to geostationary satellite link for fade threshold levels of 6, 11 and 21 dB. These correspond to the Rec. ITU-R P.618-10 (2009) predicted fades approximately at time exceedances of 0.15%, 0.03% and 0.01% respectively. Figure 5.6 compares the GINSIM simulated results, for the years 2004, 2005 and 2006; with the P.1623-1 model predictions.

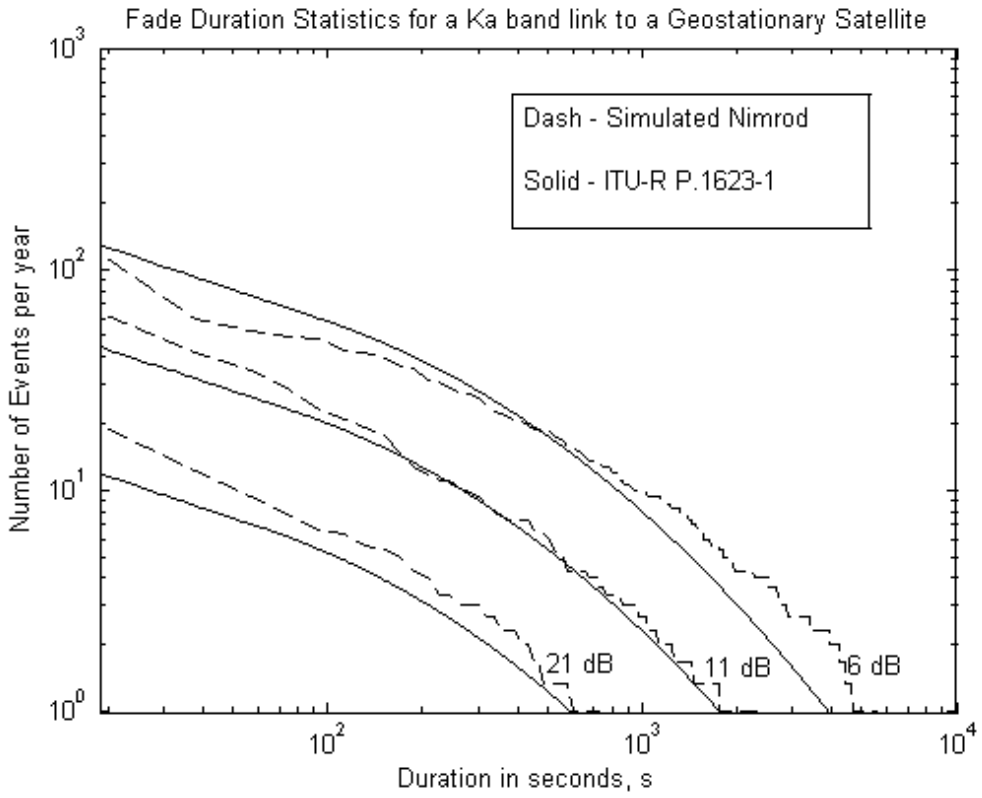

Figure 5.6: Comparison of annual fade duration statistics from the Rec. ITU-R P.1623-1 (2005) model and from simulation.

Figure 5.6 describes that the fade durations from the simulated Nimrod data are

consistent with the fade durations model from P.1623-1 including for lower threshold level (6 dB), middle (11 dB) and the higher level (21dB).

The GINSIM simulated fade duration distribution for a fade threshold of 11 dB for each calendar year and averaged the three years, are illustrated in Fig. 5.7. The large year to year variation suggests that the differences between the three-year simulation results and the model are not significant.

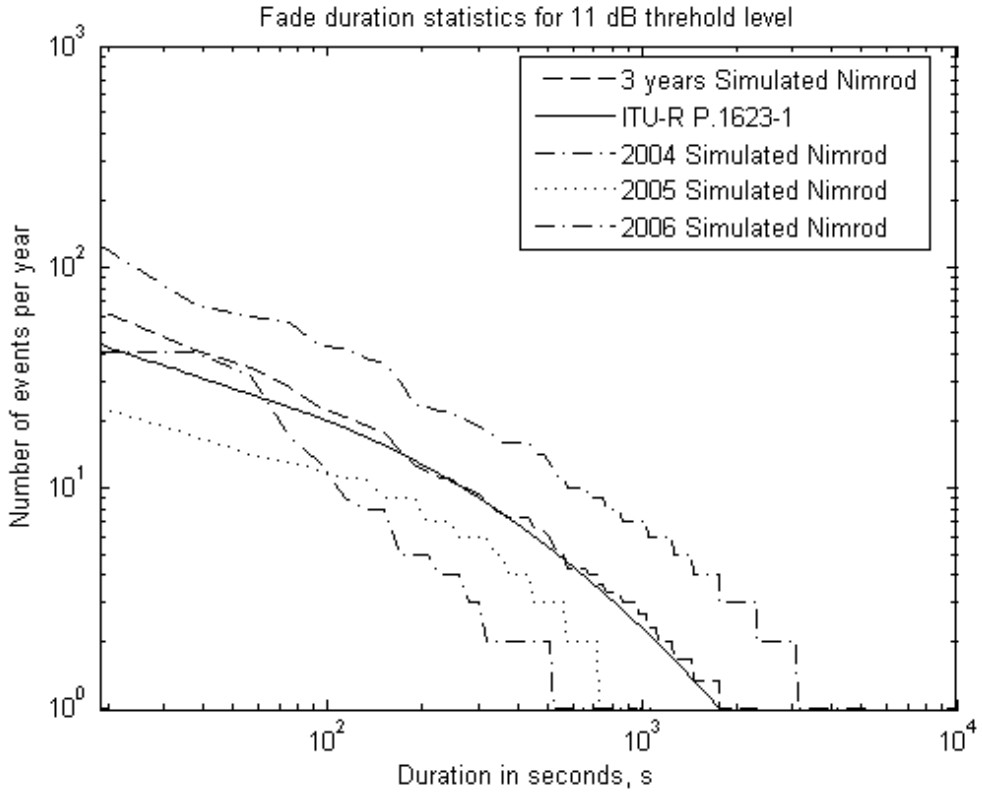

Figure 5.7: Comparison of annual fade duration statistics from Rec. ITU-R P.1623-1 (2005) model and simulation for the three years 2004 to 2006 at 11 dB threshold level.

5.3.2 Fade Slope

Fade slope is defined as the rate of change of attenuation with time. Fade slope is another important parameter when designing FMTs at it constrains the time in which a system needs to react to increasing fade. Information on the fade slope of the signal

can be used for short term prediction of the propagation conditions and the optimisations of FMTs. The fade slope model in Rec. ITU-R P.1623-1 (2005) is applicable to satellite links with elevation angles between 10 and 50 degrees and frequencies from 10 GHz to 30 GHz. The distribution of fade slopes is strongly dependent upon the fade measurement integration interval. Typically, short integration intervals yield more extreme fade slopes. The integration interval is chosen to typical FMT response time and to focus on fade mechanisms with correlation intervals of this order or longer. An integration interval of 10 s is often used as this yields the variation due to rain but greatly reduces the effects of scintillation. Rather than box-car integration, many systems sample a low-pass filtered fade time-series and this can be parameterized by the 3 dB cut-off frequency.

The following equation shows how the fade slope ¸ was derived from samples of attenuation data:

$$¸(i) = \frac{A(i+1) - A(i-1)}{2\Delta t} \quad \text{dB/s} \tag{5.1}$$

where A is the attenuation level, i is the sample index and Δt is the sampling period.

$$p(¸ / A) = \frac{2}{®\pm_{¸}\left(1+\left(\frac{¸}{\pm_{¸}}\right)^2\right)^2} \tag{5.2}$$

Equation (5.2) is the conditional fade slope probability density model provided by Rec. ITU-R P.1623-1 (2005). The only parameter that is required is the standard deviation of the conditional fade slope, $\pm_{¸}$. Equation (5.3) shows how to estimate $\pm_{¸}$

.

$$\pm_{¸} = SF(f_B, \Delta t)A \quad \text{dB/s} \tag{5.3}$$

Function F gives the dependence on the time interval length and the 3 dB cut-off frequency of the low pass filter and can be calculated in (5.4):

$$F(f_B, \Delta t) = \sqrt{\frac{2®^2}{(1/f_B^b + (2\Delta t)^b)^{1/b}}} \tag{5.4}$$

where A is the attenuation level (dB);

f_B is the 3 dB cut off frequency of the low pass filter (Hz);

Δt is the time interval used to calculate the fade slope;

b = 2.3

S is a parameter that depends on elevation angle and climate. For Europe, the average of S is 0.01;

Figures 5.8 and 5.9 illustrate the fade slope probability density function, conditional upon the fade level, for the notional Ka band link between London and a geostationary satellite with 0.02 Hz for f_B and the time interval or Δt is 37.5 seconds. Figure 5.8 shows the conditional fade slope distribution predicted by GINSIM at fade threshold levels of 1, 3 and 10dB, compared with the Rec. ITU-R P.1623-1 (2005) fade slope model. The results shows reasonable agreement between the GINSIM simulation and the P.1623-1 model at all the tested fade threshold levels. The low numbers of fade samples at the target fade thresholds yields large uncertainty in the conditional distributions and sizable fluctuation in the simulated distribution. However, the simulated and model distributions are very similar in shape, at all fade levels, and fluctuations in the GINSIM distributions are around means close to the ITU-R model values.

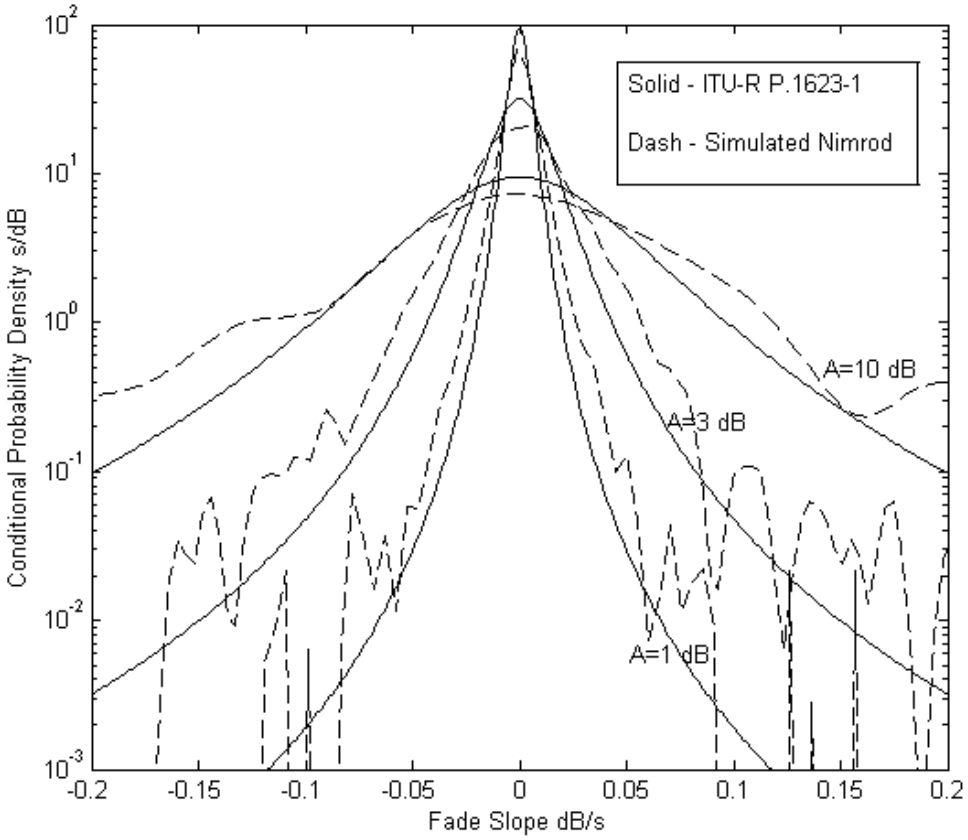

Figure 5.8: Comparison of annual fade slope statistics from Rec. ITU-R P.1623-1 (2005) model and simulated Nimrod data at 1, 3 and 10 dB threshold levels

The predicted distribution provided by P.1623-1, the distributions measured over three individual years and the average distribution, are compared in Figure 5.9. A threshold at the 0.01% exceedance levels has been used. The ITU-R model is well within the range of results from the three individual years of GINSIM simulation and is consistent with the model. The deviation is within that expected given year-to-year variation.

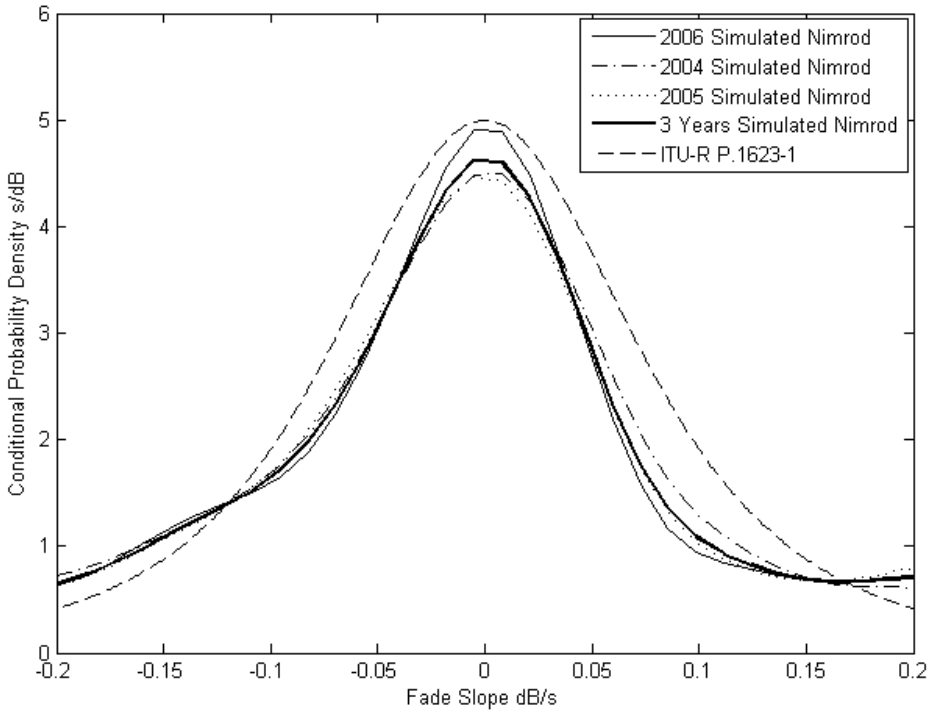

Figure 5.9: Annual fade slope distribution at approximately 0.01% fade level or 19 dB, for a Ku band geostationary Earth-Space link, as predicted by Rec. ITU P.1623-1 (2005) and determined from three years of simulation.

Chapter 5 Summary

The GINSIM system has been verified by simulating a variety of notional terrestrial and Earth-Space links, situated in the southern UK. The simulated distributions of fade and fade duration and fade slope have been compared to ITU-R models and agreement has been demonstrated, within the limits of the three-year simulation period and the expected accuracy of the prediction models. Comparison with ITU-R models is a fairly weak as only average annual distributions are compared. The system requires further validation of time-series, in particular with the first and second order statistics of measured terrestrial and Earth-Space links which will be shown in the next chapter.

CHAPTER 6 VALIDATION WITH MEASURED TERRESTRIAL AND EARTH-SPACE LINKS

In the previous chapter, simulation results from GINSIM are compared to ITU-R model predictions, including the annual fade distributions of terrestrial and Earth-Space links and the average annual second order statistics of fade duration and slope. The simulation results show good agreement with the ITU-R models. However, comparison with the ITU-R models is a weak test as the models themselves are only adequate for the regulation and coordination of radio networks and for assigning fixed fade margins and offer limited use for the design of fade mitigation techniques (FMTs) and for the design and optimization of Dynamic Network Management (DNM) systems. Therefore, further validations of time-series are required. This chapter presents comparisons between GINSIM simulations and measured radio link fade time-series. Joint fade distributions for pairs of terrestrial and Earth-Space links and these are compared with measured results from links in the southern UK and Scotland. The experimental setup, output expectations, the results and discussions are described further in the following sections.

6.1 Measurement data

All the measured link fade data that will be used for validation were obtained from the British Atmospheric Data Center (BADC). Earth-Space fading was measured using a Global Broadcast Service (GBS) beacon operating at 20.7 GHz. Ground station receivers were operated by Rutherford Appleton Laboratory and had a dynamic range of approximately 13 dB. Data are available from three ground receivers, two in the southern UK and one is Scotland. Sparsholt (51°04'N, 01°26'W) provided data spanning October 2003 to March 2005, Chilbolton (51°08'N, 01°26'W) provided data from August 2003 to March 2005; while the Scottish data from Dundee (56.45811°N, 2.98053°W) spans February 2004 to August 2006. The collection and analyses of these data are described in Callaghan et al. (2008). Figure 6.1 illustrates

the geometry or positions of the measured radio links in south of UK.

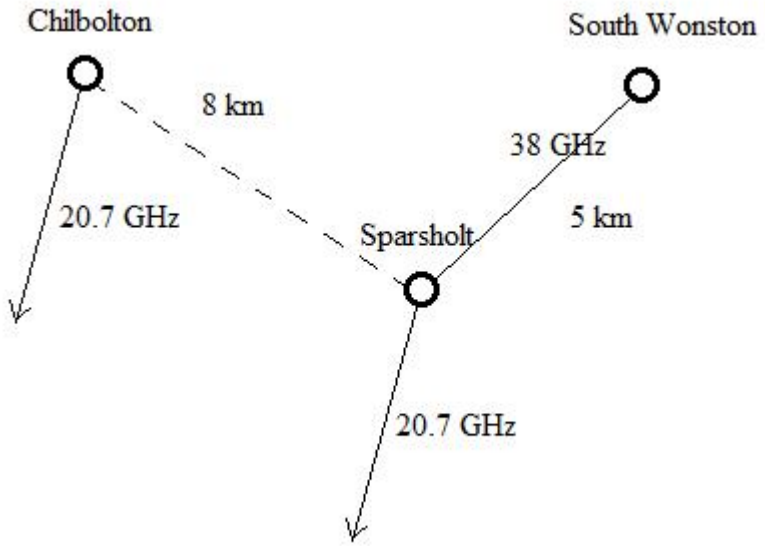

Figure 6.1: Geometry of the measured radio links in south of UK

Chilbolton and Sparsholt data will be examined to determine the accuracy of simulated, individual and joint fade distributions. In addition, diversity gain from simultaneous use of the two ground stations will be simulated and compared to measured distributions. Fade data is also available from a terrestrial link, Sparsholt to South Wonston (51.0838°N, 1.3908°W), with length of 5 km operating at 38 GHz with data starting in October 2002 and ending in March 2005. These data allow joint distributions of fade on convergent Earth-Space and terrestrial links to be compared to distributions predicted by the GINSIM.

The resolution of Nimrod data changed in April 2004 and the GINSIM uses the newer, finer resolution. For this reason, only data collected after April 2004 is used in the following analyses. Furthermore, it should be noted that the downscaling does not attempt to reproduce the fine-scale, spatial-temporal rain field variation that existed at the time. It produces fine-scale rain fields that are consistent with an expected statistical model of spatial-temporal variation. For this reason, direct comparison between measured and simulated fade time-series, over the same period of time, have similar coarse features but the fine-scale features are not expected to be similar.

However, long term first and second order statistics derived from measurements and simulation should be drawn from the same underlying distributions.

6.2 Comparison of simulated and measured fade data

In this section, measured and simulated, joint fade distributions are compared. The network examined consists of the terrestrial 38 GHz link and the Earth-Space 20.7 GHz link that converges at Sparsholt. Measured and simulated fade time-series are collected for the same one-year period: April 2004 until the end of March 2005. The fade data archived on the BADC is relative to a notional clear-sky level. The measured Earth-Space data exhibits Gaussian noise with a standard deviation of approximately 1 dB and some drift around the 0 dB reference level. For the comparisons in this section, Gaussian noise with a standard deviation of 1 dB has been added to the GINSIM simulated fade time-series and the fade capping effect of the 13 dB receiver dynamic range has been added. The simulated outputs are compared with the measured fade data in terms of annual fade distributions for terrestrial and Earth-Space links, joint exceedance statistics between terrestrial and Earth-Space links in Sparsholt, site diversity between two Earth-Space base stations and auto covariance. The outputs from the simulation are expected to be consistent (particularly at higher exceedance level) with the measured radio links for annual fade distributions including the joint distributions and the site diversity comparison. For auto covariance experiment, the simulated outputs of terrestrial and Earth-Space links may not be consistent with the measured links due to the presence of scintillation and multipath on measured links. The following sections contain the results including the discussions.

6.2.1 Distributions and Joint Distributions of Fade

The joint fade distribution has then been estimated form the joint 2D histogram of measured and simulated fade data. Figure 6.2 shows fade distributions of the two links, both measured and simulated, independently. These results agree within

expected simulation accuracy. Differences between measured and simulated distributions can be due to a range of effects. Fading due to fog causes low fade levels for long periods on the terrestrial link. Both the terrestrial and Earth-Space links are affected by statistical variation of the specific attenuation – rain rate relationship which is known to vary by a factor of two for the same rain rate. Fade on the Earth-Space link is also affected by the incidence of convective rain. The simulator assumes a vertically stratified atmosphere and convective events can cause significantly more fade than expected. In this case, the limited dynamic range removes extreme fade events. Before introducing the effects of the limited 13 dB dynamic range of the receiver, the simulated fade reached 30 dB on the Earth-Space link at 0.001% of time. This is more plausible than the measured data.

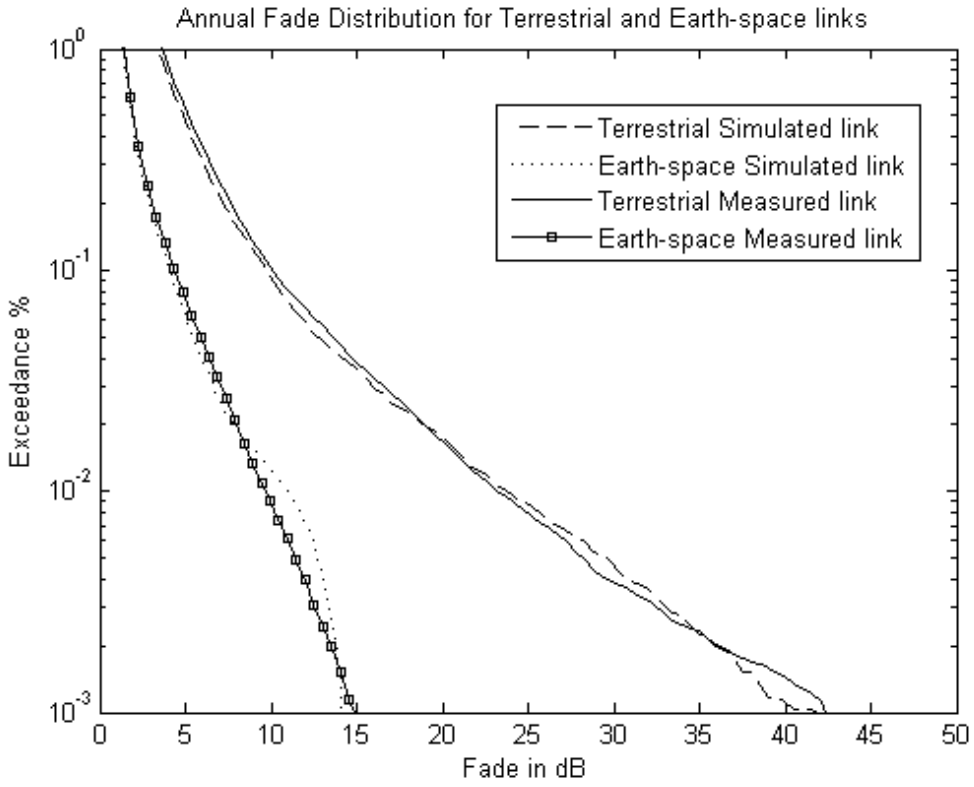

Figure 6.2: Average annual fade distribution for the Global Broadcast Service (GBS) Earth-Space link to Sparsholt and terrestrial link (South Wonston - Sparsholt), both measured and simulated, from April 2004 – March 2005.

Figure 6.3 illustrates the 2D, joint fade exceedance statistics for the two links. For

exceedance times greater than 0.01% of time, the joint statistics agree very well. At lower time percentages the contours are very uncertain due to the poor sampling statistics.

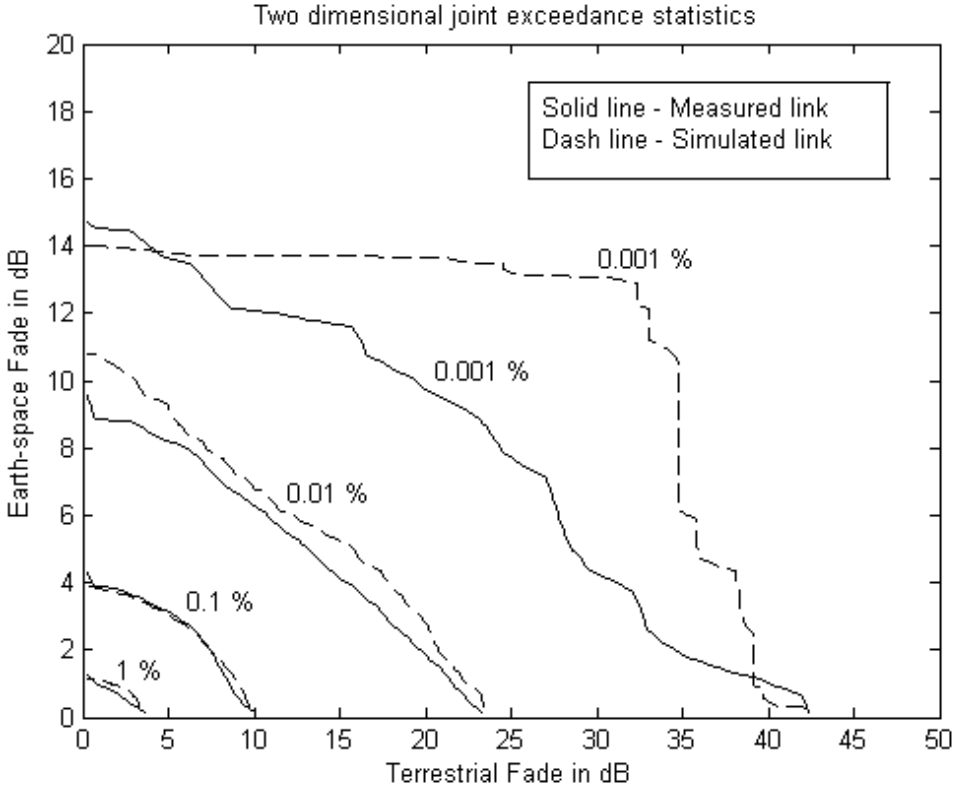

Figure 6.3: Joint fade exceedance statistics for the Earth-Space and terrestrial links from April 2004 – March 2005.

6.2.2 Distributions of Fade at different spatial and temporal scales

In this section, we test the ability of the simulator to produce annual fade distributions at different spatial and temporal scales with the same experimental setup in section 6.2.1. The motivation for these comparisons is to study on whether the downscaling algorithms managed to improve the output results in terms of distributions (especially dealing with different spatial scales). The comparisons will include various ranges of spatial-temporal scales from the original spatial and temporal resolutions (1 km and 5 minutes) to the resolutions of the final downscaled data (125 meters and 18.75 seconds) that are used for validations in Chapter 5 and 6. The simulator only downscaled to these specific spatial and temporal scales due to huge computational

resources that are required to maintain smaller spatial and temporal scales of downscaled data. The Nimrod rain maps are also downscaled at 500 and 250 meters spatially and 1 min temporally for the comparison purposes. I expect lower fade distributions for spatial scales that are larger than 125 meters since smaller spatial integration volume tend to have higher rain rates, see Zhang (2008). For annual fade distribution comparison at temporal scales, we expect all the distributions to look similar regardless at any temporal scales since interpolation algorithm is designed to preserves the distribution statistics, Zhang (2008). The following figures illustrates the annual fade distribution for terrestrial (Figure 6.4) and for Earth-Space link (Figure 6.5) at different spatial scales with fixed temporal scale at 18.75 seconds.

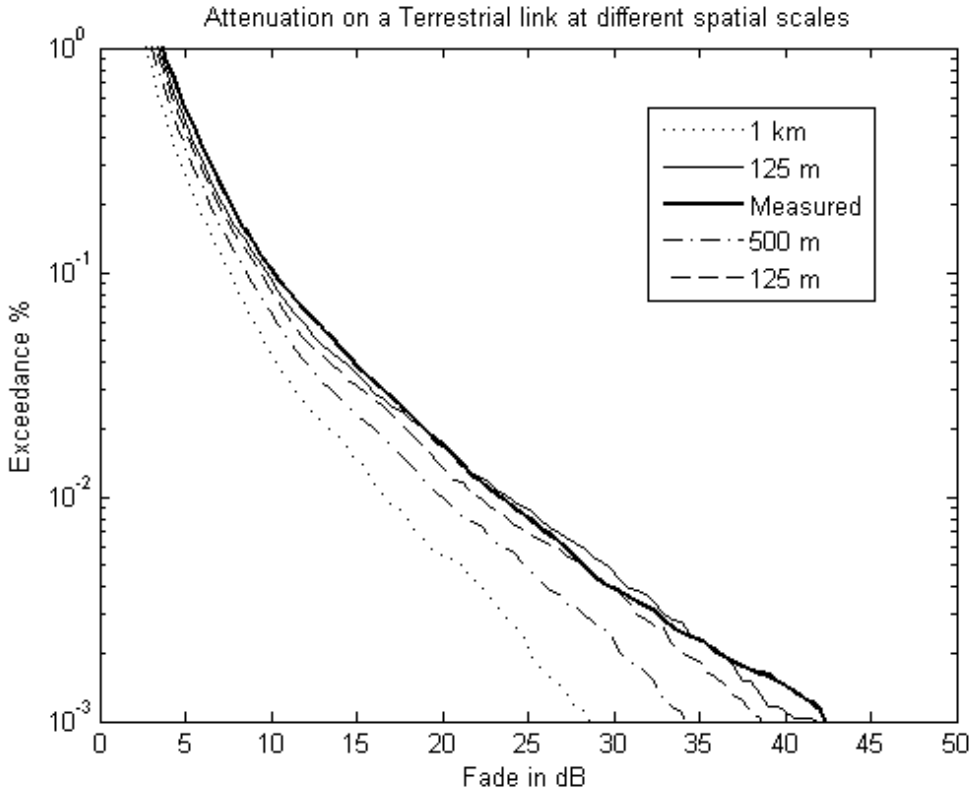

Figure 6.4: Average annual fade distribution for terrestrial link (South Wonston - Sparsholt) with 1 km scale to 125 meters from April 2004 – March 2005.

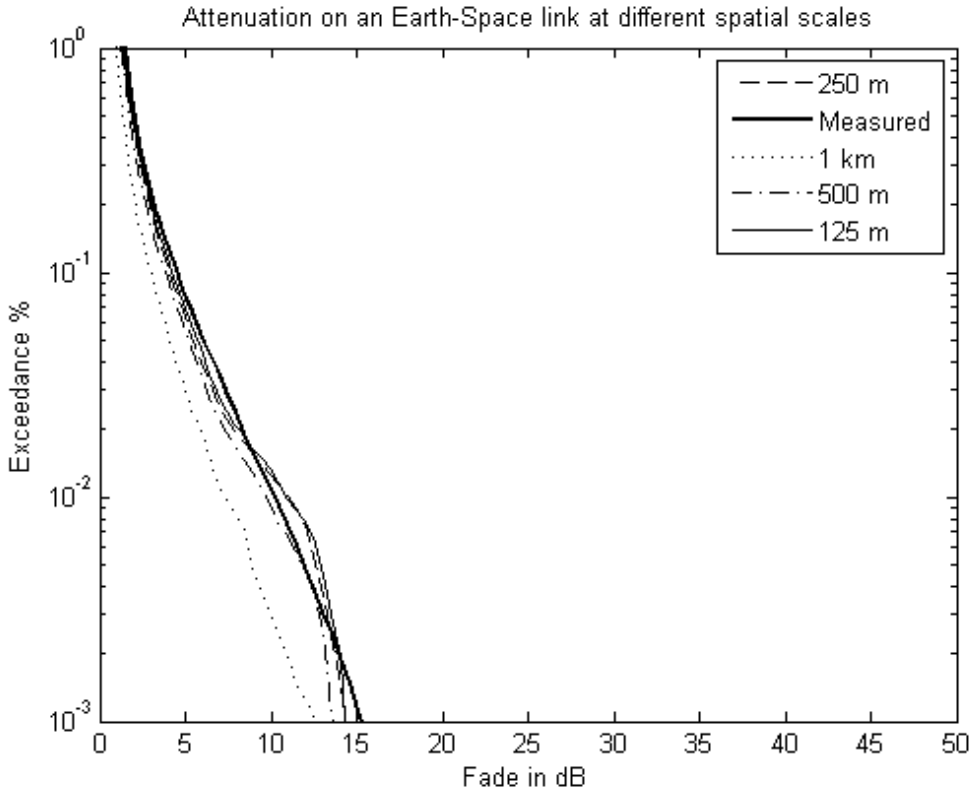

Figure 6.5: Average annual fade distribution for Earth-Space link (Sparsholt) with 1 km scale to 125 meters from April 2004 – March 2005.

Figure 6.4 and 6.5 illustrate that the downscaling algorithms manage to improve the distribution results. As expected, the simulated output results becoming more consistent with the measured link as the spatial scales decreasing from 1 km to 125 meters. The following figures illustrates the annual fade distribution for terrestrial (Figure 6.6) and for Earth-Space link (Figure 6.7) at different temporal scales with fixed spatial scale at 125 meters.

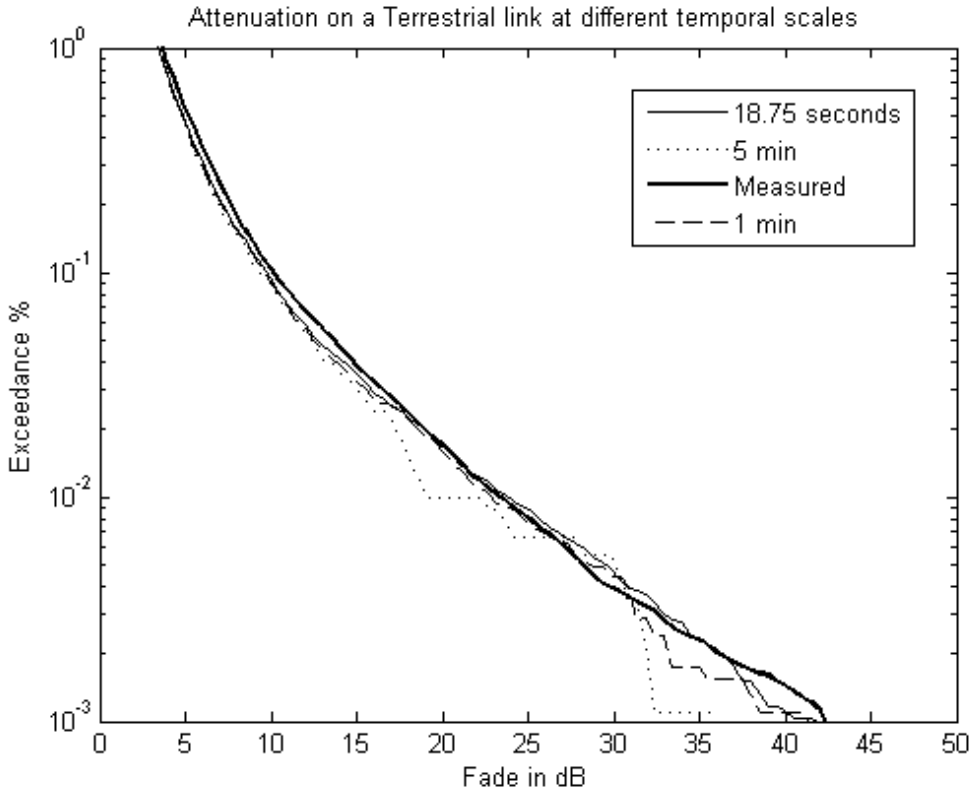

Figure 6.6: Average annual fade distribution for terrestrial link in Sparsholt from 5 min to 18.75 seconds (April 2004 – March 2005).

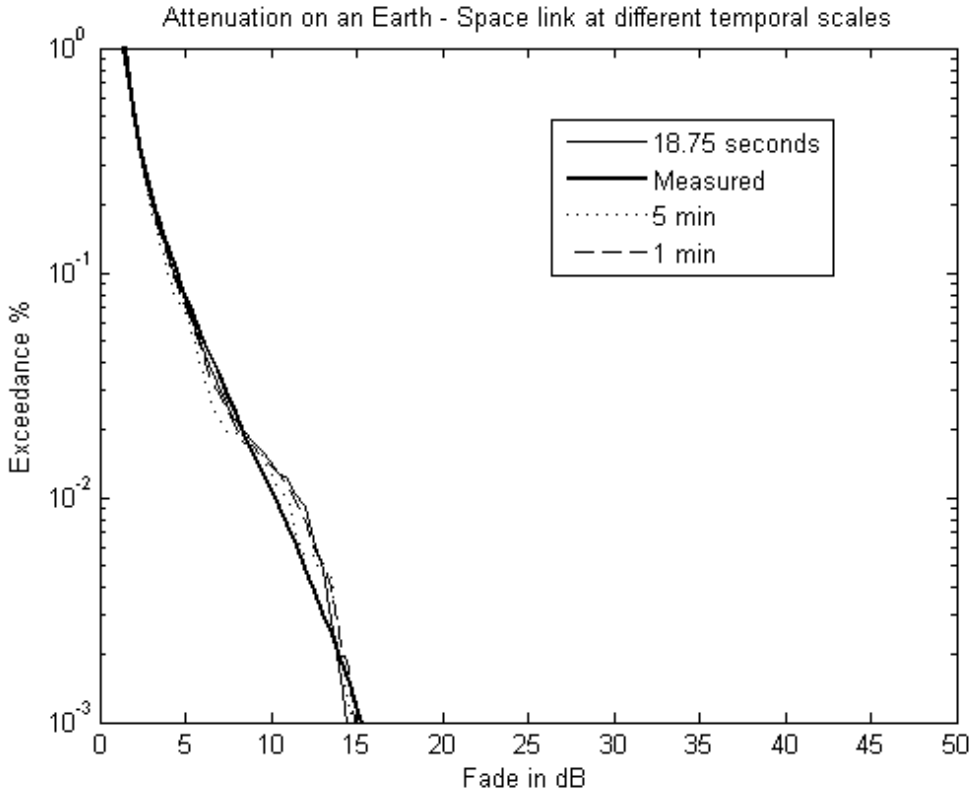

Figure 6.7: Average annual fade distribution for Earth-Space link in Sparsholt from 5

min to 18.75 seconds (April 2004 – March 2005).

Figure 6.6 and 6.7 illustrates that the distributions are consistent with one another as expected despite at different temporal scales. Based on the results from Figure 6.4, 6.5, 6.6 and 6.7, we can conclude that the simulator managed to produce results as expected and improves the distribution results (in the case with the spatial scales).

6.2.3 Site Diversity Comparison

In this section, we test the ability of the simulator to predict site diversity performance. The two ground stations at Sparsholt and Chilbolton are approximately 8 km apart and so have very similar fade distributions. However, if both ground stations can be used as a diversity receiver, then the effective fade is the instantaneous minimum of the fade experienced by the two links. The distribution of instantaneous minimum fade is important when evaluating the site diversity performance.

Figure 6.8 illustrates the measured and simulated fade distributions for the two Earth-Space links, derived from data spanning April 2004 till end of March 2005, showing good agreement. Also illustrated are the measured and simulated, minimum joint fade distributions. These show excellent agreement down to 0.01% of time. Deviation below this time percentage may be due to the movement of small intense rain events such as convective events that are not sufficiently described or captured by the 5 minute sample interval of the Nimrod data, or may just reflect large uncertainty due to low numbers of samples.

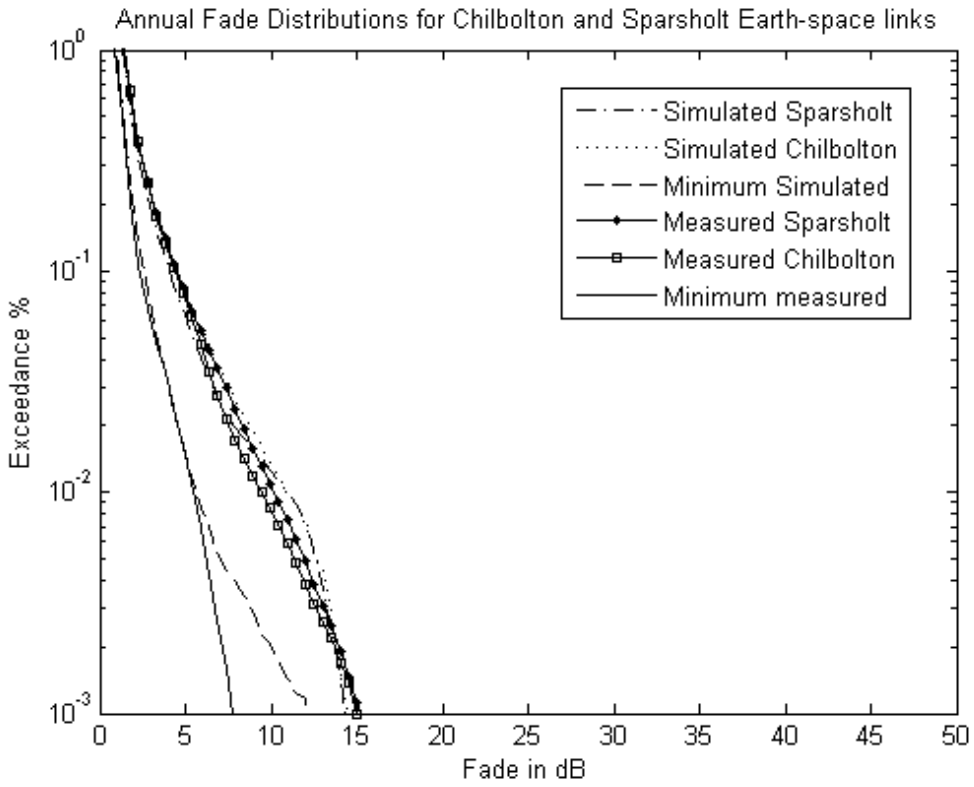

Figure 6.8: Annual single and joint statistics for Chilbolton and Sparsholt from April 2004 – March 2005.

Figure 6.9 illustrates the individual fade distributions, and the instantaneous minimum fade distribution, for the Sparsholt receiver and the Scottish receiver in Dundee. The measured and simulated results are in broad agreement. The Dundee link experiences higher fade levels than the simulation predicts at time percentages above 0.02% of time, possibly due to the high incidence of light rain that is poorly determined by Nimrod radars. Due to the large spatial separation between Sparsholt and Dundee, approximately 500 km, the fade experienced by these links is largely uncorrelated and so considerable diversity advantage exists.

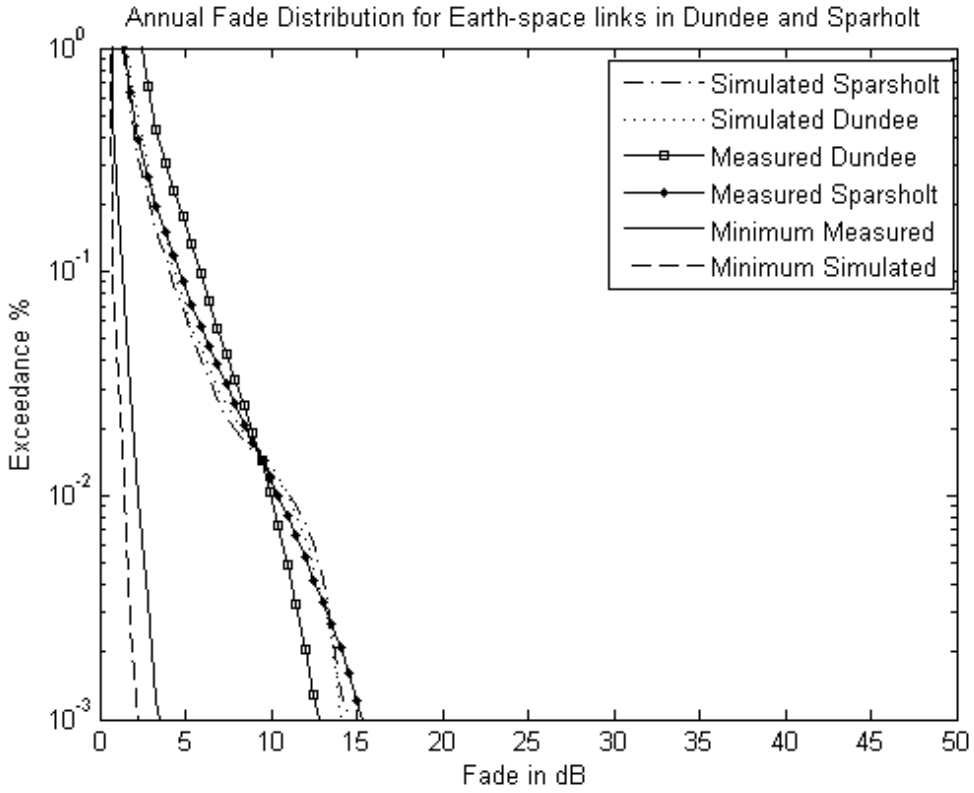

Figure 6.9: Annual single and joint statistics between Dundee and Sparsholt from April 2004 – March 2005.

Figure 6.10 and 6.11 shows the diversity gain performance, both simulated and measured, for the Sparsholt and Chilbolton Earth-Space links. According to ITU-R P.618, diversity gain is defined as the difference of attenuation, in dB, between the single site and joint site for the same percentage of time. The measured and simulated diversity gains are in excellent agreement.

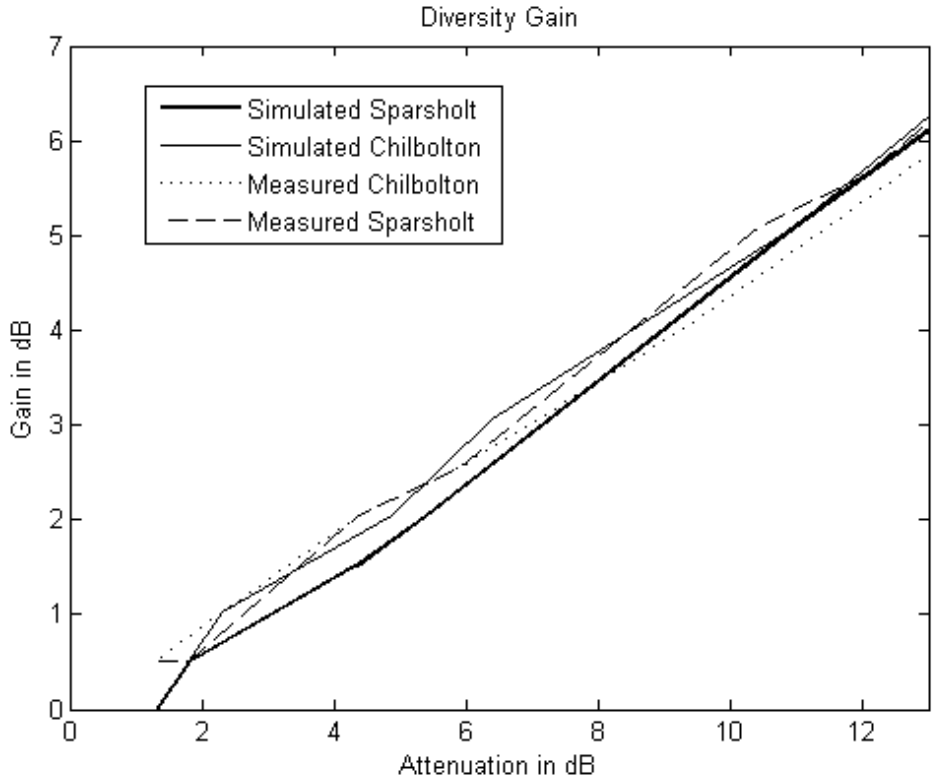

Figure 6.10: Diversity Gain for two Earth-Space links in Sparsholt and Chilbolton, April 2004 – March 2005.

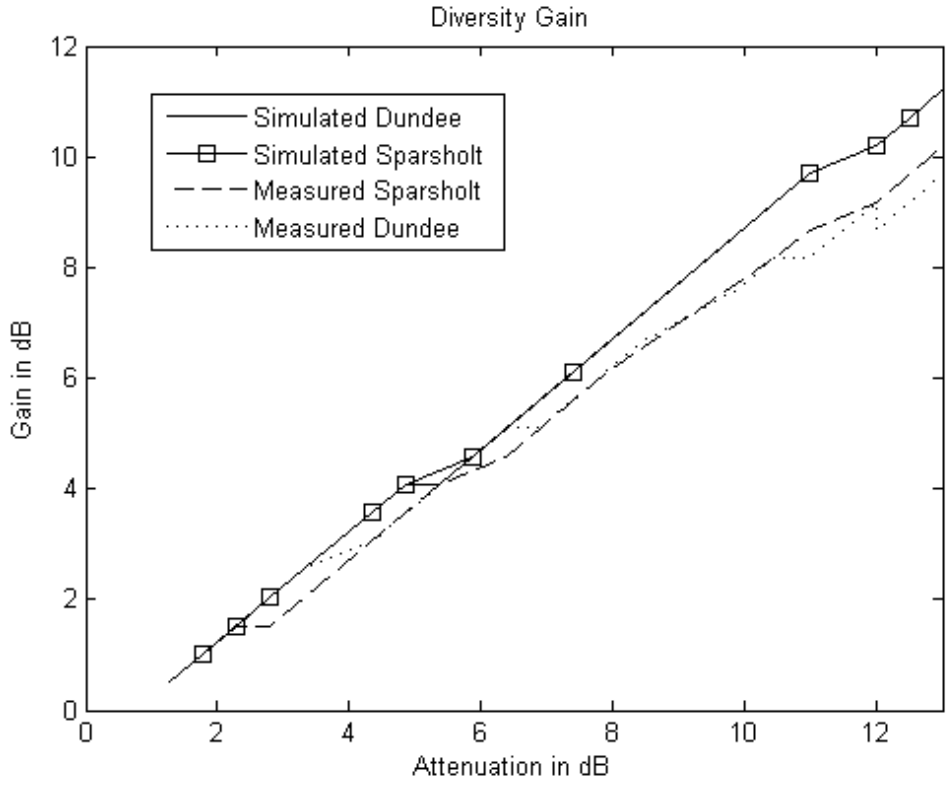

Figure 6.11: Diversity Gain for two Earth-Space links in Sparsholt and Dundee, April 2004 – March 2005.

6.2.4 Validation of Autocovariance

Autocovariance is defined as the covariance of the variable with itself or the variance of the variable against a time-shifted version of itself. Autocovariance is given by:

$$C_{xx}(t,t+k) = E(X_t - \overline{X})(X_{t+k} - \overline{X}) \tag{6.1}$$

where *E(Y)* is the expected value of the random variable *Y*, X_t is the variable at a time t and $\overline{X}$ is the mean of the variable. Normalised autocovariance, known as the autocorrelation is formed by dividing the autocovariance C by the variance $\pm^2$. The autocorrelation is restricted to the closed interval [-1,1]. Autocovariance and autocorrelation are a mathematical tools frequently used in signal processing for analysing functions or series of values, such as time domain signals. The autocovariance function of a fade time-series contains a lot of information on the fade dynamics and, with other information, can be related to the fade slope and fade duration statistics. The autocovariance can be used in the development of FMTs. In this Section, autocovariance functions derived from the measured and simulated fade time-series are compared.

As with fade slope and duration, autocovariance is sensitive to sample integration time, non-stationarity and the presence of noise. To allow direct comparison, measured fade time-series are integrated to a sample period of 18.75 seconds, the same sampling time of the downscaled rain maps from GINSIM. The measured Earth-Space fade time-series experience random variation with a standard deviation of about 1 dB during clear-sky conditions; due to a combination of multipath, interference and equipment noise. In the UK rain occurs for approximately 5% of an average year and so the autocovariance of the random clear-sky variation can overwhelm rain fade autocovariance, despite the lower fade magnitudes, due to the much greater period on incidence. To address this, before estimation of covariance

both measured and simulated fade time-series are numerically processed so that any fades less than 1.5 dB, and all enhancements, are replaced by zero fade. Figures 6.12, 6.13 and 6.14 compare measured and simulated autocovariance functions.

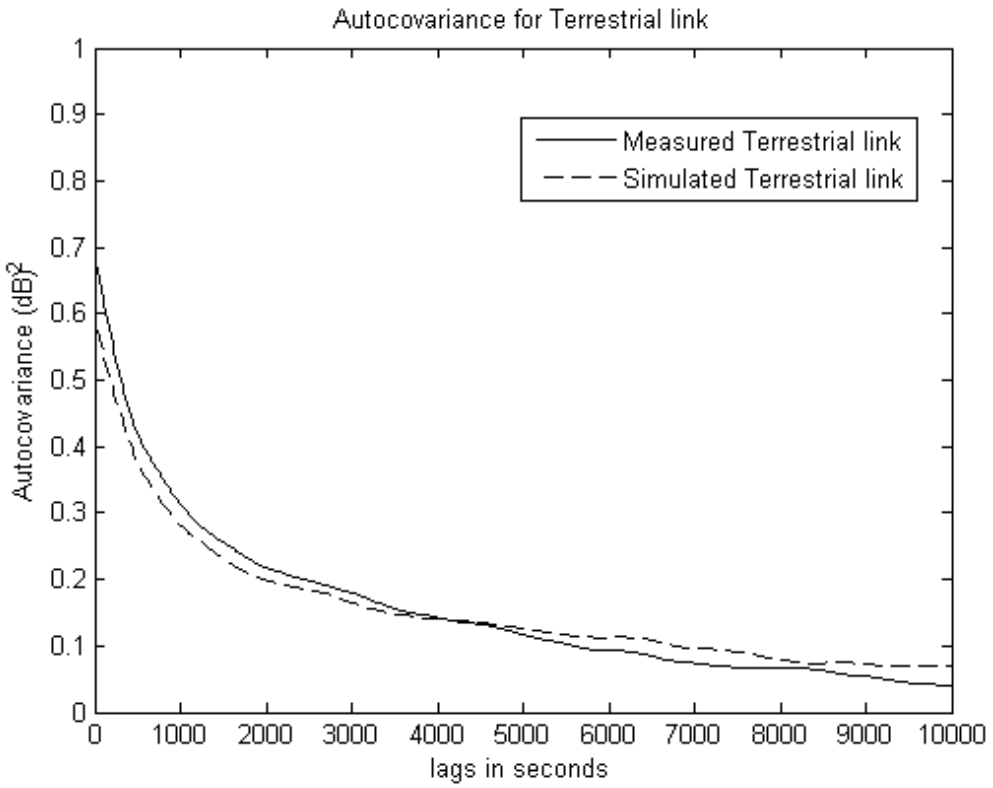

Figure 6.12: Autocovariance of the measured measured terrestrial link fade time-series compared to the GINSIM prediction.

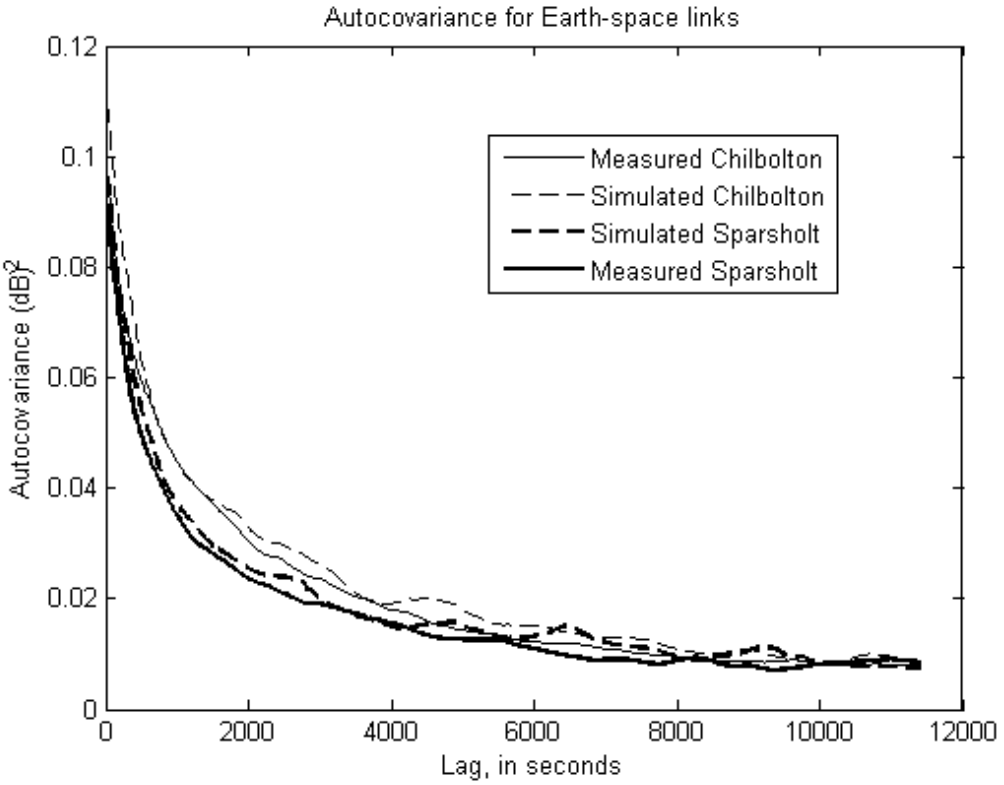

Figure 6.13: Autocovariance function statistics of the measured Earth-Space link fade time-series compared to the GINSIM prediction.

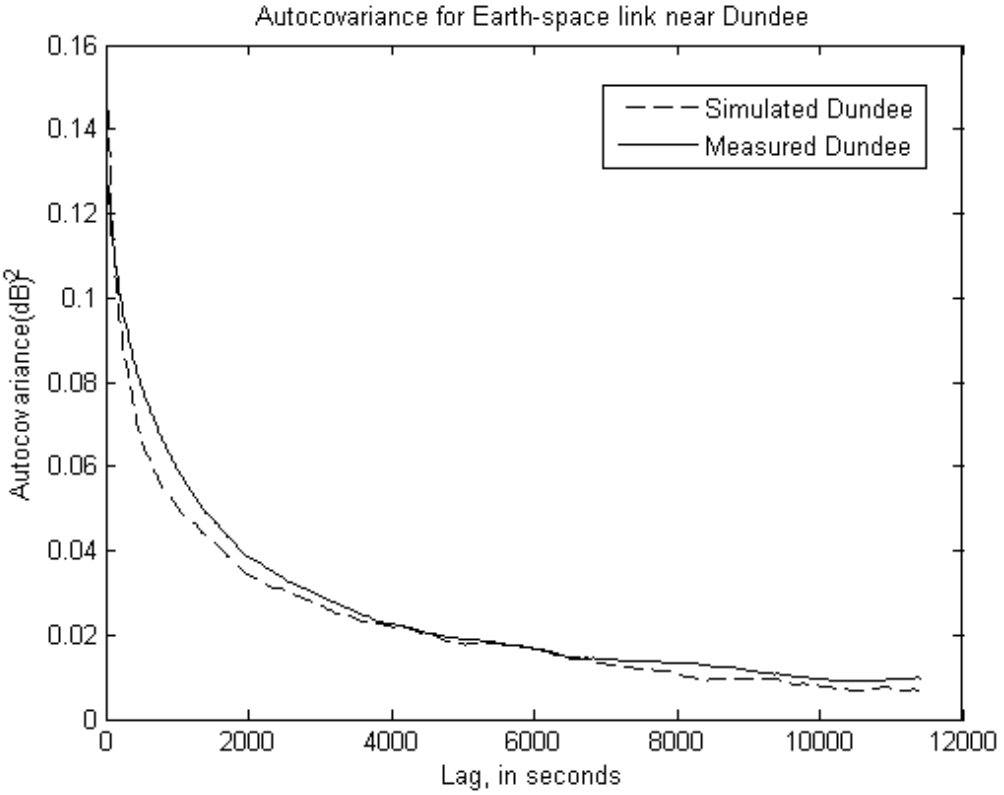

Figure 6.14: Autocovariance function statistics of the measured Earth-Space link fade

time-series compared to the GINSIM prediction.

Some systematic variation is to be expected between measured and simulated autocovariance due to non-hydrometeor fade mechanisms e.g. variation in absorption by atmospheric gasses, multipath, scintillation etc. Despite this, measured and simulated results show useful agreement.

Chapter 6 Summary

GINSIM time-series have been subjected to validation tests by comparison with measured link data. GINSIM has produced joint fade time-series with very similar joint fade distributions to measured results from pairs Earth-Space links and the combination of an Earth-Space and terrestrial link. Joint fade distributions allow the performance of multi-hop and route diverse networks to be predicted. The simulator has also reproduced measured fade autocovariance for both terrestrial and Earth-Space links. The validation evidence provided in this chapter supports the conclusion that GINSIM can produce joint hydrometeor fade time-series with the correct first and second order statistics. There are several reasons not to expect the simulations to exactly match measured results. The downscaling of rain fields is a statistical process that yields different results each time and can produce arbitrarily intense rain cells with finite probability. Furthermore, the simulator does not currently attempt to model non-hydrometeor fading mechanisms, which dominate for 95% of the time.

The simulator has only been tested against data acquired in the UK. Further work is required to verify its performance in other regions. As composite rain radar images spanning Europe become available from the OPERA project, with consistent quality, this validation will be performed. In particular, better data position information is required.

CHAPTER 7 CONCLUSIONS AND FUTURE OUTLOOK

This thesis is focused on the development of a new network fade simulation tool called GINSIM. GINSIM is a network fade simulation tool that can produce joint fade time-series for arbitrary networks of SHF and EHF radio links, with a temporal resolution adequate for the development and optimization of dynamic resource management systems. GINSIM operates by overlaying networks onto specific attenuation fields derived from the numerical downscaling of recognized databases of coarse-scale meteorological fields, particularly rain rate.

The use of newly available, historical databases of Nimrod (UK coverage) and OPERA (Europe coverage) composite rain fields have allowed the application area to be greatly increased so it now spans the UK and, subject to verification, most of continental Europe, (Paulson and Basarudin, 2011). The OPERA projects produces composite rain field images with a resolution of 1 km, every 5 minutes, based on a large number of rain radars operated by European national meteorological agencies. The downscaling methods developed for the HRFNS, Zhang (2008), have been adapted to the finer temporal sampling and coarser spatial integration of the Nimrod and OPERA data compared to CRIE data. Furthermore, more sophisticated descriptions of advection, applicable over much larger areas, have been developed. The downscaling of rain fields, both by disaggregation and interpolation, has been verified by comparison with ITU-R models and rain gauge data.

GINSIM is an extension to the HRFNS enabling the simulation of joint fade time-series for Earth-Space links and shorter slant paths such as those to HAPs and UAVs. Vertical variation of specific attenuation has been introduced using the Bacon-Tjelta sleet model combined with the assumption of a stratified atmosphere. The system has been tested against both ITU-R models and measured radio link data. Good agreement has been found in both the first and second order statistics i.e. average annual distribution of hydrometeor fade, fade slope and fade duration. Also,

predictions of long term autocorrelation and diversity gain have been verified. Currently GINSIM is one of the most powerful, verified, network fade simulation tool available. However, GINSIM still requires further enhancement and validation. The following sections describe the limitations of GINSIM, recommendations for further development and the future outlook for GINSIM.

7.1 Assumptions, Limitations and Recommendations

7.1.1 Disaggregation

The disaggregation process (Deidda, 1999) was used to refine spatial resolution to smaller integration volumes. In GINSIM, the coarse scale Nimrod rain maps are downscaled from 1 km to 125 metres. In the algorithm, each volume within the rain map is independently downscaled into smaller volumes. Generally, rain rate measurements made with smaller integration volumes tend to exhibit greater variation such as high rain rates. The algorithm is designed to reproduce the multi-scaling exponents measured on CRIE data. However, the undressed cascade is also known to produce non-stationary autocovariance which will not match the autocovariance of rain fields over scales less than 1 km. One way of addressing this would be to disaggregate to smaller voxels and then to re-aggregate onto a translated grid. Hodges et al. (2003) suggest filtering the disaggregated field. Both these approaches greatly reduce the spatial variation in the autocovariance but also change the multi-fractal exponents. These problems will only be apparent at scales below 1 km and, except for very short links, are unlikely to seriously affect the attenuation time-series produced.

7.1.2 Advection

Use of Nimrod or OPERA data allows more accurate modeling of the advection of events between rain field measurements due to the fine temporal sampling. This requires more sophisticated advection transformations for regions larger than

approximately 50x50 km^2. The HRFNS assumed a linear translation between radar scans. The advection vector may be estimated by maximising the cross-covariance for different sub-regions. Currently the complex advection field is produced by smoothly interpolating between region centres. The advection of rain events is known to be highly correlated to the 700 mBar wind vector, Jeannin et al. (2009). This parameter is commonly provided by NWP databases, albeit on quite coarse grids, and could be used to constrain or condition the advection field. Fig 7.1 illustrates a 700 mBar wind vector field from NOAA's NCEP/NCAR Reanalysis I data.

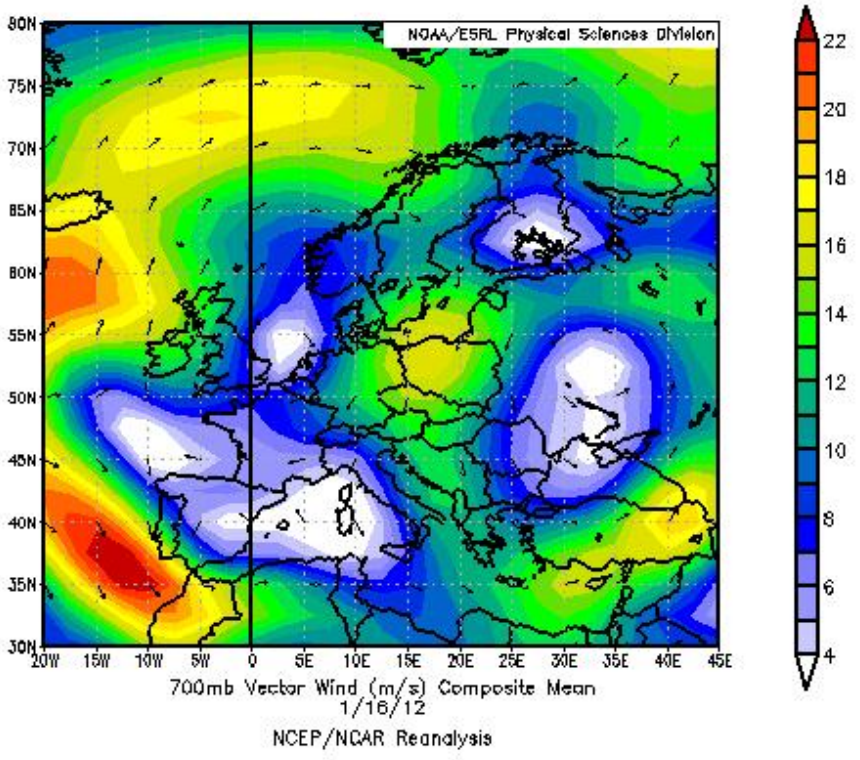

Figure 7.1: Vector wind (m/s) at 700 mBar pressure level. (Courtesy of NOAA)

7.1.3 Specific Attenuation

One of the major assumptions that are made in GINSIM is the use of the Rec. ITU-R P.838-3(2005) model to transform rain rate into specific attenuation, the ¥-R relation. Studies have shown that the specific attenuation can to vary by a factor of two or

more either side of the 838 value for the same rain rate. This variation is due to variations in drop size distribution (DSD). In practice, if the specific attenuation varied around the ITU-R model values along a link path, the pseudo-integration to calculate the total attenuation would greatly reduce the error introduced. Even if this was not the case, predicted average annual link statistics may well be correct even if the mean simulated attenuation was quite different from that actually experienced. There are several approaches that could address this problem. The ¥-R relation could be conditional upon the event type. Different DSD models exist for convective and stratiform rain and these could be used to derive different ¥-R relations. Event type could be approximately determined from rain rate and event size, as in Capsoni et al (2009). This classification could also be used in the estimation of rain height. Alternatively, as Nimrod radars switch to dual polarization, two DSD parameters can be determined from the radar reflectivity and these can be used to condition the ¥-R relation. Currently it is not clear if this is a problem. Time-series of measured link data will need to be compared with many simulations to determine is a significant bias exists. It is possible that the current simulator will be adequate for many regions but require adaption in climates with extreme convective-stratiform mixes e.g. in the tropics.

7.1.4 Rain Height model

Another major assumption is that of a stratified atmosphere. This is used when calculating the vertical variation of specific attenuation. The current stratified atmosphere models of specific attenuation variation with altitude are probably sufficient for stratiform events but absolutely inadequate for convective events. These events exhibit tall columns of mixed phase hydrometeors which cause extreme fading due to the long path lengths for slant path links. Rain height for stratiform rain events usually extend up to 360 m above ZDI. For convective evens the ZDI may not exist and mixed phase hydrometeors can exist up to altitudes of 10 km due to very strong updrafts and downdrafts which also prevent the formation of melting layer

(Capsoni et. al., 2009). Since the melting layer cannot be formed during a convective rain event, the Bacon-Tjelta sleet model (Tjelta et. al., 2005) is certainly not applicable for convective rain. Ultimately, two separate rain height models are needed to describe the different vertical specific attenuation profiles, one for stratiform and the other for convective type of precipitations as demonstrated by Capsoni et al. (2009). The group have develop an improved version of exponential cell (EXCELL) called SC EXCELL which can distinguish between stratiform and convective rain events by having two separate physical rain heights, derived from ERA-15 database for each type of rain event (stratiform and convective) to calculate rain attenuation. The effects of the melting layer in terms of hydrometeor attenuation are also added into the system. SC EXCELL has shown to perform better than the previous EXCELL when comparing with radio measurements from DBSG3 database. In addition, SC EXCELL offers flexibility in terms of modifying some of its input parameters so that the model can be used for different climate regions. The physical rain height model for convective precipitation from SC EXCELL could be used for GINSIM when simulating radio links during convective rain event.

7.2 Comparison with other Network Fade Simulation Tools

As discussed in Chapter 4, there are several ways to develop a network fade simulation tools which differ in the methods used to produce the fine scale meteorological fields. Fine scale rain fields can be generated by statistical models of rain cell parameters, purely statistical models of spatial temporal rain rate variation or through downscaling coarse-scale meteorological measurement data. The three approaches currently in development each have advantages and disadvantages. Purely statistical generation of rain fields is computationally fast but limited by lack of knowledge of rain field statistics at the scales between weather systems and variation within individual events. There are also concerns that rain field statistics measured at one location may not translate to other places e.g. between temperate and tropical regions or between coastal and mountainous regions. The EXCELL and HYCELL

rain cell models are capable of producing annual fade distribution and other statistics but they cannot reproduce time-series and so are of little use for the design and optimization of FMTs. The use of NWP or direct observation data, e.g. CRIE, ERA 40, NCEP/NCAR reanalysis or OPERA rain radar data; is limited by the existence of verified downscaling methods, both disaggregation and interpolation, and the same uncertainty in constraining variation statistics that limits purely statistical methods

7.3 Future Works and Recommendations

7.3.1 Downscaling Attenuation Time-Series

The downscaling algorithms in GINSIM could be used to downscale coarse-scale rain rate fields to the very fine scale resolutions consistent with link Fresnel zones and response times of FMT systems i.e. a few seconds and a few metres. However, for regions the size of even simple networks, this requires huge computational resources in terms of processing speed and the space to store data. This problem can be addressed by numerically downscaling the attenuation time-series after the pseudo-integration process is applied to moderately downscaled meteorological fields, The ONERA SISTAR system, (Jeannin et al. 2009), operates this way. Such methods could offer huge computational gain but it is still at its early stage and has not been properly investigated. The major difficultly is the prediction of the integration-scale cross-covariance of fade on arbitrary pairs of links. This information is required for the joint disaggregation of fade time-series. For links that are widely separated, the fine-scale variation of fade can be assumed to be independent. However, for the most interesting networks i.e. convergent links; this scale dependant cross-covariance is unknown. Models for the covariance of terrestrial links have been published, e.g. Paulson et al (2006), but these have not been integration-scale dependant. The problem has many parameters i.e. radio parameters such as frequencies and polarizations, network parameters such as geometry, and climate parameters. However, simple models will need to be developed. The errors introduced by bias in

the cross-correlation model will only effect variation at fine-resolution and only for links in very close proximity. The potential benefits of this scheme seem to greatly outweight the difficulties.

7.3.2 Other Atmospheric Fade Effects

Currently GINSIM only simulates rain and sleet fade for terrestrial and Earth-Space links since these are the most dominant hydrometeors fade mechanisms. Further fade processes can be added to refine the channel models. Absorption by atmospheric gases is a process that varies slowly in time and space and the fade can be calculated from local meteorological parameters provided by standard sources. Scintillation depends upon atmospheric turbulence and system parameters such as antenna apertures. Once turbulence has been estimated, scintillation time-series can be added using the model of Tatarski (1961). Cloud attenuation is another important fade mechanism and should be taking into account especially when simulating fade for Earth-Space links at higher frequency band. Cloud data is widely available from satellite Earth observation sources.

7.3.3 Nowcasting

Network fade simulation tools such as GINSIM could utilise meteorological nowcasting rainfall products to predict link outage half an hour or an hour into the future. This information could be used to predicatively reconfigure networks and data movements. Video streaming is an important application of current and future networks. Predictive DRM systems could preload network nodes with video data before a sub-network becomes isolated by outages. Alternatively, video streams can be rerouted around outages or to reduce the required capacity of links using dynamic modulation and coding to mitigate fades. The UK's Meteorological Office operates a nowcasting system for rainfall maps (created through extrapolating a sequence of radar images to produce a very short-range rainfall forecast) in which can be

combined with output from numerical weather prediction models to extend the period of predictability.

7.3.4 Global Applications and Different Climate Regions

The simulator has only been tested against ITU-R models and measured data acquired in the UK. Further work is required to verify its performance in other regions with different climates such as the alpine and Mediterranean regions of Europe. As composite rain radar images spanning Europe become available from the OPERA project, with consistent quality, this verification will be performed. In particular, better data position information is required. With the increasing deployment of weather radars across the world, it is possible to extend the application of a current simulation tool to a global scale where OPERA could combine with other large rain radar networks such as NEXRAD (Next-Generation Radar) in the U.S operated by NOAA. Alternatively, the simulation tool could also be applied to the space-borne rain radars, which have wider coverage than ground base rain radars and have becoming increasing popular, such as the TRMM (Tropical Rainfall Measuring Mission) by NASA. Recently, China has begun developing their own space-borne rain radar and it is expected to be launched in 2016 (Yang et. al., 2010). Currently, space-borne rain radars may not have the same quality as the surface-based rain radars, see Chapter 3. However, they can still provide data for complex algorithms, such as the Multi-Precipitation Estimates (MPE), to provide rainfall maps with global coverage. Over the years, the techniques and algorithms for systems such as MPE are improving and it may only be a matter of time to have a global rainfall map with rainfall accuracy and resolutions similar to the current ground-based rain radars.

7.3.5 Climate Change

Network fade simulation tool such as GINSIM could be used to investigate the climate change effects on radio links including terrestrial and Earth-Space links. Climate change phenomena are usually associated with natural disasters but recently researchers have begun exploring the effects on radio links. Where propagation important parameters, such as rain height, rain rate distributions and the mixture of stratiform and convective events; are reflected in the input data to simulation systems such as GINSIM, these tools can be used to demonstrate the effects of climate change on networks. NWP simulations of future climates will also allow the extrapolation of these effects into the future.

7.4 Future Outlooks

A network fade simulation tool, GINSIM, has been developed and verified. The tool can currently be applied to networks that span Europe, but have only been verified in the UK. The methods developed can potentially be used in a global simulation tool when global meteorological data is available at similar scales to that currently available in Europe. GINSIM has the potential to augment or replace ITU-R models and provide answers to questions that ITU-R models will never address. Applications include the design and optimization of Dynamic Network Management systems and managing the introduction of new systems into populated telecommunications bands. Combining the current system with nowcasting could provide the input data necessary for predicted DNM.

REFERENCES AND BIBLIOGRAPHY

Barclay L., “Propagation of Radiowaves”, second edition, *MPG Books Ltd*, UK, 2003.

Battan L. J., “Radar observations of the atmosphere”, *University of Chicago press*, 324 pp, 1973.

Beard K. V., and Chuang C., “A new model for the equilibrium shape of raindrop”, in: *Journal of the Atmospheric Sciences*, vol. 44, pp. 1509 – 1524, 1987.

Bell T. L., “A space-time stochastic-dynamic model of rainfall for satellite remote sensing studies”, in: *Journal of Geophysical Research*, vol. 92, No. D8, 1987.

Bosisio V., Carlo Riva, “A novel on method for the statistical prediction of rain attenuation in site diversity systems: theory and comparative testing against experimental data”, *International Journal of Satellite Communications*, Vol. 16, Issue 1,pages 47-52, doi:10.1002/(SICI)1099-1247(199801/02)16:1<47::AID-SAT592>3.0.CO;2-C, 1998.

British Atmospheric Data Centre’s website. In: *badc.nerc.ac.uk/home/index.html*. Accessed: 2009.

Callaghan S. A., Boyes, B., Couchman, A., Waight, J., Walden, C. J., and Ventouras, S., “An investigation of site diversity and comparison with ITU-R recommendations”, *Radio Science*, vol. 43, RS4010, doi:10.1029/2007RS003793, 2008.

Callagan S. A., “Rain field for fixed radio systems using fade mitigation Techniques”, URSIGA 2008 Chicago, USA, 2008.

Callaghan S. A., “Fractal Analysis and Synthesis of Rain Fields for Radio Communication Systems”, PhD thesis, University of Portsmouth, UK, 2004.

Capsoni C., Luini L., Paraboni A., Riva C., Martellucci A., “A New Prediction Model of Rain Attenuation That Separately Accounts for Stratiform and Convective Rain”, in: *Antennas and Propagation, IEEE Transactions on*, vol. 57, pp 196 – 204, doi:10.1109/TAP.2008.2009698, 2009.

Capsoni C., Fedi F., Magistroni C., Paraboni A., and Pawlina A., “Data and theory for a new model of the horizontal structure of rain cells for propagation applications”, in: *Radio Science*, vol. 22, no. 3, pp. 395-404, 1987.

Chilbolton radar website. In: *www.stfc.ac.uk/Chilbolton/default.aspx*. Accessed: 2009.

Christian Roland, “Spatial and seasonal variations of air temperature lapse rates in Alpine regions”, in: *Journal of Climate, American Meteorological Society*, vol. 16, pp 1032-1046, 2002.

Christopher Haslett, “Essentials of radio wave propagation”, *Cambridge University Press*, 2008.

Cluckie I. D., and Rico-Ramirez M. A., “Weather radar technology and future developments”, in: *GIS and Remote Sensing in Hydrology, Water Resources and Environment, IAHS Publ. 289*, 2004.

COST 280. “Propagation impairment mitigation for millimetre wave radio systems”, in: *www.cost280.rl.ac.uk/*, 2001 – 2005.

COST 255. “Radiowave propagation modelling for new satcom services at Ku-band”, in: *www.cost255.rl.ac.uk/*, 2002.

COST 210 Management Committee, COST210. “Influence of the atmosphere on interference between radio communications systems at frequencies above 1 GHz”, ISBN 9282780236, EUR 13407 EN, 1991.

Crane R. K., “Electromagnetic wave propagation through rain”, *John Wiley&Sons, Inc.*, 1996.

Deidda, R., “Rainfall downscaling in a space-time multifractal framework”, *Water Resources Research*, 36, 1779-1794, 2000.

Deidda R.: “Multifractal analysis and simulation of rainfall fields in space”, *Phys. Chem. Earth Part B - Hydrology*, vol. 24, No. 1-2, pp. 73-78, 1999.

Diaz H. F., Eischeid J. K., C. Duncan, and R. S. Bradley, “Variability of freezing levels, melting season indicators, and snow cover for selected high-elevation and continental regions in the last 50 years”, *Kluwer Academic Publishers* , Climate Change 59: pp 33-52, 2003.

Dissanayake A., Allnutt J., and Haidara F., “Cloud Attenuation Modelling for SHF and EHF applications”, *Int. J. Satell. Commun*, vol. 19, pp 335-345, doi: 10.1002/sat.67, 2001

Ebert E., and Manton M., “Performance of satellite rainfall estimation during TOGA COARE”, in: *J. Atmos. Sci.*, vol. 55, pp 1537-1557, (1998).

European Organisation for the Exploitation of Meteorological Satellites (EUMETSAT) Multi sensor Precipitation Estimate (MPE): concept and validation. In: *www.eumetsat.int/groups/ops/documents/document/mpe_conceptvalidation_uc2003.pdf*. Accessed 2011.

Fenton G. A., and Vanmarcke E., “Simulation of Random Fields via Local Average Subdivision”, *ASCE Journal of Engineering Mechanics*, 116(8), 1733-1749, 1990.

Féral L., Lemorton J., Castanet L., and Sauvageot H., “HYCELL: a new model of rain fields and rain cells structure”, Proceedings of the 2nd International Workshop of Action 280 Joint with COST272, ESTEC, NL, May 2003. In: *www.cost280.rl.ac.uk/documents/WS2%20Proceedings/documents/pm-5-065.pdf.* Accessed: 2011.

Féral L., Sauvageot H., Castanet L. and Lemorton J., “HYCELL—A new hybrid model of the rain horizontal distribution for propagation studies: 1. Modeling of the rain cell”, in: *Radio Science*, vol. 38, No. 3, 2003, 1056, doi:10.1029/2002RS002802, 2003a.

Féral L., Sauvageot H., Castanet L. and Lemorton J., “HYCELL—A new hybrid model of the rain horizontal distribution for propagation studies: 2. Statistical modeling of the rain rate field,” in: *Radio Science*, Vol. 38, No. 3, 2003, 1057, doi:10.1029/2002RS002803, 2003b.

Goddard J. W. F., and Cherry S. M., “The ability of dual-polarisation radar (copolar linear) to predict rainfall rate and microwave attenuation”, in: *Radio Science*, vol. 19, pp 201–208, 1984.

Goldhirsh J., and Katz I., “Useful experimental results for Earth-Satellite rain attenuation modeling”, in: *IEEE Trans. Ant. Prop.*, AP-27, pp 413-415, 1979.

Gremont B., and Filip M., “Spatio-Temporal rain attenuation model for application to fade mitigation techniques”, in: *IEEE Trans. Antennas and Propagation*, pp 1245-1256, 2004.

Groisman P. Ya., and Legates D. R., “The accuracy of United States precipitation data”, in: *Bull. Amer. Meteor. Soc.*, vol. 75, pp 215–227, 1994.

Harrison D. L., Driscoll S. J. and Kitchen M., “Improving precipitation estimates from weather radar using quality control and correction techniques”, in: *Met. Appl.*, vol. 6, pp 135–144, 2000.

Hodges, D., Watson, R., Page, A., Watson, P., “Generation of attenuation time-series for EHF SATCOM simulation”, in: *Military Communications Conference*, 2003. MILCOM 2003. IEEE, Vol.1, page 505 – 510, ISBN 0-7803-8140-8, doi:10.1109/MILCOM.2003.1290154, 2003.

Hunter S. M., “WSR-88D radar rainfall estimation: Capabilities, limitations, and potential improvements”, in: *Natl. Wea. Dig.*, vol. 20 (4), pp 26–38, 1996.

ITU-R., “Attenuation due to clouds and fog”, in: *Recommendations* ITU-R P. 840-4, 2009.

ITU-R., “Attenuation by atmospheric gases”, in: *Recommendations* ITU-R P. 676-8, 2009.

ITU-R., “Propagation data and prediction methods required for the design of Earth-Space telecommunication systems”, in: *Recommendations* ITU-R P. 618-10, 2009.

ITU-R., “Propagation data and prediction methods required for the terrestrial line-of-sight systems”, in: *Recommendations* ITU-R P. 530-13, 2009.

ITU-R., “Prediction procedure for the evaluation of interference between stations on the surface of the Earth at frequencies above about 0.1 GHz”, in: *Recommendations*

ITU-R P. 452-14, 2009.

ITU-R., “Characteristics of precipitation for propagation modeling”, in: *Recommendations* ITU-R P. 837-5, 2007.

ITU-R., “Specific attenuation model for rain for use in prediction methods”, in: *Recommendations* ITU-R P. 838-3, 2005.

ITU-R., “Prediction method of fade dynamic on Earth-Space paths”, in: *Recommendations* ITU-R P. 1623-1, 2003.

ITU-R., “Rain height model for prediction methods”, in: *Recommendations* ITU-R P. 839-3, 2001.

Jeannin N., Castanet L., Lemorton J., Feral L., Sauvageot H. and Lacoste F., “A space-time channel model for the simulation on continental satellite coverages: overview of the modelling and potentiality for adaptive resource management optimization”, in press, *IEEE Transactions on Antennas and Propagation*, 2009.

Joss J., and Waldvogel A., “Comments: Some observations on the Joss-Waldvogel Rainfall disdrometer.”, in: *Journal of Applied Meteorology*, vol. 16, pp. 112 – 113, 1977.

Kalnay E., Kanamitsu, M., Kistler, P. Collins, W. Deaven, D. Gandin, L. Iredell, M. Saha, S. White, G. Woollen, J. Zhu, Y. Cheillab, M, Ebsuzaki, W. Higgins, W. Janowiak, J. Mo, K. C. Ropelewski, C. Wang, J. Leetma, A. Reynolds, P. Jenne 1. and Joseph, D. , “The NCEP/NCAP 40-year reanalysis project”, in: *Bull. Amer. Meteor.* Soc., 77, pp 437-470, 1996.

Kitchen M., and Jackson P. M., “Weather radar performance at long range—

Simulated and observed", in: *J. Appl. Meteor.*, vol. 32, pp 975–985, 1993.

Laws J. O., and Parsons D. A., "The relationship of rain-drop size to intensity", in: *Trans. Amer. Geophys*. Union, 24, pp. 432-460, 1943.

Lempio G. E., Bumke K., and Macke A., "Measurement of solid precipitation with an optical disdrometer", published by *Copernicus GmbH on behalf of the European Geosciences Union*, doi:10.5194/adgeo-10-91-2007, 2007.

Liebe H. J., "MPM-An atmosphere millimeter wave propagation model, in: *Int. J. Infrared Millimeter waves*, 10(6), 631-650, 1989.

Lilley M., S. Lovejoy, N. Desaulniers-Soucy and D. Schertzer, "Multifractal large number of drops limit in rain", in: *J. of Hydrology*, vol. 328, Issue 1-2, pp 20-37, doi:10.1016/j.jhydrol.2005.11.063, 2006.

Liolis, K. P., A. D. Panagopoulos, and P.G. Cottis, "Multi-Satellite MIMO Communications at Ku Band and above: Investigation on Spatial Mutiplexing for Capacity Improvement and Selection Diversity for Interference Mitigation" in: *EURASIP Journal on Wireless Communications and Networking*, May 2007.

Lovejoy S., and Schertzer D., "Multifractals and Rain". New Uncertainty Concepts in Hydrology and Hydrological modelling, Ed. A. W. Kundzewicz, pp 62-103, Cambridge press, 1995.

Luini L., and Capsoni C., "MultiEXCELL: a new rain field model for propagation applications", accepted for publication in *IEEE Transactions on Antennas and Propagation*, vol. 59, No. 11, doi: 10.1109/TAP.2011.2164175, 2011.

Marshall J. S., and Palmer W. McK., "The distribution of raindrop with size", in:

J.Meteor., vol. 5, pp. 165-166, 1948.

Maseng, T., and Bakken, P.M., ”A Stochastic Model For Rain Attenuation”, in: *IEEE Trans Commun.*, vol. COM-29, No5, May 1981, pp. 660-669, 1981.

Max M. J. L. van de Kamp, “Statistical Analysis of Rain Fade Slope”, in: *IEEE Transactions on antennas and propagation*, vol. 51, pp 1750-1759, August 2003.

Morrison and Cross. “Scattering of a plane electromagnetic wave by axisymmetric rain drops”, in: *Bell System Technical Journal*, vol. 53, pp. 955–1019, 1971.

National Oceanic and Atmospheric Administration (NOAA)’s Physical Science Division (PSD) website. In: www.esrl.noaa.gov/psd/, accessed: 2009.

Page A., Watson R. J., Watson P. A., “Time-series of attenuation on EHF and SHF fixed radio links derived from meteorological forecast and radar data”, in: *IEE Proc., Microw. Antennas Propag*, vol. 152, issue 2, pp124–128, doi:10.1049/ip-map:20041034, April 2005.

Paraboni, A.,Gino M., and Antonio E., “The effects of precipitation on microwave LMDS networks – Performance analysis using a physical rain cell model”, in: *IEEE Journal on Selected Areas in Communications*, vol. 20, No. 3, S 0733-8716(02)03382-6, 2002.

Paraboni A., Capsoni C., and Riva C., “Spatial rain distribution models for the prediction of attenuation in point-to-multipoint and resource-sharing systems in the Ka and V frequency bands”, in: *Proceedings of URSI Commission F meeting, Open Symposium on Propagation and Remote Sensing*, Germany, 2002.

Patra K. C., “Hydrology and water resources engineering and applications”, in: *Alpha*

Science International Ltd., India, 2001.

Paulson K. S., and Basarudin H., "Development of a heterogeneous microwave network, fade simulation tool applicable to networks that span europe," in: *Radio Science*, doi:10.1029/2010RS004608, 2011.

Paulson K. S., and Basarudin H., "Verification of a Heterogeneous Microwave Network, Fade Simulation Tool," in: *Radio Science*, in press.

Paulson K. S., and Xiaobei Zhang, "Simulation of rain fade on arbitrary microwave link networks by the downscaling and interpolation of rain radar data", in: *Radio Science*, vol. 44, RS2013, doi:10.1029/2008RS003935, 2009.

Paulson K. S., and Xiaobei Zhang, "Estimating the scaling of rainrate moments from radar and rain gauge", in: *Geophys. Res. – Atmos*, vol. 112, doi:10.1029/2007JD008547, 2007.

Paulson K. S., Usman I. S., and Watson R. J., "A general route diversity model for convergent terrestrial microwave links", in: *Radio Science*, vol. 41, RS3004, doi:10.1029/2005RS003411, January 2006.

Paulson K. S., "The effects of variation in atmosphere absorption on millimetric, terrestrial, telecommunications links, in: *Radio Science*, vol. 40, RS6004, doi:10.1029/2004RS003218, 2005.

Paulson K. S., "Fractal interpolation of rainrate time-series", *J. Geophys. Res.-Atmos.*, vol. 109 (D22): art. no. D22102, doi:10.1029/2004JD004717, 2004.

Paulson K. S., "The spatial-temporal statistics of rainrate random fields", in: *Radio Science*, vol. 37, No. 5, art. No. 1088, doi:10.1029/2001RS002527, 2002.

Peck E. L., “Quality of hydrometeorological data in cold regions”, in: *J. Amer. Water Resour. Assoc.*, vol. 33, pp 125–134, 1997.

Pruppacher H. R., and Beard K. V., “A wind tunnel investigation of the internal circulation and shape of water drops falling at terminal velocity in air”, in: *Quarterly Journal of the Royal Meteorological Society*, vol. 96, pp. 247 – 256, 1970.

Pruppacher H. R., and Pitter R. L., “A semi-empirical determination of the shape of cloud and rain drops”, in: *Journal of the Atmospheric Sciences*, vol. 28, pp. 86 – 94, 1971.

Radar Meteorology Tutorial by Brian McNoldy from Multi-community Environmental Storm Observatory (MESO). In: *w8lrk.org/article/RadarTutorial.pdf.* Accessed 2010.

Report by the Electronic Communications Committee of CEPT on “The use of the Frequency Bands 27.5-30.0 GHz and 17.3-20.2 GHz by satellite networks”, Gothenburg, September 2010.
In: www.erodocdb.dk/docs/doc98/official/pdf/ECCRep152.pdf. Accessed 2012.

Scofield R. A., and Kuligowski R. J., “Status and Outlook of Operational Satellite Precipitation Algorithms for Extreme-Precipitation Events”, in: *National Environmental Satellite, Data, and Information Service, Camp Springs, Maryland*, vol. 18, pp 1037-1051, 2003.

Shkarofski I. P., “Dependence of rain attenuation and cross-polarization on drop size distribution”, in: *IEEE Trans. on Ant. and Prop.*, vol. AP-27, No 4, pp. 538-542, July 1979.

Shuttle Radar Topography Mission (SRTM)'s website. In: *www2.jpl.nasa.gov/srtm/*. Accessed: 2009.

Skolnik M. I., "Introduction to Radar Systems", *McGraw-Hill*, third edition, 2002.

Smith J. A., Seo D. J., Baeck M. L., and Hudlow M. D., " An intercomparison study of NEXRAD precipitation estimates", in: *Water Resour. Res.*, vol. 32, pp 2035–2045, 1996.

Smith J. A., Bradley A. A., and Baeck M. L., "The space–time structure of extreme storm rainfall in the southern plains" in: *J. Appl. Meteor.*, vol. 33, pp 1402–1417, 1994.

Takada M., and Nakamura S., "Attenuation of 11 Gc Waves by Wet Snowfall", in: *Review of the Electrical Communication Laboratory*, 14(1-2), pp. 27-42, January 1966.

Tatarski V. I., "Wave propagation in a turbulent medium", in: *McGraw-Hill Book Company*, New York, 1961.

Taylor G. I., "The spectrum of turbulence", in: *Proc. Roy. Soc. London*, A164, 1938, pp. 476–490, 1938.

The Nilometer in Cairo. In (www.waterhistory.org/histories/cairo/). Accessed in 2012.

Thurai M., and Woodroffe J. M., "Precipitation induced co and cross-polar effects from a 9 km link operating at 38 GHz", in *Proc. of International Conference on Antennas and Propagation (ICAP)*, Conf. Publ. No. 436, 2, pp. 222-225, 14-17 April 1997.

Tjelta T., and Bacon D., “Predicting Combined Rain and Wet Snow Attenuation on Terrestrial Links”, in: *IEEE Transactions on Antennas and Propagation*, vol. 58, No. 5, 2010, pp. 1677-1682, 2010.

Tjelta T., Bråten L. E., Bacon D., “Predicting the attenuation distribution on line-of sight radio links due to melting snow”, in: *Proc. ClimDiff*, Cleveland, U.S.A., 26-27, Sept. 2005

Trevor Manning, “Microwave Radio Transmission Design Guide”, in: *Artech House Microwave Library*, Chapter 3, Second Edition, 2009.

Tropical Rainfall Measuring Mission (TRMM) website. In: *trmm.gsfc.nasa.gov/*. Accessed 2010.

UK Meteorological Office’s National Meteorological Library and Archive, Fact sheet No. 15 – Weather Radar. In: *badc.nerc.ac.uk/data/nimrod/factsheet15.pdf*. Accessed: 2009.

UK Meteorological Office’s website. In: *www.metoffice.gov.uk.* Accessed: 2009.

Ulbrich C. W., “Natural variations in the analytical form of the raindrop size distribution”, in: *J. Clim. Appl. Meteorol.*, vol. 22, pp. 1764-1775, 1983.

Usman I. S., “Development of point to multipoint models for available and fade mitigation in the millimeter wave frequency range”, PhD thesis, University of Bath, UK, 2005.

Veneziano D., Bras R. L., and Niemann J. D., “Nonlinearity and self-similarity of rainfall in time and a stochastic model”, in: *J. of Geophys. Research*, vol. 101, D21, 26371-26392, Nov. 27, 1996.

Voss R. F., “Random fractal forgeries”, in “Fundamental Algorithms for Computer Graphics”, editor R. A. Earnshaw, NATO ASI Series F, in: *Computer and System Sciences*, vol. 17, 1985.

W. Zhuang., J.-Y. Chouinard and D. Makrakis., “Dual-Space Diversity over Land Mobile Satellite Channels Operating in the L and K Frequency Bands”, in “Wireless Personal Communications”, volume 4, Number 3, pp. 277-298, 1997.

Walden C.J., Wilson C.L., Goddard J. W. F., Paulson K. S., Willis M. J., and Eastment J. D., “A study of the effects of melting snow on communications links in Scotland”, in: *Proc. of International Conference on Antennas and Propagation (ICAP)*, 2003.

Waldvogel A., “The N0 jump of raindrop spectra”, in: *J. Atmos. Sci.*, vol. 31, pp 1067–1078, 1974.

WeatherQuestion’s website. In: *www.weatherquestions.com*. Accessed: 2011.

Wheater H. S., Isham V. S., Onof C., and Chandler R. E., “Generation of spatially consistent rainfall data”, report to Ministry of Agriculture, Fisheries and Food, Feb. 2000.

Williams C. R., and Gage K. S., “Raindrop size distribution variability estimated using ensemble statistics”, in: *Annales Geophysicae*, vol. 27, pp 555-567, doi:10.5194/angeo-27-555-2009, 2009.

William Myers, “Comparison of Fade Models for LMDS, Comparison of Propagation Models”, Broadband Wireless Access Working Group, *IEEE 802.16cc-99/13*, 1999.

WTEC panel report on Global Satellite Communications Technology and Systems. In: *www.wtec.org/pdf/satcom2.pdf*. Accessed in 2012.

Yang H., Shang J., Wu Q., Yin H., and Guo Y., “Development of spaceborne rain radar in China: The first results from airborne dual-frequency rain radar field campaign”, in: *Geoscience and Remote Sensing Symposium (IGARSS), 2011 IEEE International*, pp 1551 – 1553, doi:10.1109/IGARSS.2011.6049365, 2011.

Zhang X., “Fine-scale modelling of rain fields for radio network simulation”, PhD thesis, Department of Engineering, University of Hull, UK, 2008.

APPENDIX A: DISAGGREGATION

A two dimensional spatial multi-fractal disaggregation method is required for a network simulator that preserves spatial statistical properties as observed in actual rainfall. Disaggregation is a process to refine existing sample into smaller spatial integration volumes. Multi-fractal cascade method from Deddia (2000) has been employed for the disaggregation process. The random cascade is created via a multiplicative process. Each son rain rate R_j^i at *j*th level can be gained by multiplying the related father at level (*j-1*) by an independent and identical distributed random variable w_i .Therefore $R_j^i = w_i R_{j-1}$ where the scale at the *j* level is half of the scale at the level (*j-1*). Collection average or mean of *q* moments of random variables *R* can be related to the statistics of the generator *w* as following:

$$\overline{R_j^q} = R_0^q \overline{w^{q^j}} \tag{A1}$$

Moment scaling structure function can be established if the information of the rain rate distribution at the coarsest scale is known. The structure function as shown by Deddia (1999 and 2000) obeys the scaling law with expected multi-fractal exponent *ζ(q)* depending only on the ensemble averages of the moments of the generator *w*.

$$¸(q) = q(2 + \log_2 \overline{w}) - \log_2 \overline{w^q} \tag{A2}$$

ζ(q) can be proven as a convex and nonlinear function of the moments *q* by using the Cauchy-Schwarz inequality. Hence, the model is appropriate for the generation of multi-fractal fields. The selection of probability distribution for the random generator *w* characterises the multi-fractal behaviour and the scale covariance of synthetic signals. In GINSIM, the log-Poisson distribution has been employed. $w_i = e^{\,q}\beta^{\,y}$, where *y* is an i.i.d. or independent and identically distributed sample from a Poisson

distribution of mean *c*.

The q-order moment of the log-Poisson distribution is given by:

$$\overline{w^q} = \exp[qa + c(\quad^q - 1)] \tag{A3}$$

When q=1, then $a=c(1-\beta)$. Conclusively, the expected scaling of synthetic fields can be assessed:

$$\text{،}(q) = 2q + c\frac{q(\quad -1) - (\quad^q - 1)}{\ln 2} \tag{A4}$$

where c and β are the parameters for multi-fractal exponent $\zeta(q)$. Parameters of c and β must be scale-independent in order to replicate a scaling regime in synthetic fields. The parameters c and β from the model can be estimated by solving the minimisation equation as following:

$$\min_{c,} \sum_{q} [\frac{\text{،}_s(q) - \text{،}(q)}{q-1}]^2 \tag{A5}$$

where $\zeta_s(q)$ are the sample multi-fractal exponents, $\zeta(q)$ is the theoretical expectation as above, q-1 is a weight that accounts for the estimation error which is the standard deviation of $\zeta(q)$.

APPENDIX B: INTERPOLATION

Interpolation is a process to introduce new rain rate measurements where there were none. In GINSIM, the interpolation is used to introduce new rain rates between existing scans. Methods for interpolation are based on series of algorithms including Random Midpoint Displacement algorithm of Voss (1985) and the Local Average Subdivision algorithm of Fenton and Vanmarcke (1990).

Assume a pair of log rain rate fields to be from a Gaussian fractional Brownian process:

$$L_1 = \ln\left(R(\mathbf{x} + \mathbf{y}_A, t_1)\right)$$

$$L_2 = \ln\left(R(\mathbf{x}, t_1 + \Delta_t)\right)$$

Where $\mathbf{y}_A$ represents the advection vector between scans. A Maximum Likelihood algorithm is used to estimate the marginal mean μ_L and variance σ_L^2 for censored data, $L > L_{min}$ where L_{min} is the smallest measurable log rain rate. The set of spatial sampling points is assumed to be $A \equiv \{A_i \in (x, y)\}$ and let $T \equiv \{t_1 \leq T_i \leq t_1 + \Delta t$ be the equi-spaced interpolation times. Then, the discrete interpolation volume will be $V \equiv \{(\mathbf{x}, t): \mathbf{x} \in A, t \in T\}$.

The values of the interpolated log rain rate are calculated via a hierarchical algorithm that introduces fresh samples. These samples are separated by distances that decrease exponentially with every iteration. Voss's Random Midpoint Displacement (RMD) algorithm (1985) was developed to increase the resolution of isotropic FBfs. This algorithm has been used as a foundation and existing samples are conserved at each iteration process. The following paragraphs explain the development of an algorithm for asymmetrically sampled FBfs. The technique is based on the Local Average Subdivision algorithm by Fenton and Vanmarcke (1990).

The RMD algorithm starts with a FBf that evenly sampled at scale Δ in each dimension and produces new samples to generate a FBf sampled at half of the

original scale or Δ/2. Assume $L_\Delta = \{L_i; i = 1, \dots N_\Delta\}$ to be the log rain rate samples in a region of scale Δ around the interpolate L_Y at position $\boldsymbol{Y}$. The new value from the interpolation process is selected to be:

$$L_Y = S(L_\Delta) + \sigma_\Delta \varepsilon_Y \qquad \text{B1)}$$

where $S(L_\Delta)$ is a smoothly interpolated value and ε_Y is an independent and identically distributed (i.i.d.) standard Normal distribution sample. A linear estimator i.e. $S(L_\Delta) = a_0\mu_L + \sum_{i=1}^{N_\Delta} a_i L_i$ will be implemented for the asymmetric algorithm. The coefficients a_i depend upon the distribution and shape of samples in the scale area and are selected to fulfil:

$$E(L_Y) = \mu_L, \qquad \text{(B2.1)}$$

$$E(L_y L_j) = B_{FBf}(\delta_{yj}) \text{ and} \qquad \text{(B2.2)}$$

$$E(L_Y^2) = B_{FBf}(0). \qquad \text{(B2.3)}$$

$B_{FBf}(\delta)$ is the expected value of the product between two log rain rates that are separated by a distance δ, with known FBf assumption. It may be obtained from the marginal distribution i.e. $B_{FBf}(\delta) = E(L^2) - \delta^{2H}\sigma^2/2$. By substituting the equation in (B1) into the expected value in (B2) and using the independence of L_i and ε_Y produces:

$$E(L_Y) = a_0\mu_L + \sum_{i=1}^{N_\Delta} a_i E(L_i) = \sum_{i=0}^{N_\Delta} a_i \mu_L, \qquad \text{(B3.1)}$$

$$E(L_y L_j) = a_0\mu_L^2 + \sum_{i=1}^{N_\Delta} a_i\, B_{FBf}(\delta_{ij}) \text{ and} \qquad \text{(B3.2)}$$

$$E(L_Y^2) = a_0^2\mu_L^2 + 2a_0\mu_L^2 \sum_{i=1}^{N_\Delta} a_i + \sum_{i=1}^{N_\Delta}\sum_{j=1}^{N_\Delta} a_i\, a_j\, B_{FBf}(\delta_{ij}) + \sigma_\Delta^2\,. \qquad \text{(B3.3)}$$

The equations in (B2.1) and (B3.1) indicate that $\sum_{i=1}^{N_\Delta} a_i = 1$. In addition, the equations in (B2.2) and (B3.2) yield a further N_Δ equations linear in a_i. The value of the coefficients $\{a_i\}$ can be extracted via solving the $N_\Delta + 1$ linear equations. The coefficients $\{a_i\}$ obtained yield an expression for σ_Δ^2, using (B2.3) and (B3.3).

The midpoint interpolation of regularly spaced samples and L_Δ taken to be the $N_\Delta = 2^n$ nearest or adjacent neighbours, generated FBfs via Voss's RMD algorithm with $a_0 = 0$, $a_i = N_\Delta^{-1}$ and noise variance exponentially decreasing with scale. In this situation, the calculation for interpolation coefficients is insignificant. Nevertheless, Nimrod rain data is sampled finer in space than in time in which the units are decorrelation intervals. The second order moment of the measured rain data is defined as:

$$B_L(\mathbf{y}, \tau) \equiv E(L(\mathbf{x}, t)L(\mathbf{x} + \mathbf{y}, t + \tau)) \quad \text{(B4)}$$

Interpolation scale of $N = 2^m$ sample units can be determined:

$$B_L((N+1)\Delta_x \mathbf{e}, 0) \cong B_t(0, \Delta_t) \quad \text{B5)}$$

where *e* is a unit vector. In order to produce samples symmetrically distributed in space and time, $N - 1$, new, equi-spaced, log rain rate fields need to be interpolated. The process can be achieved in *m* iterations of an asymmetric RMD or ARMD through equations in (B1), (B2) and (B3). During the first iteration, interpolation region with diameter $\Delta_0 = 2N$ in sample units are used and the diameter is halved at each following iteration. For each scale, the interpolation coefficient $\{a_i\}$ for the recognised/known L_i within the interpolation volume or dimension, and the variance σ_Δ^2 must be established. For interpolation regions located on the boundary of L, need coefficients that are consistent with the asymmetry of L_Δ, i.e. the existence of finely scaled measured rain data on a pair of log rain rate fields (L_1 and L_2) or the lack of samples located outside the boundary of L. On the other hand, same coefficients can be applied for all regions that are located away from the boundary.